Tampere University

TOMI RYYNÄNEN

Alternative Electrode Materials for Prototyping Cell Model-Specific Microelectrode Arrays

Tampere University Dissertations 123

Tampere University Dissertations 123

TOMI RYYNÄNEN

Alternative Electrode Materials for Prototyping Cell Model-Specific Microelectrode Arrays

ACADEMIC DISSERTATION
To be presented, with the permission of
the Faculty of Medicine and Health Technology
of Tampere University,
for public discussion in the auditorium TB109
of the Tietotalo building, Korkeakoulunkatu 1, Tampere,
on 8 November 2019, at 12 o'clock.

ACADEMIC DISSERTATION
Tampere University, Faculty of Medicine and Health Technology
Finland

Responsible supervisor and Custos	Prof. Emeritus Jukka Lekkala Tampere University Finland	
Pre-examiners	Adj. Prof. Bruce C. Wheeler University of California San Diego USA	Prof. Sami Franssila Aalto University Finland
Opponent	Prof. Andreas Offenhäusser Forschungszentrum Jülich Germany	

The originality of this thesis has been checked using the Turnitin OriginalityCheck service.

Cover design: Roihu Inc.

ISBN 978-952-03-1230-5 (print)
ISBN 978-952-03-1231-2 (pdf)
ISSN 2489-9860 (print)
ISSN 2490-0028 (pdf)
http://urn.fi/URN:ISBN:978-952-03-1231-2

PunaMusta Oy – Yliopistopaino
Tampere 2019

ABSTRACT

A microelectrode array, MEA, is a tool used by biologists for measuring the electrical activity of cells *in vitro*. Instead of only studying random cell clusters and monolayers, an increasing number of biological research questions are aimed at studying well-defined cell networks or single cells. This places special demands on the location, size, and overall performance of the MEA electrodes, which the standard, commercially available layouts cannot usually meet. Therefore, custom-designed MEAs are needed for a wide range of applications from basic cell biology and disease model development to toxicity testing and drug screening. This thesis focuses on the fabrication of microelectrodes made of titanium, atomic layer deposited (ALD) iridium oxide (IrOx), and ion beam-assisted e-beam deposited (IBAD) titanium nitride (TiN). These MEAs are characterized, for example, in terms of their impedance, noise level, and surface morphology, and their biocompatibility and functionality are verified by simple experiments with human stem cell-derived neuronal cells and cardiomyocytes. The aim of these studies is to offer more alternatives for MEA fabrication, enabling researchers and practitioners to choose the electrode material that best fits their application from their available resources.

Pure titanium is commonly disregarded as an electrode material because of its oxidation tendency, which destabilizes the electrical performance. However, when prototyping customised MEAs, the time and cost of fabricating the subsequent iterations of the prototype can be more decisive factors than the device's ultimate electrical performance, which is typically evaluated by the impedance value at 1 kHz. As might be expected, although titanium electrodes underperformed in terms of impedance (>1700 kΩ), when used in the cell experiments, the field potentials from both neuronal cells and cardiomyocytes were still easily distinguishable from the noise. There are a number of benefits to using titanium as an electrode material. Besides the fact that it is about hundred times cheaper than other commonly-used materials, such as gold or platinum, it usually requires fewer and often simpler process steps than the most common alternatives.

IrOx and TiN are common electrode coatings which, when applied on top of e.g. a titanium electrode, can lower the impedance and the noise level of the electrode.

In this study, two alternative deposition methods, ALD and IBAD, were used for IrOx and TiN in MEA applications. Even if the impedance of these 30 μm electrodes (450 kΩ for ALD IrOx and ~90 kΩ for IBAD TiN) did not quite reach the impedance levels of the industry standards, i.e. sputtered TiN (30-50 kΩ) and Pt black (20-30 kΩ), in cell experiments the IBAD TiN electrodes in particular showed no tangible differences in peak amplitudes and noise levels compared with sputtered TiN electrodes. This makes IBAD TiN an attractive alternative material for those who prefer to use TiN electrodes, but do not have access to a sputter coater, for example. ALD IrOx, on the other hand, relies on the potential of the general properties of ALD and IrOx (yet unverified) to provide exceptional performance in designs requiring excellent step coverage or stimulation capability.

Finally, as an application example of a custom-designed MEA, a version capable of measuring cardiomyocytes at the single-cell level was developed. The benefit of such an MEA is to offer a unique noninvasive method to study single cells without destroying them with the time-consuming patch clamp method, and without losing cell-specific information, which often occurs if the cell clusters studied with standard MEAs are too heterogenous. This was achieved with a number of innovations. For example, the electrodes were placed near the perimeter of the cell culturing area and had a larger diameter (80 μm) than the usual 30 μm electrodes. This simplified the plating of the cells to the electrodes and enabled the beating of the cells to be electrically recorded. It is also possible to combine that with image-based analysis of mechanical beating through transparent indium tin oxide (ITO) electrodes.

TIIVISTELMÄ

Mikroelektrodimatriisi (MEA, microelectrode array) on biologien käyttämä väline solujen sähköisen toiminnan mittaamiseen *in vitro* olosuhteissa. Pelkkien satunnaisten soluryppäiden ja yksikerroksisten soluviljelmien tutkimisen rinnalla yleistymässä ovat biologiset tutkimuskysymykset, joissa tutkitaan ohjatusti muodostettuja soluverkkoja tai yksittäisiä soluja. Nämä aiheet asettavat sellaisia erityisvaatimuksia elektrodien koolle ja sijainnille MEA-levyllä, sekä ylipäätään MEA-levyn suorituskyvylle, että kaupasta saatavat vakiomalliset MEA-levyt eivät yleensä niitä täytä. Räätälöidyille MEA-levyille onkin tarvetta monella sovellusalueella perussolubiologiasta ja tautimallien kehittämisestä myrkyllisyystutkimuksiin ja lääketestaukseen. Tässä väitöstyössä on valmistettu mikroelektrodeja, joiden materiaalina on käytetty titaania, atomikerroskasvatettua (atomic layer deposition, ALD) iridiumoksidia (IrOx) sekä ionisuihkuavusteiselle elektronisuihkuhöyrystyksellä (ion beam assisten e-beam deposition, IBAD) tuotettua titaaninitridiä (TiN). Elektrodit on karakterisoitu mm. niiden impedanssin, kohinatason ja pinnan morfologian osalta. Lisäksi bioyhteensopivuus ja toimivuus on varmistettu kokeilla, joissa on käytetty ihmisperäisistä kantasoluista johdettuja hermo- ja sydänsoluja. Näiden tutkimusten tarkoituksena on tarjota MEA-valmistukseen lisää vaihtoehtoja, mistä valita eri sovelluksiin parhaiten sopivat ja käytettävissä olevat resurssit parhaiten huomioivat elektrodimateriaalit.

Titaanin käyttöä puhtaasti metallimuodossa on mikroelektrodimateriaalina yleisesti vältetty sen johtavuusominaisuuksia häiritsevän hapettumistaipumuksen vuoksi. Valmistukseen kuluva aika ja kustannukset voivat kuitenkin olla räätälöityjen MEA-prototyyppien kehittämisessä olennaisempia tekijöitä kuin prototyypin huippuunsa viritetty suorituskyky, jota usein arvioidaan 1 kHz taajuudella mitatun impedanssin avulla. Kuten odotettua, titaanielektrodien impedanssi oli huomattavan korkea (>1700 kΩ), mutta silti solumittauksissa sekä hermo- että sydänsolujen tuottamat kenttäpotentiaalisignaalit olivat erotettavissa kohinasta. Titaanin etuihin elektrodimateriaalina kuuluvat yleisimpiin vaihtoehtoihin verrattuna vähäisempien ja yksinkertaisempien prosessivaiheiden tarve sekä noin sata kertaa pienemmät raaka-aine kustannukset kultaan ja platinaan verrattuna.

IrOx ja TiN ovat yleisesti käytettyjä elektrodien pinnoitusmateriaaleja, joiden tarkoitus on laskea esimerkiksi titaanista tehtyjen elektrodien impedanssia ja kohinatasoa. Tässä työssä tutkittiin mahdollisuutta tehdä pinnoitukset vaihtoehtoisilla, MEA sovelluksissa uusilla menetelmillä, ALD:llä ja IBAD:lla. Vaikka näillä menetelmillä pinnoitettujen 30 μm elektrodien impedanssit (450 kΩ ALD IrOx:lle ja ~90 kΩ IBAD TiN:lle) eivät aivan laskeneetkaan yleisesti käytettyjen sputteroidun TiN:n (30-50 kΩ) ja huokoisen platinan eli Pt black:n (20-30 kΩ) tasolle, niin solumittauksissa etenkään IBAD TiN elektrodien ja sputteroitujen TiN elektrodien välillä ei ollut käytännössä lainkaan havaittavaa eroa kohinatasossa ja signaalipiikkien korkeuksissa. Täten IBAD TiN onkin täysin varteenotettava materiaalivaihtoehto niille, jotka suosivat TiN elektrodeja, mutta joilla ei ole sputteriointiin sopivaa laitetta käytettävissä. ALD:n ja IrOx:n yleiset ominaisuudet sen sijaan puoltavat ALD IrOx:n sopimista erityisesti geometrialtaan haastaviin tapauksiin tai sovelluksiin, joissa elektrodeilta vaaditaan erinomaisia stimulointiominaisuuksia.

Lopuksi tässä väitöstyössä kehitettiin esimerkkinä räätälöidyn MEA-levyn vaativasta sovelluksesta yksittäisten sydänsolujen mittaamiseen soveltuva MEA-levy. Tällainen MEA-levy tarjoaa yleisesti käytetylle, mutta työläälle patch-clamp menetelmälle ainutlaatuisen soluja vahingoittamattoman vaihtoehdon yksittäisten solujen tutkimiseksi, sekä mahdollistaa yksittäisen solun ominaisuuksien havainnoinnin paremmin, kuin usein varsin heterogeenisen soluviljelmän tutkiminen vakiomallisella MEA-levyllä. Ratkaisuna tähän oli elektrodien sijoittaminen lähelle solualueen ulkokehää sekä elektrodien halkaisijan kasvattaminen 80 μm:iin tavanomaisesta 30 μm:stä, mikä helpotti solujen asettamista elektrodeille ja mahdollisti solujen sähköisen sykesignaalin mittaamisen. Indiumtinaoksidi (ITO) elektrodien läpinäkyvyys mahdollisti lisäksi mekaanisen sykinnän analysoimisen kuvaan perustuvan mittaamisen avulla.

PREFACE

I have always admired PhD graduates, whose discoveries and revolutionary ideas arouse the public interest and are discussed on morning TV shows and in the national newspapers. However, I won't be one of those graduates. Instead, I belong to the vast majority of PhD candidates, most of whose findings will be forgotten almost as soon as the exit door from the dissertation hall closes behind them. But I am not sad. As a researcher, I have learned many valuable skills and my all-too-many years as a PhD student have given birth to many other great things that will stay alive. Two great sons, state-of-the-art cleanroom facility, and plenty of research done with my support by my students and colleagues – these I have the privilege to be proud of. And in general, many of the greatest scientific discoveries and inventions in natural sciences and engineering are usually attributed to the work of one man, but nowadays there are no more Newtons and Einsteins - the modern science is based on co-operation and multidisciplinary team work. No lone researcher's contribution to a teamwork project will make the news, but the total outcome of the whole team, that might change the world. Who knows, maybe there is some tiny finding in this thesis that will one day be a facilitator for such a change.

The work for this thesis was carried out in the now defunct Tampere University of Technology and in its many historical departments and faculties - MIT, ASE, BMT as well as BioMediTech, which now continues its life in the new Tampere University. I would like to thank Professor Emeritus Jukka Lekkala for giving me the opportunity to do the PhD in his group and entrusting me with the development of the department's cleanroom activities and facilities. I would also like to show my appreciation for all the additional help and guidance I have received from so many other PIs in our from Stemfunc via Human Spare Parts to the Centre of Excellence research consortium. I would particularly like to thank my current group leader, Prof. Pasi Kallio, for arranging the China exchange periods and Adj. Prof. Susanna Narkilahti, Prof. Katriina Aalto-Setälä, and Prof. Jari Hyttinen for being the first ones to understand the need for and possibilities of custom-designed MEAs.

Among my many colleagues, I want to highlight Dr. Jarno Tanskanen as my mentor to the MEA world, Joose Kreutzer as my destiny mate of having too much other responsibilities, but also many common trips to a variety of CHEMSEM

events and throughout Europe, Markus Karjalainen and Antti Karttu for sharing office, knowledge and troubles, and Dr. Timo Salpavaara as peer support sharing the frustration during the writing phase of our theses, and for valuable comments. I am also grateful to Dr. Laura Ylä-Outinen and Dr. Mari Pekkanen-Mattila for sharing their expert knowledge of cells, Dr. Jani Hämäläinen as the ALD guru, and the list could go on. To all my many other colleagues, co-authors, administrative and technical support persons, equipment manufacturers and suppliers, thank you all!

Thinking back, I would also like to thank my former supervisors and colleagues at the University of Jyväskylä and at Modulight, Inc. for giving me such a solid foundation in microfabrication. Going back even further, I must acknowledge my elementary and high school math teachers, Juhani Vaaherkumpu and Jussi Makkonen, and also my childhood friend Tuomas Hollman. Without the early inspiration to science and engineering given by all of you, I might now be driving a bus, the dream job of mine in the 80's.

CHEMSEM, the Academy of Finland, Business Finland, the Finnish Cultural Foundation and its Pirkanmaa Regional Fund, the Ulla Tuominen Foundation, the Automation Foundation in Finland, the Council of Tampere Region, BioneXt, and the Tampere Scientific Foundation, thank you all for funding my research and providing me with the tools to do it. I also want to thank my proof-reader, Adrian Benfield, my pre-examiners, Prof. Sami Franssila and Adj. Prof. Bruce C. Wheeler, and my opponent Prof. Andreas Offenhäusser for the time and trouble they have taken to examine my thesis.

And last, but clearly not least, my childhood family, my sons Veeti and Kaapo, deputy godson Joel, and lately especially my dear Petra & Co., thanks to you there was and always will be life also outside the lab, both through good times and bad. This is one of the good times.

"You must write a thesis that you are able to write" – Umberto Eco

Hämeenlinna, August 2019

Tomi Ryynänen

TABLE OF CONTENTS

ABBREVIATIONS AND SYMBOLS

2D	Two dimensional
3D	Three dimensional
A	Area
A_{cov}	Electrode are covered by the cell
A_G	Plain geometric area
A_S	Total surface area
A_{tot}	Total electrode area
AC	Alternating current
AFM	Atomic force microscope (device) or Atomic force microscopy (method)
ALD	Atomic layer deposition
ALE	Atomic layer epitaxy
Al_2O_3	Aluminum oxide, alumina
BNCD	Boron doped nanocrystalline diamond
C_{dl}	Interface capacitance
C_{in}	Input capacitance
$C_{m,s}$	Membrane capacitance within the seal area
C_p	Parasitic capacitance
CMOS	Complementary metal oxide semiconductor
CNT	Carbon nano tube
cps	Counts per second
CV	Cyclic voltammetry
EDS	Energy-dispersive X-ray spectroscope (device) or Energy-dispersive X-ray spectroscopy (method)
EIS	Electrochemical impedance spectroscopy
ERDA	Elastic recoil detection analysis
eV	Electrode volt
FBS	Fetal bovine serum
FP	Field potential
hESC	Human embryonic stem cell

HF	Hydrofluoric acid
HfO_2	Hafnium oxide, hafnia
(h)iPSC	(Human) induced pluripotent stem cell
hPS-CM	Human stem cell-derived cardiomyocyte
HTP	High-throughput
i_{sig}	Ionic diffusion current
IBAD	Ion beam assisted (e-beam) deposition
IC	Integrated circuit
IrOx	Iridium oxide
ITO	Indium tin oxide
k_B	Boltzmann constant
l	Length
MCS	Multi Channel Systems MCS GmbH
MEA	Microelectrode array or Multielectrode array
ML	Molecular layering
MLS	Maskless lithography system
PCB	Printed circuit board
PDMS	Polydimethylsiloxane
PECVD	Plasma enhanced chemical vapor deposition
PEDOT	Poly(3,4-ethylenedioxythiophene)
PEI	Polyethyleneimine
PEN	Polyethylene napthalate
Piranha	Cleaning solution consisting of sulfuric acid and hydrogen peroxide
Pitch	Electrode-to-electrode distance (from center to center)
Poly-Si	Polycrystalline silicon
Pt black	Platinum black (electrochemically fabricated porous platinum)
PSS	Poly(styrene sulfonate)
R	Resistance
R_{ct}	Charge transfer resistance
R_m	Membrane resistance
$R_{m,s}$	Membrane resistance within the seal area
R_r	Track and conductor wire resistance
R_s	Seal resistance

R_S	Solution resistance
$Re(Z)$	Real part of the electrode impedance
RIE	Reactive ion etcher (device) or Reactive ion etching (method)
RMS	Root mean square
SAR	Surface-area-ratio
SEM	Scanning electron microscope (device) or Scanning electron microscopy (method)
SiC	Silicon carbide
SIMIT	Shanghai Institute of Microsystem and Information Technology
Si_3N_4	Silicon nitride
SiO_2	Silicon dioxide
SNR	Signal-to-noise ratio
SOG	Spin-on-glass
SU-8	Negative photoresist/epoxy
T	Absolute temperature
TiN	Titanium nitride
TiO_2	Titanium dioxide, titania
V	Voltage
V_{cov}	Voltage from the cell covered part of the electrode
V_e	Potential at the electrode
V_{in}	Input voltage signal to the recording amplifier
V_m	Intracellular potential
V_n	(Thermal) noise
Z_{CPA}	Constant phase angle impedance
Z_W	Warburg impedance
Δf	Measurement bandwidth
ϱ	Resistivity
ω	Angular frequency
Ω	Ohm

ORIGINAL PUBLICATIONS

The present thesis is based on the following publications that are referred to in the text as Publications I-IV. The publications are reproduced with the permission of the copyright holders.

Publication I **Ryynänen, T.,** Kujala, V., Ylä-Outinen, L., Korhonen, I., Tanskanen, J.M.A., Kauppinen, P., Aalto-Setälä, K., Hyttinen, J., Kerkelä, E., Narkilahti, S., Lekkala, J., 2011. All Titanium Microelectrode Array for Field Potential Measurements from Neurons and Cardiomyocytes–A Feasibility Study. Micromachines, 2(4), 394–409. doi: 10.3390/mi2040394

Publication II **Ryynänen, T.,** Ylä-Outinen, L., Narkilahti, S., Tanskanen, J.M.A., Hyttinen, J., Hämäläinen, J., Leskelä, M., Lekkala, J., 2012. Atomic layer deposited iridium oxide thin film as microelectrode coating in stem cell applications. Journal of Vacuum Science & Technology A, 30(4), 1–5. doi: 10.1116/1.4709447

Publication III **Ryynänen, T.,** Toivanen, M., Salminen, T., Ylä-Outinen, L., Narkilahti, S., Lekkala, J., 2018. Ion Beam Assisted E-Beam Deposited TiN Microelectrodes–Applied to Neuronal Cell Culture Medium Evaluation. Frontiers in Neuroscience, 12:882, 1–13. doi: 10.3389/fnins.2018.00882

Publication IV **Ryynänen, T.,** Pekkanen-Mattila, M., Shah, D., Kreutzer, J., Kallio, P., Lekkala, J., Aalto-Setälä, K., 2018. Microelectrode array for noninvasive cardiomyocyte measurements at the single-cell level. Japanese Journal of Applied Physics, 57:117001, 1–7. doi: 10.7567/JJAP.57.117001

AUTHOR'S CONTRIBUTION

Publication I This paper evaluates the suitability of titanium (Ti) metal as a microelectrode material. The author participated in designing the experiments, designed and fabricated the all-titanium microelectrode arrays (MEAs) except for the outsourced Ti and silicon nitride (Si_3N_4) deposition steps, performed the atomic force microscope (AFM) measurements, and analyzed AFM and noise data. The author also wrote the text about the above-mentioned topics and compiled it with the texts from the other authors into a complete manuscript. Jarno Tanskanen and Pasi Kauppinen performed the impedance measurements and analysis. Laura Ylä-Outinen, Ismo Korhonen, and Ville Kujala conducted the cell experiments. The rest of the authors participated in designing the experiment and contributed to writing the introduction and the conclusions.

Publication II In this paper, atomic layer deposited (ALD) iridium oxide (IrOx) is presented as a candidate low impedance electrode material. The author participated in designing the experiments, designed and fabricated the MEAs except for the outsourced Ti, ALD IrOx, and Si_3N_4 deposition steps, performed AFM and impedance measurements, participated in noise and impulse measurements headed by Jarno Tanskanen, and analyzed the AFM, impedance, impulse and noise data. Laura Ylä-Outinen performed the cell experiments and Jani Hämäläinen did the ALD IrOx depositions. The author also wrote the entire manuscript excluding some minor additions to the ALD and cell experiment sections by the rest of the authors, who also participated in designing the experiments.

Publication III This paper introduces ion beam assisted e-beam deposition (IBAD) as an alternative for sputtering in the fabrication of low impedance titanium nitride (TiN) microelectrodes. In addition, the electrodes were used in an experiment where two cell culture media were evaluated. The author was responsible for the IBAD TiN process development, IBAD TiN MEA (referred as BMT MEA in the paper) design and fabrication, the AFM, impedance, and cyclic voltammetry (CV) measurements, and all the technical data analysis excluding noise analysis, which was done together with Maria Toivanen and Laura Ylä-Outinen. Maria Toivanen was responsible for the cell

experiments and cell data analysis. Turkka Salminen operated the scanning electrode microscope (SEM) and energy-dispersive X-ray spectroscope (EDS). The author wrote the manuscript together with Maria Toivanen. Laura Ylä-Outinen, Susanna Narkilahti, and Jukka Lekkala participated in the project design along with the author and Maria Toivanen, and provided additional support for analysis and writing of the manuscript.

Publication IV In this paper a custom-designed microelecrode array was developed for noninvasive electrical and video measurements of single cardiomyocytes. The author was responsible for the MEA engineering part of the study, including MEA design, fabrication and characterization, and writing the corresponding parts of the manuscript. Mari Pekkanen-Mattila was responsible for the biological part of the study – both the cell experiments and the writing. Disheet Shah assisted in the cell experiments and Joose Kreutzer fabricated the polydimethylsiloxane (PDMS) rings. Together with the rest of the authors they provided additional support in designing the experiments and writing the manuscript.

1 INTRODUCTION

1.1 Motivation

A microelectrode array (MEA) is, in essence, that part of an electronic circuit that is used as an interface between the measurement electronics and the biological cells or tissues, whose electrical activity is measured or stimulated by the array. One common field of application for MEA experiments is studying stem cell-derived neuronal or cardiac cells, either to increase our basic understanding of biology and to develop disease models, or to harness the cells as tools in drug screening and toxicity tests. This is the application field also in the research environment in which this thesis was made.

Multi-disciplinary research is now a buzzword in most academic fields. However, the development of multi-disciplinary research teams is relatively recent. For example, in the mid 2000s, stem cell biologists from the former University of Tampere and biomedically-oriented engineers from the former Tampere University of Technology realised that together they had common goals which neither institution could achieve on their own. Therefore, in 2008 the Academy of Finland funded 'Stemfunc', a project that combined the research aims of four biologist groups and four engineering groups from the two universities. It is now 11 years on, and those groups are still working together in Centre of Excellence in Body-on-Chip Research, as well as in many other multidisciplinary projects. All this research is based on combining biological and engineering knowledge to better understand stem cell-derived cardiac, neuronal and some other cell types, and developing better technical tools to harness the biological cells for various applications and cell models. This co-operation not only lead to common projects, but also formed the core of the common BioMediTech institute between the two former universities, which in some sense was a multidisciplinary test platform for the new combined Tampere University.

Since the introduction of the first MEAs by Thomas et al. (1972), most of the *in vitro* MEA experiments have been performed with MEAs having a simple n × n electrode layout, or one of a few other commercially available standard layouts. However, owing to the recent development of microfabrication and MEA technologies, advances in our understanding of biological processes, and especially the rise of more intensive multidisciplinary co-operation between biologists and engineers, the trend is increasingly towards more advanced biological experiments, for which standard MEAs are no longer a practical choice, if they are a valid choice at all. Such studies often need customised design for the sizes, locations and/or even the shapes of the electrodes. Furthermore, the requirements for the noise level and signal-to-noise ratio (SNR) might rule out some of the common material choices, or even require the introduction of completely new materials. In addition, an increasing number of add-ons, such as chemical or physical sensors, now have to be integrated into the MEAs. Similary, there can be more imaging, perfusion, gassing tools etc. around the MEA than ever before. All of these features may also set special requirements for the layout and structure of the MEA. No matter what kind of features the custom-designed MEA has to exhibit, and no matter how carefully the prototype MEA is planned and modelled, it is probable that the first version will not be successful, meaning that more iterations will be needed. Therefore, in order to keep the cost and time involved in building a new prototype as low as possible, the materials and fabrication processes should be simple, cheap and readily available.

Already Thomas et al. introduced platinum black (Pt black), the all-time most popular MEA electrode material, or actually a coating intended to lower the impedance and the noise level of the underlying electrode. Only sputtered titanium nitride (TiN) introduced a quarter of decade later by Janders et al. (1996) has been able to compete with it in popularity in *in vitro* MEAs. Nevertheless, as the literature review in Chapter 2 reveals, a great number of other materials have also been used as electrode materials. There are at least two common reasons why a researcher may decide to use an electrode material other than Pt black or sputtered TiN. The first is practical, the selected material must conform to the limitations of the budget, equipment, processes or expertise available. The other reason some other electrode material may be selected, (despite its poorer performance), would be in an attempt to develop an electrode material which has some particular feature or performance characteristic. Such materials may well be better than Pt black and sputtered TiN in some respects, although so far none of them can match Pt black and sputtered TiN

overall in terms of electrical performance, mechanical and long term stability, ease of fabrication, and cost. Usually, new candidate materials for electrodes try to outperform the other materials in electrical performance, but they all fail in one way or another, especially in the ease of fabrication. However, the electrical performance of Pt black or sputtered TiN is rarely a bottleneck in biological experiments and, in addition, they are both relatively easy to fabricate, assuming the required technical expertise and equipment are available. TiN does not have any known mechanical stability issues either, and the cost issues are mainly related to equipment costs. This begs the question, why bother to study new materials? Even though they don't require very specialized tools or niche expertise, Pt black and sputtered TiN are not readily available everywhere. Thus, the answer to the above question is that with so many new biomedical research applications being opened up with the use of MEAs, more choices for the electrode material and/or its deposition method will always be of value. Biological cell experiments encompass a great number of different factors, all of which have to be blended together to produce the right MEA for the job. All the MEA materials, the different molecular coatings to promote cell adhesion or guiding, the polydimethylsiloxane (PDMS) structures, the cell-culturing media, integrated sensors and, of course, the cells themselves must all be fully compatible with each other. It is only a matter of time before some researcher needs a particular MEA structure or experimental combination for which sputtered TiN or Pt black or their fabrication processes are simply incompatible with one or other of the factors listed above.

All too often, the chosen solution in studying advanced biological research questions is either to use non-optimal materials and/or to tweak the research question to suit the capabilities of standard MEAs. This usually means that the results are less valid than they would have been if the research had been carried out with custom-designed MEAs using high performance materials. This thesis aims to facilitate custom-designed MEA prototyping and fabrication by presenting three more potential electrode materials: titanium (Ti), atomic layer deposited (ALD) iridium oxide (IrOx) and ion beam assisted e-beam deposited (IBAD) TiN. Although the materials themselves are not new, their use in the fabrication of custom-designed MEAs is. With the first one, titanium (Publication I), the motivation was to find an electrode material which would enable custom-designed MEA prototyping with the very limited microfabrication resources and budget our research team had available some 11 years ago when we started our MEA project here in Tampere. In contrast,

the author studied ALD IrOx at first as pH sensing material (Ryynänen et al. 2010b) and only later applied it also to MEAs (Publication II). In both applications IrOx was already a well known material, but had not been deposited by ALD before. The original aim was to be able to use the same electrodes both as pH sensors and for field potential (FP) recordings, but it soon became clear that this aim was impractical because of the insurmountable problems associated with calibration and drift. Thus, in this thesis ALD IrOx is only utilized as an electrode coating aimed at decreasing the impedance and noise level of titanium electrodes for in-house MEAs, i.e. as an alternative to Pt black and sputtered TiN. As for IBAD TiN (Publication III), the motivation was to find an in-house deposition process for fabricating gold-standard TiN electrodes when there was no sputter coater available. Clearly, the study of these materials was initially driven more by the local resource situation than by some universally acknowledged scientific need. Nevertheless, there are many other low-resourced researchers, and even top-level well-resourced professionals who may well find the results of this research, summarized in Chapter 3, useful.

The final part of this thesis, an MEA capable of making cardiomyocyte measurements at the single-cell level (Publication IV) is presented in Chapter 4. From a broader scientific perspective, such a single-cell MEA is the answer to many biologists' quest to find an easy-to-use and noninvasive alternative to the patch clamp in single-cell studies of cardiomyocytes. From the perspective of this thesis, the single-cell MEA presented here is an example application of the fruit of years of research spent in identifying and developing alternative materials and fabrication methods for the cost-effective prototyping and fabrication of custom-designed MEAs.all headings, quotes, tables and figures the style of first paragraph is TUD Body Text 1.

1.2 Included MEA types

The MEA research field is broad as there are so many applications for different types of MEAs. Many readers will have their own ideas and experience of what an MEA is, and what kind of applications they should be used in. Covering all those applications and ideas in one thesis would be impossible, so what follows here is brief a description of what is meant by an MEA in this thesis, and what common types of MEA have been excluded.

In this thesis, an MEA is mainly understood to be a substrate-integrated two dimensional (2D) device intended to electrically measure cells and tissues in a dish, i.e. *in vitro*. The discussion is mainly focused on, but not limited to, MEAs compatible with the Multi Channel Systems' (MCS; Reutlingen, Germany) or Alpha MED Scientific's (former Panasonic; Osaka, Japan) MEA formats. These MEAs typically have about 60 passive electrodes that are usually divided between one to six wells. Alternatively, there may be some more sophisticated cell guiding arrangement created on or around the electrode area by a PDMS, plastic, or glass structure. In some cases, however, high throughput (HTP) MEAs built in well-plates, and active or *in vivo* electrodes are referred to or discussed because of their similarities, especially in terms of materials. The same applies to the so-called (quasi) three dimensional (3D) MEAs, where the electrode has some 3D shape out of the plane, but the structure is otherwise planar and thus similar to pure 2D MEAs. Similarly the focus of this thesis is on the MEAs intended for FP measurements, but because of their similarity in many structural aspects, MEAs measuring impedimetric parameters are occasionally referred to as well. Even if the same MEAs are often used for both measurement and stimulation purposes, the stimulation part is largely excluded from this thesis as the main focus in the included publications and related research by the author has been on developing MEAs for measuring the spontaneous activity of cells without the need for stimulation.

1.3 Aims of the study

The overall aim of this thesis was to find alternative electrode materials and fabrication methods to facilitate and support time- and cost-effective prototyping and the small-scale in-house fabrication of custom-designed MEAs needed for advanced stem cell studies.

The specific aims were:

- To identify and validate a simple and low cost MEA prototyping process
- To evaluate low-impedance and low-noise microelectrode materials as alternatives to the industry-standard Pt black and sputtered TiN

- To utilize the results from the above studies in order to develop an MEA which enables noninvasive cardiomyocyte measurements at the single-cell level

In order to achieve these aims, at least the following research questions had to be answered:

- Can titanium be used as the sole conducting material in MEA prototypes?
- Is ALD IrOx suitable as an MEA electrode material and what is the performance of such electrodes?
- Can low impedance TiN coating be deposited on MEA electrodes by any method other than sputtering?
- What kind of MEA electrode layout, if any, could enable the recording of the field potentials of cardiomyocytes at the single-cell level?

2 BACKGROUND AND LITERATURE REVIEW

2.1 Theory of microelectrode cell measurements

The function of the microelectrodes in an MEA is to detect the electrical activity of a cell located on top of the electrode, or at least near it. As the cell measurements are done in a dish filled with an electrolyte, typically a cell culturing medium, there is a so called double-layer interface on the electrode surface; the metal interface of the electrode against either the liquid interface of the medium or the biological interface of the cell. The double-layer interface transforms the electric charge carried by the ions in the medium or in the cell into the electric current carried by electrons or holes in the metallic electrodes and tracks. In its simplest form, the electrode-electrolyte double layer can be presented as an equivalent circuit, as shown in Figure 1, where Z_{CPA} is the constant phase angle impedance that represents the interface capacitance impedance, R_{ct} is the charge transfer resistance and R_S is the solution resistance (Franks et al. 2005).

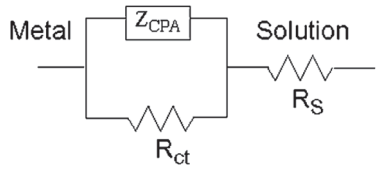

Figure 1. Simplified equivalent circuit model for the double layer interface between the microelectrode and the cell culturing medium. ZCPA is the constant phase angle impedance, Rct is the charge transfer resistance and RS is the solution resistance. (Franks et al. 2005)

An analytical form of the impedance of such a circuit can be calculated from the formula

$$Z = Re(Z) + Im(Z) = R_S + \frac{R_{ct}}{1+R_{ct}^2 \cdot \omega^2 \cdot Z_{CPA}^2} - j\frac{R_{ct}^2 \cdot \omega \cdot Z_{CPA}}{1+R_{ct}^2 \cdot \omega^2 \cdot Z_{CPA}^2} \quad (1)$$

where ω is the angular frequency of the alternating current (AC) voltage applied to the double layer interface (Trantidou 2014).

A more detailed representation has been suggested by Guo et al. (2012) and is presented in Figure 2a. There, C_{dl} corresponds to Z_{CPA} in the simplified model and Z_W is the Warburg impedance, which is basically the diffusion of chemical reactants in the solution. This value can be considered negligible with typical materials and frequencies used to sense field potentials, and has thus been excluded from the simplified model. Similarly, R_r representing the track and conductor wire resistances from the electrode to the amplifier input is typically negligible in comparison with the total resistance.

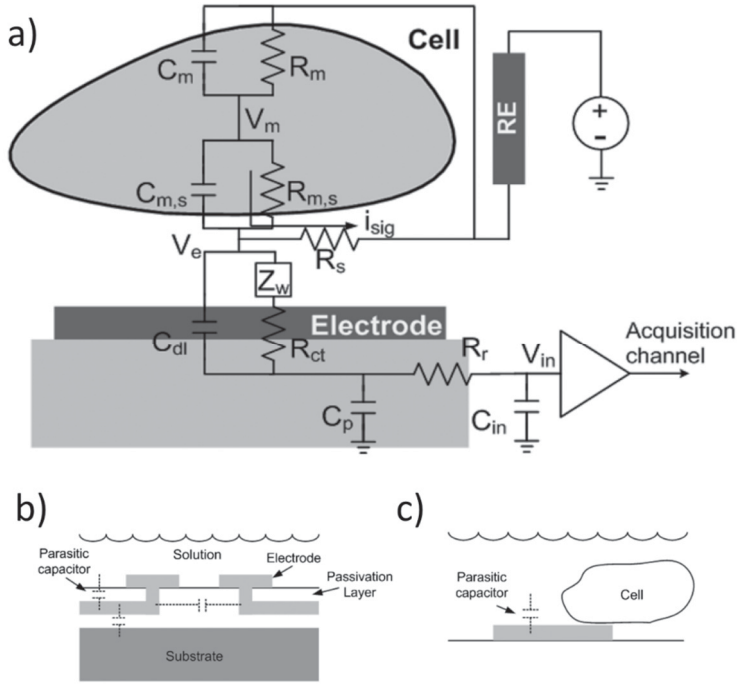

Figure 2. **a)** Detailed microelectrode-cell interface model. Parasitic capacitance **b)** from the track metal, and **c)** from the uncovered electrode. V_m is the intracellular potential, C_m is the membrane capacitance, R_m is the membrane resistance and $C_{m,s}$ and $R_{m,s}$ are the same components within the seal area. Z_W is Warburg impedance, R_s is seal resistance, i_{sig} is the ionic diffusion current, V_e is the potential at the electrode, C_{dl} is the double layer capacitance, R_{ct} is the charge transfer resistance, R_r is the wire resistance, C_p is the parasitic capacitance, C_{in} is the input capacitance, and V_{in} is the input voltage signal to the recording amplifier. (Guo et al. 2012)

Parasitic capacitance, C_p, can be divided into two components, as illustrated in Figures 2b and 2c. The first component is the coupling capacitance to the solution, the tracks, or to the conductive substrate, if there is one. If the electrode is not fully covered by the cell, then there is another component because of the double-layer capacitance of the uncovered part of the electrode to the liquid. (Guo et al. 2012)

The noise of a microelectrode is mainly regarded as thermal noise, which can be calculated from the standard Johnson noise equation

$$V_n = \sqrt{4 \cdot k \cdot T \cdot Re(Z) \cdot \Delta f} \qquad (2)$$

where k is the Boltzmann constant, T is the absolute temperature, $Re(Z)$ is the real part of the electrode impedance, and Δf is the measurement bandwidth. Huigen et al. (2002) have shown that the noise of an electrode is inversely proportional to the electrode area,

$$V_n \propto \frac{1}{\sqrt{A}} \qquad (3)$$

The explanation for this is rather obvious; ideally, if the temperature and measurement bandwidth are kept constant, then it is only the real part of the impedance (resistance) of the electrode that can change the thermal noise in Formula 2. At high frequencies, the capacitive component starts to dominate the impedance, but otherwise the resistance is the major factor in the impedance. By its fundamental definition, $R = \varrho l/A$, the resistance is inversely proportional to the area. Thus, lower noise and impedance of an electrode can be achieved by increasing the electrode area. One way is to increase the diameter of the electrode. However, this may: 1) limit the resolution of the microelectrode array as there must be enough space between the electrodes to avoid interfering effects from the neighboring electrodes; and 2) decrease the SNR as the contribution from the cell on which the electrode averages its signals from the environment gets smaller. If V_{cov} is the voltage from the cell-covered part of the electrode, then according to Xiao et al. (2010), the measured voltage V depends on both the total electrode area, A_{tot}, and the area of the electrode covered by the cell, A_{cov}, as follows:

$$V = V_{cov} \cdot \frac{A_{cov}}{A_{tot}} \quad (4)$$

A more efficient way to increase the electrode area is to increase its roughness or porosity (Heim et al. 2012). This increases the active surface area against the cell or medium without affecting the planar size of the electrode compared with the cell size. It should be remembered that even though the impedance of the electrode and the cell-electrode coupling contribute most to the noise in MEA recordings (Urbanová et al. 2011), one should also pay attention to the proper use of the amplifier electronics, as they may be highly sensitive to temperature changes (Ryynänen and Lekkala 2018). In stimulation electrodes, the electrode area is also a critical factor because a larger area increases the charge transfer capacity to the cells or tissues under stimulation. Therefore, porous electrodes that are capable of supplying high-density electrical charge are favored in stimulation use (Weiland et al. 2002).

2.2 MEA types

2.2.1 Normal MEAs

In its simplest and most typical form, an MEA consists of three layers: 1) a planar substrate; 2) a conductive layer, which contains the microelectrodes, grounding or reference electrodes, tracks, and contact pads; and 3) an insulator layer, which has openings above the electrodes and the contact pads. Often, there is also a fourth layer as the electrodes (and contact pads) are typically coated with an additional porous conductive layer in order to decrease the impedance and noise levels of the electrodes or to improve their mechanical durability. In addition, a well or wells for the cells and the cell culture medium is attached on top of the MEA. This kind of MEA is referred to as a "normal MEA" or even just an MEA in this thesis (Fig. 3a). This kind of structure can be used to take two types of measurements, field potential measurements and impedimetric measurements, in addition to which they can also be used for cell stimulation. In the first type of measurement, the electrodes are typically round or square in shape, whereas the impedimetric measurements need interdigitated finger electrodes. This thesis focuses on MEAs for FP measurements.

Figures 3b and 3c illustrate two common normal MEA versions, a single well MEA with an 8 × 8 electrode layout, which is often called a "standard MEA", and a so-called "6-well MEA", which has six wells with 9 electrodes in each.

Normal MEAs are currently commercially available only from two manufacturers, MCS and Alpha MED. One of the former manufacturers of normal MEAs, Axion Biosystems (Atlanta, USA), has recently abandoned their production of normal MEAs and now focuses on high-throughput (HTP) MEAs only. Another former MEA manufacturer, Qwane Biosciences (formerly Ayanda Biosystems, Lausanne, Switzerland) has been out of business since 2016. A recent newcomer to the field is BMSeed LLC (Phoenix, USA), but so far this company has only focused on their own stretchable MEA concept. MCS's MEAs are actually manufactured by NMI, a research institute of the University of Tübingen, and in this thesis MCS and NMI are used interchangeably. In the past, the MEA pioneer Guenter Gross's research group at the University of North Texas and Plexon, Inc. (Dallas, Texas) were involved in the commercial production of some MEAs.

In addition, there are a couple of companies offering well-plate MEAs, which primarily contain impedimetric electrodes, but may also have a couple of FP electrodes. These, however, are excluded from this thesis. Even though this thesis focuses on normal MEAs, the next five sections give a brief introduction to some other common MEA types or other closely related arrangements used in electrophysiological *in vitro* studies of cells.

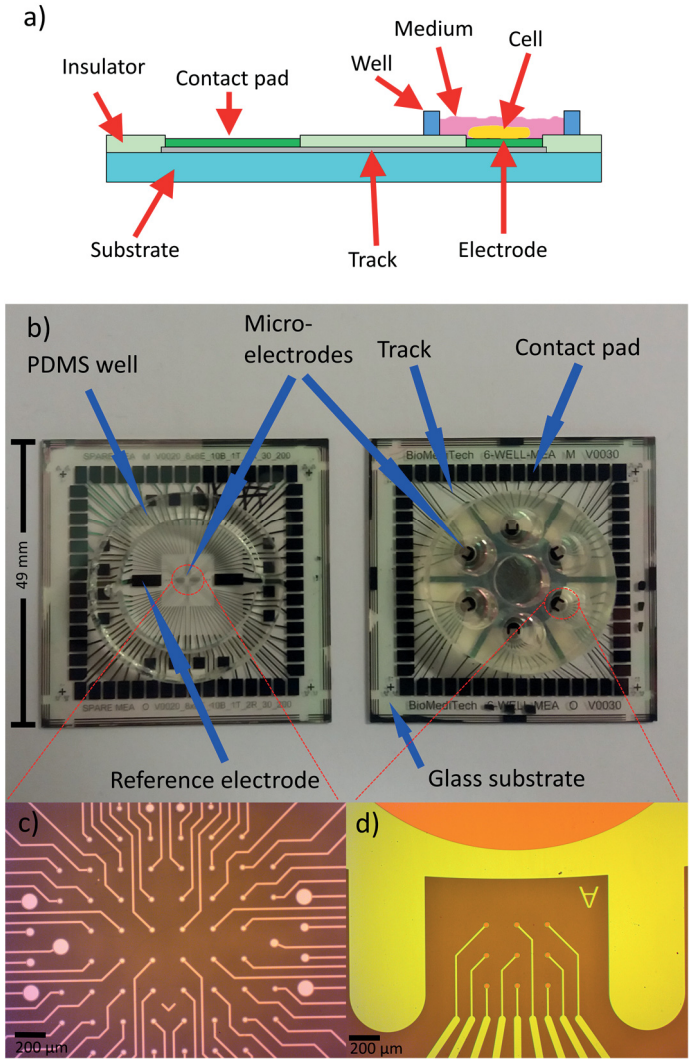

Figure 3. Design of the normal MEA. **a)** Cross-sectional structure of the normal MEA. The green layer in the contact pad and the electrode is an optional, often porous, coating that is used for decreasing the impedance of the electrode and/or improving the mechanical durability of the contact pad. The image is not to scale. **b)** Examples of common MEA layouts; a single well MEA on the left and a 6-well MEA on the right. The magnified representations of the electrode areas of **c)** a single well MEA with the author's version of a standard 8 x 8 electrode layout (including some additional bigger electrodes for process characterization) and **d)** one well of the 6-well MEA. The electrode diameter is 30 µm and the electrode to electrode distance is 200 µm in both MEA designs.

2.2.2 High throughput MEAs

In drug screening and toxicity testing in particular, the fact that a normal MEA has only one, or at best only a few wells, is a very limiting factor. For these reasons, and also to increase the sample number in other studies, an HTP MEA is a far better choice. Basically, this is an MEA that is integrated into the wells of the well-plate instead of being built on a planar substrate. Commercially-produced HTP MEAs are available from both Alpha MED, Axion (McConnell et al. 2012), and MCS (Fig. 4). However, purely academic versions (Eggermann et al. 2016; Eichler et al. 2015) are rare. Commercial versions are currently available in 12, 24, 48, 72 and 96 well formats and include a total of 384 (Alpha MED), 384 or 768 (Axion), or 288 or 1152 (MCS) electrodes divided equally between each well.

Figure 4. One 96-well (back) and two 24-well (front) and HTP MEAs by Multi Channel Systems. [Picture from www.multichannelsystems.com.]

The outer dimensions and well locations of HTP MEAs are the same as those of standard well-plates, which enable the HTP MEAs to be used with the automated pipetting and imaging tools developed for standard well-plates. However, in other ways the structure is more complex. Traditionally, HTP MEAs have been composed of a printed circuit board (PCB) containing the actual MEA design and a plastic well-plate part glued on top. Such an arrangement can be quite cost effective to manufacture, especially if it does not need to be transparent. However, if the electrode area must be made transparent to enable microscopic inspection by an inverted microscope, then part of the PCB has to be replaced by glass chips, and

bonding or gluing those onto a PCB makes the process more complicated. Gluing the well-plate walls onto a PCB while simultaneously insulating the MEA tracks and making the whole structure leak-proof seems to be rather challenging for the manufacturers, at least from what the author has seen of HTP MEAs and from discussions with the users. Despite the challenges, the reason for using a PCB is quite clear. Unlike in normal MEAs in which the contact pads are placed on top, the contact pads in an HTP MEA have to be placed at the bottom in order to maintain the standard well-plate compatibility. Although PCB technology provides standard solutions for this, making vias through transparent glass or plastic substrates is a very expensive, specialised process. Even though Axion has suggested flexible "wrap-around" technology (Tyler and Rajaraman 2016) as an alternative to through-substrate vias, they still rely on vias through the plastic or PCB substrate in their commercial products. Unlike the other manufacturers, Alpha MED has built its HTP MEA on a glass substrate with contact pads on top, as in normal MEAs. This approach, however, has compelled them to choose non-standard base dimensions for their plates.

The medium throughput alternative is to use normal MEAs that are divided into several compartments, wells, by specially designed PDMS (Kreutzer et al. 2012) or plastic ring(s). However, the space available on a normal MEA chip and the inclusion of about 60 electrodes seriously limits the number of wells that can be included. Although Kang et al. (2009) managed to construct a separate well for each electrode of a standard 8 × 8 MEA layout, 6 wells and thus 9 electrodes per MEA is still the more common choice, and this was the layout used in Publication III of this thesis. MEA amplifier manufacturers also offer the possibility to connect 2-8 MEAs to the same amplifier system. Although this approach allows the total well count, together with multi-well rings, to be comparable to that of real HTP MEAs, the method is not compatible with standard well-plate tools.

2.2.3 CMOS MEAs

According to Heer et al. (2004), the two main limitations of normal MEAs are signal degradation and array size (i.e. the number of electrodes). The first of these limitations, basically, means the increased noise and other artifacts that the signals may pick up on their way from the electrode to the amplifier electronics via the long tracks and connecting wires. The other limitation comes from the fact that it is rather

challenging to place a large number of contact pads on one MEA substrate of only moderate size.

The obvious solution to the signal degradation issue is to place the amplifiers and AD-converters, in/on the MEA substrate. Even if there is no room for all of them, then at least the pre-amplifiers can be placed there. An approach taken by Blum et al. (2003) was to bond the amplifier chips onto an otherwise normal MEA. Pancrazio et al. (1998), on the other hand, introduced the concept of a field-portable MEA system consisting of a silicon-based MEA chip bonded onto the same circuit board as a CMOS (complementary semiconductor-metal-oxide) chip containing the electronics. These approaches, however, only solved the first issue, and at the same time the additional electronics made it difficult to reuse such MEAs because of the obvious challenges with the cleaning and sterilization protocols applicable for such systems.

The current trend is to build both the electronics and the electrodes on the same CMOS chip as a so-called CMOS MEA, also referred to as a "high-resolution MEA". Basically, this device is like a digital camera, where light sensitive elements are replaced by the microelectrodes. CMOS MEAs are commercially available from 3Brain (Wädenswil, Switzerland), MaxWell BioSystems (Basel, Switzerland), and MCS (Bertotti et al. 2014). 3Brain and MCS both have over 4000 electrodes placed very close to each other on the same chip, whereas MaxWell has 26400 electrodes either in one well (Fig 5.) or divided into 6 or 24 wells as in an HTP system. In academic CMOS MEAs, the number of electrodes has been even higher; at the moment the current record is 59760 electrodes achieved by Dragas et al. (2017). However, usually only one subset of the electrodes can be recorded simultaneously, e.g. 2048 in the case of that record-holding version. Lei et al. (2011) have reported a CMOS MEA with even more electrodes, 65000, but these only have a stimulation capability.

An array of thousands of electrodes clearly answers the array size issue, and in addition, provides sub-cellular resolution, if the electrode size and the pitch (electrode-to-electrode distance) are small enough compared with the size of the cell in question. Along with that, the greatest benefit of such high-resolution MEAs is that there is nearly always an electrode directly under the cell. Thanks to the high number of electrodes, the total sensing area is, despite the small pitch, large enough to enable the study of cell networks growing on an MEA. However, such a high number of electrodes creates its own problems for high-resolution CMOS MEAs;

they generate such a huge amount of data that it is a serious problem to handle and store it all. One partial solution is to only select the electrodes located under the interesting cell(s) for recording, and thus to customize the CMOS MEA for every measurement. However, the interpretation of the data is also challenging as, owing to the small pitch, spikes from the same cell might be registered by several nearby electrodes (Müller et al. 2015).

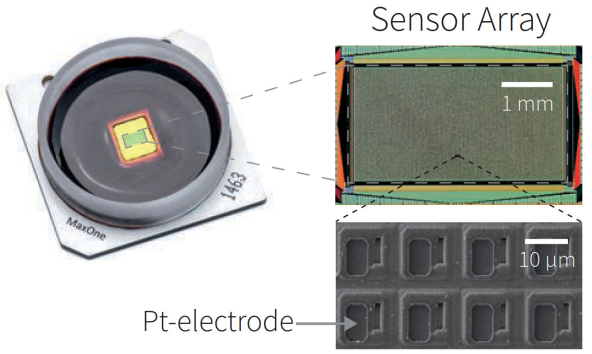

Figure 5. The CMOS MEA by MaxWell Biosystems consists of 26400 Pt electrodes (9.3×5.45 µm², 17.5 µm pitch). [Picture from MaxWell Biosystems.]

Being built on silicon, the CMOS MEAs are opaque, which rules out inverted microscopic inspection, and thus only imaging through the cell culture medium with an up-right microscope is possible, and that is a challenge. However, the software can compile some sort of image from the data recorded by the CMOS electrodes. Even if CMOS manufacturers can produce advanced circuits at low cost in large series, in the case of CMOS MEAs, the benefit is partly dissipated by the fact that the standard process leaves aluminum as the top electrode surface, so post-processing is needed to modify the CMOS MEAs to make them more biocompatible (Graham et al. 2011).

Despite all the challenges, CMOS MEAs will undoubtedly be used more and more in the future, but there will always be room for normal MEAs. From the perspective of this thesis, one fact that keeps normal MEAs viable is that in practice they can be made and customised in any microfabrication-oriented laboratory, whereas CMOS MEAs require more specialised expertise both in CMOS technology and electronics in general.

2.2.4 FET MEAs

In a field-effect transistor (FET) MEA, the non-metallized gate of the transistor acts as a substitute for the measurement electrode. The action potential generated by the cell above the gate modulates the source-drain current, and the shape of the measured signal matches with the shape of the action potential (Fromherz et al. 1991). A variant of the FET MEA is the extended gate MEA, where the metal electrode is connected via tracks to the gate of a FET located outside the cell culturing area (Krause 2000). There has been much recent research into evaluating the suitability of silicon nanowire (SiNW) FETs for MEA recordings. However, so far at least, the traditional passive Pt black electrodes have had lower noise levels than the SiNW FETs (Kang et al. 2017).

2.2.5 Light addressable MEA alternatives

CMOS MEAs can overcome the array size and resolution issues, but there is also an alternative approach, a light addressable electrode array. Instead of fabricating separate tracks for each of the huge number of electrodes, the same indium tin oxide (ITO) track is shared between all the electrodes in each row of electrodes in the array. In the normal state, the photo-conducting layer separating the electrodes from the track layer does not conduct electricity. To measure the signal from a certain electrode, one must activate the photo-conducting layer by pointing a laser beam at it beneath the desired electrode. (Bucher et al. 2001)

A closely related method is the light-addressable potentiometric sensor (LAPS), where illuminating the desired spot on the sensor surface with a focused and pulsed light generates a photocurrent in the underlying n-type Si layer. The local surface potential of the cell under study is related to the amplitude of the photocurrent. (Stein et al. 2004)

In both of these methods, the benefit is that one does not have to make any special arrangements to get the cell(s) over the electrode as one can freely choose the measurement spot, i.e. the electrode location, based on the location of the cell. The drawbacks of these methods are the requirement for rather complex measurement systems, including the laser pointer etc. as well as the fact that they are less sensitive than traditional MEAs. Furthermore, studying a network of several cells simultaneously would require having several laser spots, and the light sensitive layer

would have to be divided into smaller segments, which would ruin the idea of getting rid of the pre-determined "tracks". Yet one other concern is the effect of the laser light on the cells.

2.2.6 Patch clamp

In studying the electrophysiology of single cells, the patch clamp (Hamill et al. 1981) has long been the gold standard method. Many different patch clamp configurations exist, but put briefly, the operation principle is that a very thin glass capillary, a patch pipette, is pressed against the cell and the cell is partially sucked inside the capillary. This forms a high-resistance seal, a so-called giga(Ohm) seal, which isolates the cell membrane patch electrically. Ions fluxing through the membrane end up on the electrode inside the capillary. Either the voltage or the current is kept constant, depending on the configuration, and the uncontrolled value is measured with the help of very sensitive amplifier and an external grounding electrode (Fig. 6). The patch clamp method enables highly sensitive measurements of cell membrane conductance and action potentials. Despite this obvious benefit, however, the method is very laborious as one must catch the cells one by one with micromanipulators. And considering long term studies, even more severe drawback is that the process usually damages or finally even kills the cell.

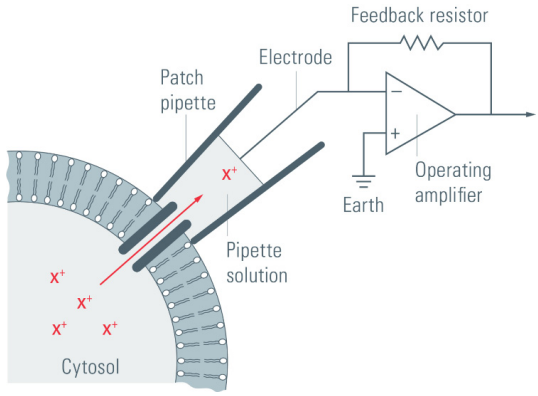

Figure 6. The patch clamp technique. A patch pipette is pressed against the cell membrane and the ion flux through the cell membrane is measured by the electrode inside the pipette. [Picture from Leica Microsystems.]

2.3 MEA measurement setup

The measurement setup used in typical cell measurements with an MEA only consists of a couple of components. The MEA (sometimes called the MEA plate, for clarity) acts as the interface between the cells and the measurement electronics. In the case of normal MEAs, it does not include any electronic components apart from the electrodes, tracks and contact pads. In the setup, the MEA plate is placed in a connector, which typically includes a heater plate under the MEA and contact pins on top to make a contact with the contact pads. The connector by MCS also includes the amplifier electronics, analog-to-digital converters, and stimulus generators in what is called a head-stage. The head-stage is connected to a separate interface board, which includes a signal processor and connects the system to the computer. Alpha MED, on the other hand, relies on an external amplifier unit between the connector and the computer (Fig. 7). The connector itself has no amplifier electronics.

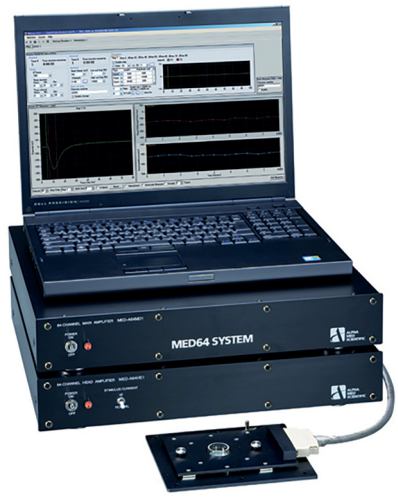

Figure 7. MED64-Basic MEA measurement setup by Alpha MED Scientific. The MEA is in the connector unit in front of the amplifier units. [Picture from www.med64.com/]

The benefit of MCS's approach is that no additional wires are needed between the connector and the amplifier, which reduces the risk of picking up noise from the environment. In contrast, Alpha MED's electronics-free connector can be placed

more freely inside the humid environment of an incubator. Temperature controllers are separate units in both cases. Axion has taken the productisation some steps further and offers all-in-one systems which only need to be connected to a computer. In all cases, the computer is equipped with dedicated software that records and displays the signal, and typically also includes tools for signal analysis and temperature control, as well as stimulation features. Depending on the system, the sampling rate is typically 10-50 kHz, digitizer resolution 16 or 24 bits, and bandwidth 0.1-10 kHz or some smaller range. Some research groups do not use commercial systems, but have built their own amplifiers and/or connectors (Bachmann et al. 2017; Buehler et al. 2016; Eichler et al. 2015).

2.4 MEA fabrication

2.4.1 Typical MEA fabrication process

The fabrication of a normal MEA with no special features is a relatively simple process, as a normal MEA basically consists of only three layers: the substrate, the conductor layer and the insulator layer. The conductor layer includes the electrodes, the contact pads, and the tracks connecting them. Frequently there is what can be regarded as a fourth layer, as the electrodes (and sometimes also the contact pads) are often coated with an additional material, whose purpose is to lower the noise and impedance of the electrode. Pt black and sputtered TiN are the best examples of such coatings. However, in the literature, and even in this thesis, the terminology can be rather problematic. That is because usually the topmost material of an electrode is considered as the material of the electrode and not necessarily referred to as a separate, low-impedance electrode coating. On the other hand, biologists tend to add their own coatings onto an MEA (e.g. to promote or inhibit cell adhesion) and those coatings have nothing to do with the electrode coatings mentioned above, although they do usually also cover the electrode. To make the terminology even more confusing, the low impedance electrode coatings made of IrOx are usually electrochemically activated after the deposition process to get the best performance, but can be used also without this activation (e.g. in Publication II). Occasionally, researchers have presented alternative fabrication processes for MEAs, but these are

usually more complex, and it seems that it is not really possible to simplify the basic structure further. Nevertheless, researchers have tried out some interesting approaches, such as replacing the built-in insulator layer by a separate replaceable insulator sheet as suggested by Nam et al. (2006). However, this thesis won't present any completely new MEA structures, but will focus on the basic fabrication process of a normal MEA as presented below, in Figure 8, and in the subsequent description of the process.

The MEA fabrication process starts with the cleaning of the substrate (Fig. 8a). Typically, this is done by the ultrasonication of the substrate in one or more solvents (acetone, isopropanol, methanol, ethanol) followed by a rinse with de-ionized water. More rigorous cleaning protocols including, for example, piranha treatment can also be used. Assuming that the conductor layer patterning is done by etching and not lift-off, the next step is to deposit the conducting layer, usually either by sputtering or e-beam evaporation (Fig. 8b). Typically, the layer is only a few hundreds of nanometers thick. After that, the photoresist is spin-coated and baked on the substrate (Fig. 8c). The desired electrode, track and contact pad pattern is exposed to the photoresist in a mask aligner through a chrome or film mask (Fig. 8d), or by using a maskless lithography system (MLS), and the photoresist is then developed (Fig. 8e). Next, the pattern is transferred to the conductor layer either by wet or dry etching (Fig. 8f) and the remaining photoresist is removed by acetone or a dedicated resist remover.

The insulator layer is either deposited by plasma-enhanced chemical vapor deposition (PECVD) (silicon nitride [Si_3N_4], silicon dioxide [SiO_2]) or spincoated (SU-8, polyimide, polystyrene etc.) (Fig. 8g). If the insulator is not photo-patternable, the photoresist layer has to be applied again (Fig. 8h). The photoresist or the directly photo-patternable insulator (SU-8) is again exposed to UV-light and the pattern containing openings for the electrodes and contact pads is transferred from the mask to the resists (Fig. 8i) and developed (Fig. 8j). In the case of a photo-patternable insulator, the development already creates the openings through the insulator, but otherwise the photoresist is used as the etching mask to etch the openings to the insulator layer (Fig. 8k). Typically, reactive ion etching (RIE) is used.

If no additional low-impedance electrode coating (e.g. Pt black or TiN) is needed, the MEA is ready to be used after the remaining photoresist has been removed. If an additional coating is applied, the resist should not be removed and the process would be continued by depositing the additional coating either by sputtering, IBAD,

ALD or electrochemical methods (Fig. 8m). Prior to that however, it is good practice to clean the electrode surface by sputter-etching, or some other means, in order to remove possible native oxides and other residuals adsorbed on the electrode surface (Fig. 8l). Finally the MEA fabrication process concludes with a lift-off process, either in acetone or with a resist remover (Fig. 8n). If the process is done on wafer that is larger than the MEA, one more step would be to cut the substrate down to the MEA size. If the conductor layer patterning is done with the lift-off process, the process is the same but the first photoresist layer is applied and patterned before the conductor deposition, and instead of etching, the pattern is transferred to the conductor layer by lift-off after the deposition.

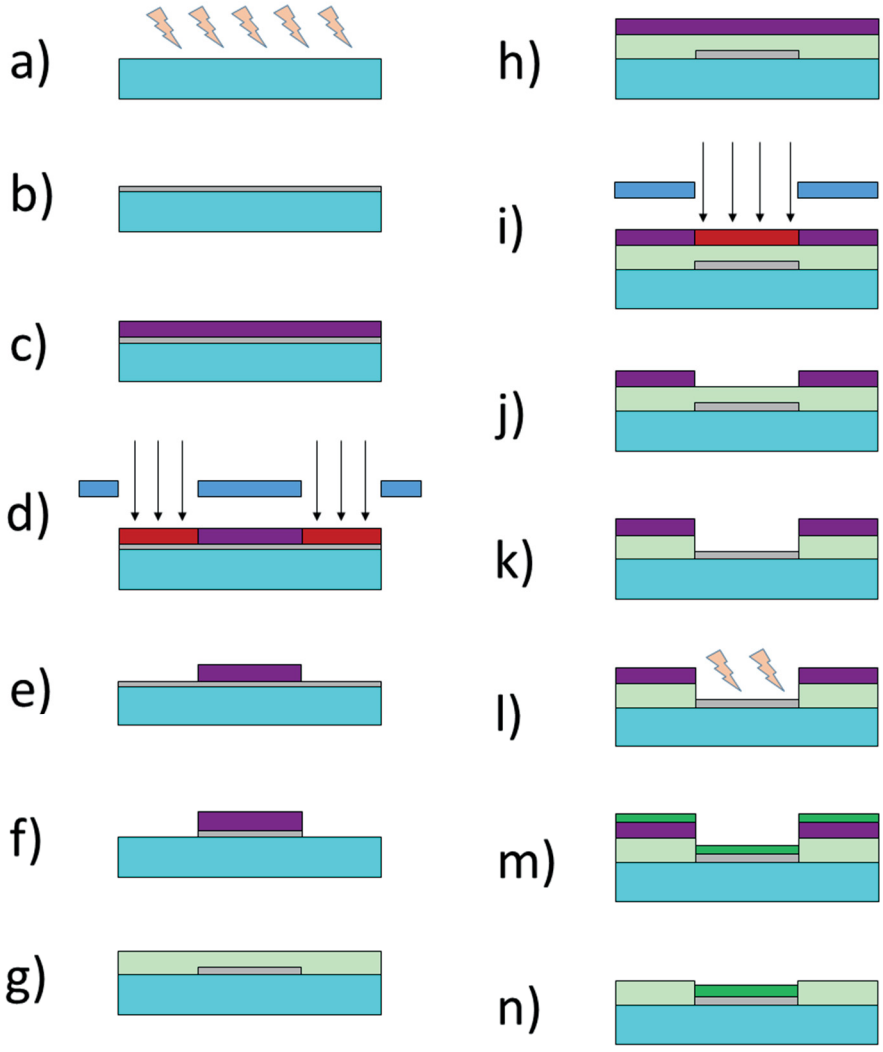

Figure 8. MEA fabrication process. **a)** Clean the substrate, **b)** Deposit conducting layer for the electrodes, tracks and contact pads, **c)** Spin-coat photoresist, **d)** Expose electrodes, tracks and contact pads pattern to the photoresist, **e)** Develop the photoresist, **f)** Etch the pattern from the photoresist to the conducting layer, **g)** Deposit insulator layer, **h)** Spin-coat photoresist, **i)** Expose openings for the electrodes and contact pads**, j)** Develop the photoresist, **k)** Etch the openings to the insulator layer, **l)** Clean the conductor surface, **m)** Deposit low impedance coating, **n)** Lift-off. The images are not to scale and follow the established practice where e.g. resist and etching profiles are idealized and misalignments do not exist.

2.4.2 Atomic layer deposition - ALD

Atomic layer deposition, ALD, is a thin film deposition method developed independently in the Soviet Union in the 60's as molecular layering, ML, and in Finland in the 70's as atomic layer epitaxy, ALE, (Puurunen 2014). The operation principle of ALD relies on alternating saturating surface reactions, which result in the formation of a thin film of material one atomic layer at a time. In fact, the term 'molecular layer' originally used in the former Soviet Union may be a more accurate description.

In brief, the process flow (Fig. 9) is that, firstly, the precursor material A is fed into the reaction chamber as a gas phase and the precursor molecules react with the surface under deposition by forming a single molecular layer on it. Once that is done, the film stops growing as there are no more free bonding locations available, even if there were some free precursor molecules left. The remaining free precursor molecules are then removed from the chamber with an inert flushing gas or by vacuum. Next, precursor B molecules are fed into the chamber and they react with the molecular layer formed in the first step and form another single molecule layer on top of the first layer. After flushing, the process can be continued with precursor A or with other precursors, depending on how complex the ALD material is. The more times the process is repeated the thicker the film layer gets.

In addition to selecting the correct precursor material, the most important parameter in the ALD process is the temperature. Too low a temperature does not initiate the chemical reactions and too high a temperature might promote unwanted reactions. The main benefits of ALD are the precise control of thickness owing to the layer by layer addition of the atoms, and its excellent step coverage. As the precursor is in its gas phase, the molecules can go everywhere on the substrate surface, even inside cavities and deep holes, which are not reachable by line-of-sight processes like e-beam deposition. The major drawback, however, is the low deposition rate, while finding suitable precursors for new materials may also be challenging. Even though ALD is generally considered to be incompatible with lift-off, because of it has such excellent step coverage, Publication II, for example, shows that at least in some cases, lift-off with ALD is achievable. However, such a process requires careful attention to the ALD process temperature in order to avoid burning the photoresist.

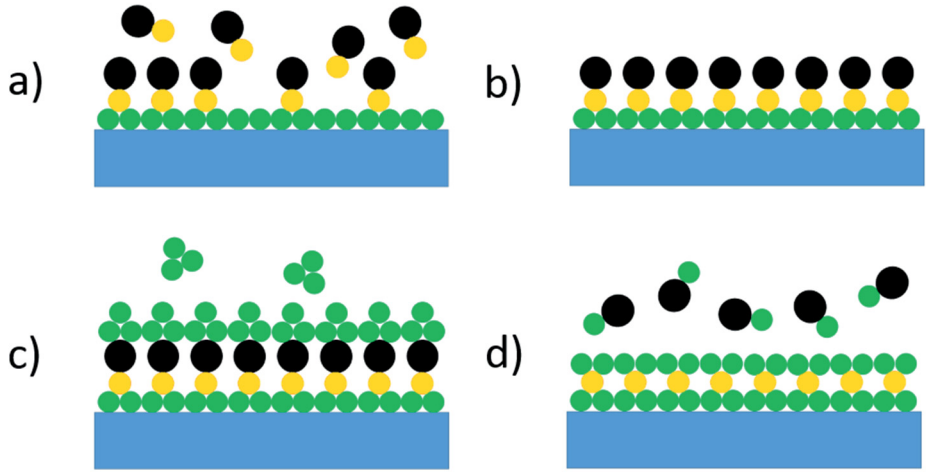

Figure 9. Simplified illustration of the principle of the ALD process. **a)** Precursor A molecules (red and black balls) attach to the functionalized substrate surface. **b)** After flushing excess molecules out of the chamber, a single molecule layer of precursor A is left on the surface. **c)** Precursor B molecules (triplets of green balls) are introduced to the chamber to react with the previous layer. **d)** Reaction products (black and green balls) are flushed away with nitrogen, leaving a single molecule layer (green balls) on the surface. The final film thickness depends on how many times the steps a)-d) are repeated.

2.4.3 Ion beam assisted deposition - IBAD

Ion beam assisted deposition, IBAD, is a thin film deposition method in which the deposited molecules are bombarded with gas ions during deposition in order to form a compound thin film on the substrate (Fig. 10). If the gas is oxygen, the thin film will be an oxide, and of course, if it is nitrogen then it will be a nitride. Often the bombardment efficiency is enhanced by simultaneous bombardment with argon ions. Argon ions on their own can be used for sputter etching, i.e. cleaning the substrate surface prior to thin film deposition. The final composition of the thin film depends on several factors, e.g. the deposition rate, gas flow rates, and the filament current and anode voltage of the ion source. IBAD can be utilized both for sputtering and e-beam deposition. In this thesis, e-beam evaporation was the basic deposition method, and as TiN was the desired compound film, nitrogen and argon were used as the reactive bombardment gases.

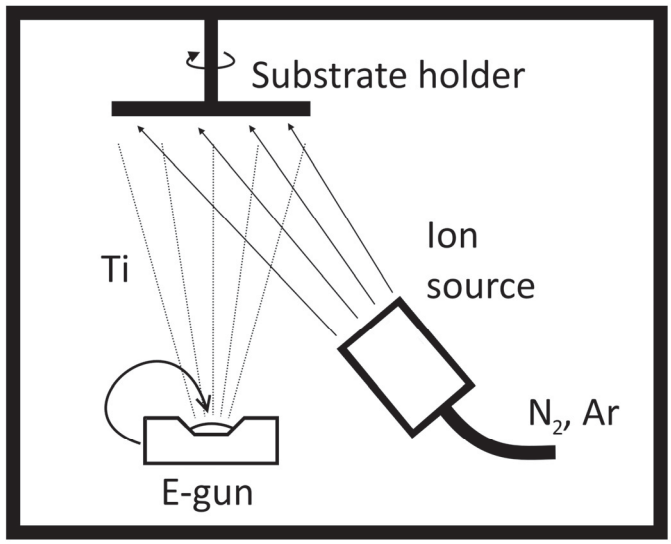

Figure 10. Principle of IBAD TiN deposition. Evaporated titanium is bombarded with nitrogen and argon ions to form a TiN thin film on the substrate.

2.5 Literature review of MEA materials

2.5.1 Substrates

Any optimal MEA substrate material will have at least following properties: 1) it is transparent, because imaging the cells on an MEA is usually done with an inverted microscope as it is optically challenging extract images through the cell culture medium, and 2) it is compatible with the temperatures and chemicals used in microfabrication and sterilization. Ever since the introduction of the very first MEA (Thomas et al. 1972), glass has been the most common substrate material. It has been used both by the majority of the researchers making their own MEAs (Buehler et al. 2016; Gross 1979; Nisch et al. 1994; Pine 1980; Suzuki et al. 2005; Yeung et al. 2007) as well as being used as the sole or partial substrate material by all the commercial MEA manufacturers. The main reason for this is simply that it usually fulfills the above-mentioned requirements for an optimal substrate. In addition, it is a widely accepted material in facilities that process standard integrated circuits (IC).

The same cannot be said for silicone rubbers, for example, as will be discussed later. Throughout the history of MEAs, a wide range of different glass types has been used. In many papers, no specific glass type is mentioned, but among the specified glasses mentioned, Pyrex (Berdondini et al. 2006; Mohr et al. 1996; Oka et al. 1999; Xiang et al. 2007), quartz/fused silica (James et al. 2004; Jing et al. 2009; Nagarah et al. 2015), D263 (Publications I and II), and soda lime (Heuschkel et al. 2006, Publications III and IV) are the most typical examples. In some rare cases, like when boron-doped nanocrystalline diamond (BNCD) is chosen as an electrode material (Granado et al. 2015), one must be careful to select a glass type whose softening point is above the very high processing temperature (≥600 °C) of BNCD. On the other hand, the closely related single-crystal-diamond can be used as a substrate material as well (Picollo et al. 2016).

Without the transparency requirement, silicon would, undoubtedly, be the favored substrate material owing to its superior history as the standard microfabrication substrate. Silicon-based normal MEAs do exist (Brüggemann et al. 2011; Bucher et al. 1999; Gabay et al. 2007; Pancrazio et al. 1998), but they are clearly in the minority. Those cases where silicon substrates are typically used are often studies demonstrating some new material or other technical innovation where imaging features are of less importance. In CMOS MEAs, silicon is naturally the obvious choice as the substrate material (Heer et al. 2004).

Another non-transparent substrate material is the PCB (printed circuit board) used, for example, by MCS in their eco-MEAs, or as a polyimide-based flexible version by Giovangrandi et al. (2006). The main benefit of a PCB MEA is its low manufacturing costs. In addition to opaqueness and certain biocompatibility issues (Heuschkel et al. 2006), they are also restricted to using larger (> 100 μm) electrodes than those that can be used in glass or silicon based MEAs. This is due to the rougher surface and lower resolution patterning methods typically used by circuit board manufacturers. Qwane Biosciences, and some research groups (Berdondini et al. 2006; Kim and Nam 2015; Kireev et al. 2016; MacCarthy et al. 2008; Xiang et al. 2007) have used PCB as a partial substrate in their MEAs. In practice this means that the electrodes are made on a small glass (or polyimide) substrate, a chip, which is then glued or bonded onto the center of a bigger PCB substrate containing the longer parts of the tracks and the contact pads. A similar approach is also used in some commercial high-throughput (HTP) MEAs, where the bottom of a well-plate is replaced by a PCB-glass-chip structure. Instead of bonding the glass chip directly

onto the PCB, it can alternatively be bonded onto a ceramic package on the PCB (Whittington et al. 2005; Zhou et al. 2015). However, in that case microscope imaging from below may be hindered if there is no opening in both the ceramic package and the PCB.

The PCB-glass hybrid structure could, in principle, save manufacturing costs and time because more chips containing the smallest and hardest-to-manufacture features of the MEA can be fitted onto the same wafer than if the whole MEA were made on glass. However, the bonding or gluing, and the sealing processes also take up time, and, undoubtedly, the more complex the structure, the greater the risk of getting faulty electrodes, or, to be more precise, faulty tracks. There is also the unavoidable issue of the effect the increased number of interfaces has on the signal quality. Fitting a well for the cells on such a structure is also more challenging than on a glass-only structure, especially if a removable PDMS structure is planned as the well. There are major problems with the non-planarity of the dual-substrate structure.

Flexibility is another issue. Flexible MEAs are common in *in vivo* studies, where the electrode array needs to be attached tightly around a randomly-shaped 3D organ or tissue. If the MEA needs to be flexible or stretchable, then neither glass, PCB nor silicon are viable options for the substrate material. Although it is more difficult to think of any practical reasons for needing a flexible MEA in *in vitro* studies, unless some speculative future 3D tissue constructs are considered. However, there have been some proof-of-concept studies based on Polyimide/Kapton (Kireev et al. 2016; Lacour et al. 2010) and PDMS (Blau et al. 2011), for example. If a stretchable MEA is used with mechanical stimulus of the cells, the PDMS type of silicone is the most common choice (Khoshfetrat Pakazad et al. 2011; Lacour et al. 2010; Zhang et al. 2005). One special application for polyimide substrates is a perforated MEA (Stett et al. 2005), where the electrodes are fabricated on thin polyimide foil which, in addition to the electrodes, also contains small holes for suction intended to attach the cells or tissues more tightly onto the electrodes. An alternative function of the holes is to provide oxygen and nutrients for the tissue from beneath (Boppart et al. 1992; Eggermann et al. 2016). Charkhkar et al. (2012, 2016) have used both polyethylene napthalate (PEN) and polycarbonate as the substrate materials in their disposable MEAs utilising flexible display manufacturing approaches.

The somewhat limited chemical and thermal tolerances of polymer and silicone materials, however, sets some challenges in many of the subsequent microfabrication

processes or sterilization steps. That may explain why they have not replaced glass as the most important substrate material in normal MEAs. Polyimide foils, for example, tend to soak up moisture, which in the case of heating or ultrasound cleaning may lead to an irreversible deformation of the sheet because of the moisture expansion (MCS 2011). This rules out autoclaving as a sterilization method. Common PECVD deposited insulators like Si_3N_4 can also easily be discounted as candidates for these substrate materials, as the typical 300-400 °C deposition temperature cannot be used. Lower temperature PECVD processes down to 80 °C or even below do exist (Suchaneck et al. 2001), but the behavior of such films in MEAs and cell-measurement environments is not well known.

2.5.2 Electrode, track, and contact pad materials

In addition to the obvious bio- and sterilization compatibility requirements, an optimal electrode material should: provide the lowest possible impedance and noise level, be mechanically and chemically durable (i.e. retains its properties after several instances of use), promote cell adhesion, be easy and cost effective to fabricate (including good adhesion to substrate), and, if imaging is needed, the material should also be transparent. Excluding cell adhesion, these requirements are all more or less valid also for tracks and contact pads. Indeed, with contact pads mechanical durability is especially important.

Excluding the all-titanium MEA described in Publication I, it is rare to only use one metal as the conducting material on an MEA. Instead, there is often at least one additional adhesion metal between the substrate and the actual conductor metal. An even more typical trend throughout the history of MEAs has been coating the electrodes with an additional porous coating. The porosity increases the surface-area-ratio (SAR), i.e. the contact area between the electrode and the liquid medium. As the impedance of the electrode is inversely dependent on its area, this decreases the impedance. Similarly, the noise level of the electrode is related to the impedance, so lower impedance also means lower noise level and, usually, a higher SNR. These are described in more detail in the theory chapter of this thesis. Typically, porous coatings may reduce the impedance by even two orders of magnitude compared with uncoated electrodes (Borkholder et al. 1997). Numerically, an electrode is considered to have low impedance if the impedance is around or below 100 kΩ for a 30 μm electrode at 1 kHz, or at least well below the impedance of non-porous Au, Pt and

ITO electrodes (~1000 kΩ). The porous coating also usually increases the charge injection capability of the electrodes, which is particularly important if the electrodes are used for stimulation. Furthermore, the contact pads are often coated with an additional conductive layer in order to improve their scratch resistance against the contact pins of the measurement electronics.

Pt black can be considered as the all-time most popular low impedance coating in the history of MEAs. It was already used by Thomas et al. (1972) in the very first MEAs and since then it has been the material of choice for many researchers (Blum et al. 2003; Jun et al. 2007; Pine 1980; Tonomura et al. 2010) and it has also been offered by the commercial MEA manufacturers Alpha MED and Qwane. Owing to its porous structure, which increases the SAR, Pt black has excellent electrical characteristics. Its fabrication by electrochemical deposition does not require expensive microfabrication tools like an e-beam or sputter coater, and it can be done at moderate temperatures. However, it does require some expertise in electrochemistry. In addition to the high cost of the raw material, the major drawback of Pt black is its poor mechanical stability (Heim et al. 2012; Li et al. 2011; Park et al. 2010). This drastically limits how many times the MEA can be re-used for a new cell culture. It has even been suggested that the Pt black coating should be redeposited after every cell culture (Eick et al. 2009). Recently some studies aimed at improving the durability of Pt black have been published. Tang et al. (2014) electroplated gold with fuzzy morphology as an intermediate layer to improve Pt adhesion, whereas Kim & Nam (2015) evaluated the hybrid structure of multiple sequential Pt black and polydopamine layers. Sonication has also been used to remove loose Pt particles during electrodeposition (Pancrazio et al. 1998; Tang et al. 2014). A closely related material is another electroplated form of platinum, nanoporous platinum (Park et al. 2010). Compared to Pt black, which is clearly porous even at the microscale level, nanoporous Pt in the same scale still appears as a dense uniform film, sometimes including some cracks with sub-micrometer widths. Only a nanoscale view reveals the 3D nanoporous structure with pore sizes of just a few nm. Nanoporous platinum is also commercially available from Axion in some of its MEAs. Another concern with Pt black is related to the chemical solution used in the electrodeposition. This typically contains lead, which may still exist as residuals in the final coating, potentially raising cytotoxicity issues (Aryan et al. 2015; Schuettler et al. 2005). Lead-free options do exist, but they are not so well known

and there are concerns about their even lower mechanical durability, as it is this feature which the lead is considered to improve (Márton et al. 2014).

Just as for platinum, there have also been some trials with gold aimed at increasing the effective surface area in order to decrease the impedance. For example, nanoporous aluminum oxide (Brüggemann et al. 2011; Wesche et al. 2012) or polystyrene microspheres (Urbanová et al. 2011) have been used as a template to create a nano- or microporous Au surface on electrodes. Despite many demonstrations, modified Au surfaces have not achieved notable popularity; probably because the common Au-related issues still remain: the high material cost, the tendency to adsorb additional substances on the surface (Heim et al. 2012), the need for an additional adhesion layer, and the fact that even when modified, the performance of Au electrodes simply cannot compete with Pt Black or TiN electrodes. Still, Axion offers its proprietary nanotextured gold as an alternative electrode material in some of its MEAs (McConnell et al. 2012). Koester et al. (2010) proposed their gold particle electroplating method as a way to refurbish aged MEA plates. However, that can also be done with, for example, Pt black or TiN.

Unlike other commercial MEA manufacturers, MCS relies on TiN (Janders et al. 1996) as their primary electrode material. Later MEAs with TiN have also been fabricated elsewhere (Aryan et al. 2011). Excluding Publication III, where ion beam assisted e-beam deposition (IBAD) is used, TiN on MEAs has always been fabricated by sputter deposition. Fejtl et al. (2006), did state that MCS have used PECVD in their process, but this has later been denied by representatives of the company, at least verbally. The electrical properties of TiN are highly competitive with Pt black and its best features are its superior adhesion and mechanical stability properties. This, of course, can be expected from a material that is also used as a hard coating in drilling tools etc. Other benefits of TiN include its compatibility with IC-processes, and compared to Pt black and IrOx, the ease of fabrication without any electrochemical methods (Li et al. 2011), which also makes it easier to coat large areas (Norlin et al. 2002). In general, there are very few negative sides to TiN, although Weiland et al. (2002) have questioned its charge injection properties and Guenther et al. (1999) its biocompatibility. The difficulty of finding the correct parameters when depositing a composite material using reactive methods can, of course, be considered as TiN's main weakness. In addition to being used as independent coating, TiN has been used also as track material in carbon nanotube (CNT) MEAs (Gabay et al. 2007). Recently, a new MEA concept with transparent

TiN electrodes has been suggested both by MCS (Mierzejewski et al. 2018) and the author (Ryynänen et al. 2019), where the transparency is based simply on the very low thickness (a few tens of nm) of the TiN layer. MCS relies on sputtered TiN, whereas the author has chosen ALD as the TiN deposition method. Low thickness naturally makes the TiN layer more scratch sensitive, and the impedance is also higher than the traditional thicker and opaque TiN electrodes.

A demonstration of an all-polymer flexible MEA, in which the PDMS patterns were made conductive by mixing in graphite (Blau et al. 2011), led to a rather poor electrical performance with impedance from 400 kΩ to 4 MΩ for relatively large ≤120 μm electrodes. However, a previous effort by the same group, using highly porous conductive polymer PEDOT:PSS [Poly(3,4-ethylenedioxythiophene):poly(styrene sulfonate)] as the electrode material showed excellent low frequency impedance, even lower than that measured for commercial TiN electrodes (Blau et al. 2009). Sessolo et al. (2013), however, did not observe similar low frequency behavior in their PEDOT:PSS MEAs, but only ”normal” frequency behavior and impedance comparable to other low impedance electrode materials. Compared with ITO electrodes, Furukawa et al. (2013) have reported over 50 times lower impedance (270 kΩ vs 5-10 kΩ) at 1 kHz for their 20 μm square PEDOT-PSS electrodes. They also state that the recorded signals are more stable, and claim that PEDOT-PSS greatly increases biocompatibility. However, the results given in their earlier paper (Nyberg et al. 2007) suggest an opposing interpretation. As conductive polymers are softer than metals, according to Green et al. (2008) this reduces the strain mismatch between the electrode and the tissue. This, of course, is a good motivation for considering conductive polymers as an electrode material on MEAs, too. Axion has recently made PEDOT microelectrodes commercially available in their HTP MEAs. They do not state, however, whether it is just PEDOT or whether it is mixed with some other material. MCS, on the other hand, has commercialized an MEA where PEDOT is mixed with CNTs as a PEDOT-CNT composite. Although there is a lot of hype related to CNTs, and one might easily think that the PEDOT-CNT MEA is primarily a CNT MEA, the main purpose of the composite is to solve the well-known mechanical instability of PEDOT coatings, and the benefit of the good conductivity of CNTs is a fortuitous side-effect. CNTs also increase the porosity of the composite, which not only yields a higher surface area but also lower impedance. In fact, the impedance was found to be less than a third of that of comparable TiN electrodes according to Gerwig et al. (2012). Later,

they reported a novel application for PEDOT-CNT MEAs, neurotransmitter sensing, where the PEDOT-CNT composite electrodes outperform the PEDOT-only electrodes in their detection sensitivity of dopamine and ascorbic acid (Samba et al. 2014).

Naturally there are also pure CNT MEAs (Gabay et al. 2007; Keefer et al. 2008; Nick and Thielemann 2014; Suzuki et al. 2013; Wang et al. 2006). In addition to their impedance and other electrical characteristics, which are comparable to or even better than TiN electrodes, another benefit of CNT electrodes is that cells prefer to attach to nano-topographic surfaces (Gabay et al. 2005), which the bunch of CNTs certainly is. The drawbacks of CNTs as an electrode material are related to the fact that they are difficult to process as they often require special chemistry skills, for instance. There are also concerns about their biocompatibility. Even though no biocompatibility issues have been observed in the published CNT MEA papers, many in the scientific community have doubts about the biocompatibility of CNTs (Hu et al. 2010; Smart et al. 2006). In conclusion, CNT MEAs have, at least so far, remained more as an interesting academic research topic than a serious alternative for TiN or Pt black MEAs. Nevertheless, the recently introduced new HTP MEA platform by Alpha MED does have CNT electrodes.

All of the above mentioned electrode materials are capacitive, but there is also a Faradaic alternative, iridium oxide, IrOx. Despite being rather popular in *in vivo* electrodes owing to its excellent charge transfer capability and thus excellent stimulation performance, IrOx has not been commercialized in *in vitro* MEAs. However, impedance levels which are highly competitive with both TiN and Pt black electrodes have been reported for IrOx microelectrodes that have been electrochemically activated, i.e. made porous after the sputter deposition (Eick et al. 2009; Gawad et al. 2009). This separate activation step, however, makes IrOx MEAs more time-consuming to fabricate than, e.g. TiN MEAs. In addition, the results by Gawad et al. (2009) indicate that there is already a substantial increase of impedance in a wet environment after only 48 hours, which is all too short a time for many cell experiments. Publication II introduces ALD as an alternative method of fabricating IrOx coatings on MEAs. Its features are discussed in more detail in Chapter 3.

Of course there are also MEAs which do not have an additional coating or any surface modification on the electrodes. The most interesting of these is indium tin oxide, ITO, which is transparent by nature and thus enables the fabrication of transparent MEAs (Kim et al. 2013; Nam et al. 2006; Tang et al. 2006; Van Pelt et

al. 2004). Biologists appreciate such MEAs as the cells or tissues are fully visible when observed by inverted microscopes. As ITO is not a porous material like Pt black or TiN, it has rather high impedance (>1000 kΩ) and, thus, in order to get a less noisy signal the electrodes in ITO MEAs are often coated with one or other of those porous materials, both by commercial manufacturers and researchers (Gross et al. 1985; Tang et al. 2014). This, of course, partly defeats the objective of transparency, but transparent tracks already improve the visibility compared with MEAs with opaque tracks. Other reported benefits of ITO are that it promotes cell growth and its protein adsorption tendency is lower than those of Au, Ir, Pt or Ti (Selvakumaran et al. 2002).

In addition to being used in porous or surface-modified forms, gold (Jaber et al. 2009; Kim et al. 2013; Seidel et al. 2017; Van Pelt et al. 2004) and platinum (Berdondini et al. 2006; Myers et al. 2011) are also commonly used in plain form as electrode materials. They are both inert and commonly regarded as biocompatible, but despite their reputation as good conductors, the impedance of non-porous Au or Pt electrodes is some 30-50 times higher than the impedance of TiN or Pt black electrodes. Although in their non-coated form they are basically simpler to fabricate than coated electrodes, the poor adhesion of Au and Pt to glass or Si entails an additional adhesion layer of Cr (Jing et al. 2009), Ti (Novak and Wheeler 1986), Ta (Thiébaud et al. 1999), or ITO (Seidel et al. 2017), which adds an additional etching step as different etchants are required for Au and Cr, Ti, or Ta. Jun et al. (2007) and Van Pelt et al. (2004) used a thin Ti layer on top of the gold layer to improve the adhesion of the insulator layer. Kim et al. (2013), however, claimed the reason for the Ti layer was to protect the gold electrodes while dry etching the openings in the insulator layer. Platinum, has its own drawbacks. It is one of the most difficult metals to etch, which means the lift-off process is the strongly preferred and most practical patterning method. Heuschkel et al. (2006) considered a (plain) Pt electrode material to be "a good compromise between good electrical characteristics and inexpensive fabrication process". In some sense that might be true, but the same could easily be easily said for TiN. Despite not being the best-performing electrode materials, both Au and Pt have been, and will probably continue to be among the most common electrode materials, simply because they are so readily available and widely used, so people have just got used to them. An interesting Au and also maybe Pt-related fabrication method is ink-jet printing, which may enable the fabrication of low cost, disposable MEAs that perform reasonably well (Bachmann et al. 2017).

The third pure single metal electrode material is titanium, which is presented in Publication I and is discussed more in Chapter 3. In spite of its well-known biocompatibility, Ti suffers from its strong oxidation tendency in atmospheric conditions, and thus it is more popular just as a track material in TiN MEAs than as an uncoated electrode material. This is especially true of recording electrodes, although Ti electrodes have been utilized more often for stimulation use, both *in vitro* (Viitanen et al. 2011), and *in vivo* (Fofonoff et al. 2004). The two other well-known conductor materials commonly used in electronics, aluminum and copper, are not biocompatible and thus cannot be used as MEA electrodes. However, if well encapsulated under an insulator layer, they can be used as a track material (Gaio et al. 2016). Similarly, nickel has occasionally been used as track material (Nick and Thielemann 2014; Oka et al. 1999; Thomas et al. 1972) or as a catalyst layer for CNT MEAs (Gabay et al. 2007).

One of the less well known electrode materials is BNCD pioneered by research groups at the University of Torino (Ariano et al. 2009) and Ulm University (Granado et al. 2015). Its benefits not only include good transparency, but it is also claimed to be the best material for amperometric measurements. Despite these benefits, the unconventional fabrication method makes BNCD impractical for most researchers and apart from the two above-mentioned research groups, very few MEA studies have been made with this material, Kiran et al. (2012) being one of the few known examples.

All in all, if transparent electrodes are needed, there are not many serious alternatives to ITO. Over the last couple of years, graphene has been considered as a promising candidate for a wide range of applications, and transparent electrodes are no exception. Graphene is not just transparent, but it also has a reputation for having superior electrical and mechanical properties to other comparable materials. In preliminary experiments conducted by the author during a research exchange visit to Shanghai Institute of Microsystem and Information Technology (SIMIT) in the summer of 2013, there was only time to show that the fabrication of graphene electrodes is, basically, doable. However, more characterization and maybe another process iteration round would have been needed to get solid results that were reliable enough for publication. Researchers at the same institute did later publish the first graphene MEA (Du et al. 2015). However, apart from its transparency characteristics, it did not meet high expectations, as that study showed that the impedance of graphene electrodes was higher than that of gold electrodes and thus

it was scarcely any better than the impedance of ITO electrodes. The same relatively high impedance issue has also since been reported by (Kireev et al. 2017). Graphene MEAs may still have a future as Koerbitzer et al. (2016) have found it to be a promising material for stimulation purposes and Kireev et al. (2016) have managed to fabricate graphene electrodes on a flexible substrate, both of which studies may be of particular interest to *in vivo* electrode developers. Recently Kshirsagar et al. (2018) proposed that graphene can be used as a transparent base layer for the growing interest in PEDOT:PSS electrodes, which may be the most practical application for graphene on MEAs presented so far. One more carbon-based electrode material is carbon nanofiber (Fang et al. 2016; Jao et al. 2014), which competes well with TiN electrodes in performance, but requires a rather complex fabrication process with the electrospinning of SU-8, backside immersion oil lithography and carbonization at 1000 °C.

Polycrystalline silicon, Poly-Si, has occasionally been used both as electrode and track material (Bucher et al. 1999), or just as track material (Wang et al. 2006). In the first case the use of Poly-Si was justified by its CMOS-process compatibility and in the latter case the reasoning was to minimize thermal stress between different layers and thus avoid the cracking of the insulator layer in the high temperature processes needed for CNT growth. Despite the reasonableness of both propositions, and the facts that Poly-Si is not completely opaque and Bucher et al. found the impedance of Poly-Si electrodes to be acceptable, Poly-Si has still not gained any broader popularity. The possible reasons for this might be the rather laborious doping process needed to improve the conductivity of Poly-Si, as well as its tendency to form passivating native oxide on its open surfaces in an oxygen atmosphere. One more finding by Bucher et al., which may have reduced interest in Poly-Si was that, contrary to what was expected, etching a nanoporous surface onto Poly-Si did not cause any significant decrease in the impedance. Porous silicon has not been studied on MEAs since then (Heim et al. 2012).

2.5.3 Insulator materials

The basic purpose of the insulator layer in an MEA is to isolate the cells and the cell culturing medium from the tracks connecting the electrodes to the contact pads. This is very important because otherwise the tracks would also act as electrodes and it would be impossible to know whether the measured signal came from a cell on

top of an electrode or from cells located on top of the track. The thickness and dielectric constant of the insulator affect the capability of the layer to reduce the parasitic capacitance between the tracks and the cell culturing medium (Heuschkel et al. 2006) and thus ultimately the noise level of the MEA. As the insulator layer is typically the top layer of the MEA, another function which the insulator layer could have is promoting cell adhesion on the MEA surface (Blau 2013). Surprisingly, not much effort has been put into studying that function, at least not specifically from a purely MEA perspective. On the contrary, cell biologists usually apply their own cell-favoring or repelling coatings on the insulator layer. Polyethyleneimine (PEI), laminin or gelatin applied as a molecular layer are typical examples of such coatings. PEI, for example, changes the charge on the glass surface from negative to positive (MCS 2011).

As the fabrication of normal MEAs strongly relies on traditional IC processes, it is obvious that two common silicon compound insulator materials, Si_3N_4 (sometimes just referred to as SiN or SiN_x) (Berdondini et al. 2006; Buehler et al. 2016; Gabay et al. 2007; Kim and Nam 2015; Nisch et al. 1994) and SiO_2 (Jing et al. 2009; Kim et al. 2013; Zhou et al. 2015) or some sandwich structure incorporating them both (Buitenweg et al. 1998; Eick et al. 2009; Xiang et al. 2007; Yeung et al. 2007) are also favored on MEAs. The most common of these is Si_3N_4. Despite its easy processing and decent insulation properties, Si_3N_4 has three drawbacks. Firstly, it is a relatively hard material compared to the natural *in vivo* environment or the polystyrene favored in cell-culturing dishes. Therefore, Si_3N_4 is not an optimal surface for the cells. This causes problems in cell adhesion and forces the biologists to use additional coatings, as has already been mentioned. Secondly, another annoying characteristic of Si_3N_4, (albeit often glossed over by the manufacturers) is its poor tolerance of common cell-culturing mediums. For example, in a comprehensive study by Herrera Morales (2015), the Si_3N_4 degraded at about 1 μm/year in PBS at 37 °C, and in Publication III the 500 nm of Si_3N_4 500 had already disappeared in a couple of weeks in a cell culturing medium. This severely limits the MEA's life time and usability for long term cell experiments. As a solution for that problem, Nam et. al (2006) suggested inserting a replaceable PDMS insulator sheet on the degraded Si_3N_4 layer. The third drawback is that, in practice the thickness of Si_3N_4 is limited to about 0.5-1 μm. This is not always considered sufficient for the reduction of parasitic capacitance (Heuschkel et al. 2006). With its somewhat lower relative permittivity and more cell-friendly hydrophilic nature, SiO_2 should have benefits over Si_3N_4, but being

permeable to sodium ions, it is not a good choice as a sole insulator material. The SiO_2-Si_3N_4-SiO_2 sandwich structure combines the benefits of both materials. In addition, Schmitt et al. (2000) propose that the counteracting intrinsic stresses in the sandwiched layers improve the corrosion resistance of such structures compared with just one layer. Furthermore, in a layered structure it is also highly unlikely that there are equally positioned pinholes in all the layers throughout the structure. However, the need for more deposition steps and the longer etching process of the sandwich structure have persuaded most designers to opt for just Si_3N_4 as the insulator material.

The most common alternatives to Si_3N_4 and SiO_2 are SU-8 (Gawad et al. 2009; Heuschkel 2001; Ren et al. 2015) and polyimide (Du et al. 2015; Novak and Wheeler 1986; Oka et al. 1999; Stett et al. 2005). There are also other options, such as parylene-C (Charkhkar et al. 2016; Tonomura et al. 2010), PDMS (Blau et al. 2009; Gross 1979), silicone-based positive photoresist (Jimbo et al. 2003), spin-on-glass (SOG) (Morin et al. 2006), nanocrystalline diamond (Maybeck et al. 2014), and an acrylic resin used by Alpha MED on its MEAs. Excluding SOG and diamond, they are often justified by being more natural or more polystyrene-like surfaces than Si_3N_4, and as they are available in much higher thicknesses than Si_3N_4, they have the possibility of offering better electrical insulation properties. However, at least sometimes the real reason for choosing one of the above materials may well have been, once again, simply practical, process-related issues. For example, a photoresist SU-8, as well as some polyimide variants, can easily be patterned by photolithography, which saves at least one etching step in the MEA fabrication process. It is also possible to use laser pulses to make openings for electrodes on a PDMS surface without the need for any lithography or etching (Gross 1979). However, polymers also have problems of their own. Depending on the material there might be issues related to their thermal and chemical compatibility, as has already been mentioned in the substrate section of this chapter. One more issue is the adhesion of PDMS structures on non-glass surfaces. Especially for SU-8 and acrylic resin, this is a well-known problem (Morin et al. 2006; Ren et al. 2015). Thus, particularly if reversible but still non-leaking bonding is needed, those materials are not suitable candidates for the insulator material.

In addition to the materials already mentioned above, there are several other insulator materials commonly used in IC processes, which may occasionally have also been applied on MEAs, such as Tetraethyl Orthosilicate, TEOS (Gaio et al.

2016), and Al_2O_3, TiO_2, HfO_2 and SiC. But as with any material, they all have issues of their own (Herrera Morales 2015) or perhaps it is just that nobody has put in enough effort on trying to sell the idea of some new material to the biologists. This may explain why those materials have not gained any notable popularity among the MEA community. As already mentioned, the major part of cell culturing is traditionally done on polystyrene dishes. Surprisingly, for a long time the only study about MEAs with polystyrene as an insulator layer was a short experiment by the author (Ryynänen et al. 2010), and it is only recently that Hammack et al. (2018) have published another report on the topic. The major fabrication challenge with polystyrene is how to make openings for the electrodes without damaging the polystyrene layer, as it has limited compatibility with the bakes and solvents included in the normal photolithography process.

2.6 Biological background

2.6.1 Stem cells

Stem cells are cells that have two basic features. They can: 1) proliferate, i.e. make copies of themselves, and 2) differentiate, i.e. change into new cell types like bone, cardiac, neuronal or vascular cells. Put in a somewhat simplified form, depending on the stem cell origin, they can be either pluripotent, meaning that they can differentiate into any cell type, or multipotent, meaning they can only differentiate into certain cell types. With human cells, the pluripotent stem cells typically originate from the inner cell mass of a blastocyst, an early-stage preimplantation embryo, and are called human embryonic stem cells, hESCs. In contrast, adult stem cells, which are found all around the body and are there to replenish dying cells or fix damaged tissue, are a typical example of multipotent cells. As some people consider it unethical to use embryonic cells in research, a Nobel and Millenium Technology prize-winning revolution was made by professor Shinya Yamanaka's group when they introduced a method of using viral transfection to re-program somatic cells back to their pluripotent stage (Takahashi and Yamanaka 2006). Such cells are called induced pluripotent stem cells, iPSCs, or hiPSCs when of human origin. Figure 11 summarizes the transformation of stem cells from different origins into organs. A

well-reported example of the use of hiPSCs in the popular press is that it is now possible to take a skin cell sample from a patient, re-program the cells to hiPSCs and then differentiate them into, for example, cardiac cells. These cells can then safely be used to test the effects of different drugs on the cells in a dish in order to find the most suitable drug for a patient (Yamanaka 2009). Stem cells are often considered as a way to find a cure for currently incurable diseases and traumas such as spinal cord injury or multiple sclerosis. In reality, medicine is still a long way from, for example, enabling quadriplegics to walk again. Nevertheless, stem cell-derived cells offer a great tool to study cell behavior, and to develop simple disease models in a dish.

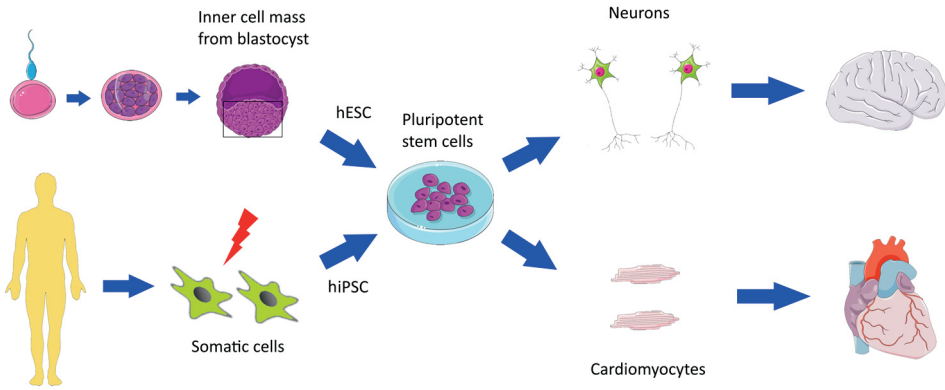

Figure 11. The life cycle of pluripotent stem cells. The stem cells originate either from embryos (hESC) or from somatic cells via viral transduction (hiPSC) and can be derived e.g. as neurons or cardiomyocytes, which are common building blogs of the brain and the heart, respectively. [The figure includes images from Servier Medical Art image bank (http://smart.servier.com/) with Creative Commons Attribution 3.0 Unported License.]

2.6.2 Other cell applications utilizing microelectrode arrays

In addition to the basic biological research, stem cell-derived cells, and also other cells and some tissue slices offer interesting *in vitro* means for drug screening and toxicity testing (Johnstone et al. 2010; Mandenius et al. 2011). This means they can at least partly replace the very contentious tests on animals. Cells in a dish may also function as material biocompatibility evaluators (Charkhkar et al. 2014). Whatever the cell application is, the functionality and well-being of the cells must be

characterized somehow. There are plenty of optical methods for this, from simple visual inspection to various microscopic imaging methods, with and without the fluorescence effect. Some by-products from the cell culturing medium can also be analyzed using chemistry techniques. But, for electrically active cells like cardiomyocytes and neuronal cells, electrical measurements offer a great tool for analysis. Traditionally, the patch clamp (Zhao et al. 2008) has been a popular and precise tool for analyzing the electrical activity of cells, but it is an invasive and very laborious procedure, so the use of MEAs for measuring the electrical activity of cells has become an increasingly important and popular method in many cell applications.

3 ALTERNATIVE ELECTRODE MATERIALS

This chapter summarizes the work described in Publications I, II and III on three new alternative electrode materials to be used in MEAs. Firstly, titanium (Publication I) is proposed as an economical and easy to process material for prototyping new MEA layouts. Then, two new candidates for low-impedance and low-noise electrode materials are presented. Publication II focuses on atomic layer deposited iridium oxide, ALD IrOx, while Publication III presents ion beam assisted e-beam deposited titanium nitride, IBAD TiN. The latter two publications utilise deposition methods which are not (yet) commonly used in MEA fabrication. It is not claimed here that ALD IrOx and IBAD TiN are better than the industry standards, Pt black and sputtered TiN. However, they are useful alternatives which have their own pros and cons. The details of the cell culturing experiments performed by Ti, ALD IrOx and IBAD TiN MEAs can be reviewed from the corresponding publications, so they are not summarized here.

3.1 Materials and methods

3.1.1 Titanium MEA

The fabrication process of the Ti MEAs stuck to the typical MEA fabrication process described in Chapter 2.4.1. The only "exception" could be the use of film masks instead of industry standard chrome masks. The ready-made MEAs were characterized by atomic force microscope (AFM) for their surface topography and by noise and impedance measurements for their electrical performance. As the Ti MEAs suffered from some processing condition failures that led to huge variations in electrode size, for the noise and impedance analysis the measured values were normalized to correspond to electrodes having a diameter of 30 μm.

3.1.2 ALD IrOx MEA

The ALD IrOx MEA fabrication was similar to that of the Ti MEAs except that in the last step the ALD IrOx coating was deposited on Ti electrodes, as illustrated in Figures 8m and 8n. The ALD IrOx depositions for Publication II were carried out at the University of Helsinki, and were based on an established process developed earlier by Hämäläinen et al. (2008). Thus, no MEA-specific ALD IrOx process development was performed for this thesis, although the same process had been shown to be feasible in a previous publication (Ryynänen et al. 2010). This study used what was basically the same structure, but for pH sensing instead of MEAs. In brief, iridium acetylacetonato $Ir(acac)_3$ and ozone were used as precursors, and nitrogen as a carrier and flushing gas. 3000 cycles of 2 second $Ir(acac)_3$ and 4 second ozone pulses separated by 2 second purges resulted in a 120 nm thick layer of IrOx, which means approximately 0.40 Å/cycle growth rate. The process temperature was 185 °C. Ready-made MEAs were characterized by AFM for their surface topography and by noise and impedance measurements for their electrical performance.

3.1.3 IBAD TiN MEA

The fabrication of the IBAD TiN MEAs also followed the same basic process as for the earlier MEAs. However, in this case chrome masks made in-house by MLS were used instead of film masks. Unlike in the case of ALD IrOx, the process development for IBAD TiN had to be started from scratch. As each vacuum evaporation system is unique, and hardly any of them are equipped with a similar Saintech Series III ST55 gridless ion source, there was little to be gained from searching through earlier publications about IBAD TiN (Guzman et al. 1998; Hubler et al. 1988; López et al. 2001) to look for ready-made process recipes. The path to using the IBAD TiN process for MEAs was as follows. Firstly, 100 nm depositions with different parameters (Table 1) were made on microscope slides. Next, an AFM, was used to measure the effective surface area ratio (SAR) on each sample as per the formula

$$SAR = \frac{A_S - A_G}{A_G} \cdot 100 \qquad (5)$$

where A_G is the plain geometric area and A_S is the total surface area of the corresponding region. As impedance is inversely proportional to the electrode area, an assumption was made that the highest SAR would give the lowest impedance. Thus, the deposition parameters of the sample with the highest SAR were selected for the MEA fabrication. The fabricated MEAs were characterized by noise and impedance, and the EDS (energy-dispersive X-ray spectroscopy) spectrum was measured to confirm that the thin film really was a nitride.

3.2 Results

3.2.1 IBAD process development

Table 1 summarizes the IBAD deposition parameters tested during the IBAD TiN process development as well as the color and SAR of the corresponding samples. Sample #2 clearly has the highest SAR so its parameters were chosen to be used in the IBAD TiN MEA fabrication. The effect of the deposition rate (2 Å/s vs. 3.5 Å/s vs. 5 Å/s) on the surface topology is illustrated in Figure 12 by the AFM images of the IBAD TiN samples #2 - #4. Clearly, the slower the deposition rate, the rougher the surface. Different deposition parameters led also to different colors of TiN (Fig. 13). The gray color, which resembles more the color of pure Ti, may indicate that the process has been unable to create TiN, whereas a goldish color is usually associated with the TiN used as a hard coating in machinery tools (Jiang et al. 2004), and the brown/bronze is closest to the almost black sputtered TiN in MCS's MEAs.

The EDS spectrum measured from the ready-made IBAD TiN microelectrode (Fig. 14) indicates that the material really is some sort of titanium nitride. As stated in Publication III, EDS is not well suited for the exact quantification of the N/Ti ratio. The Ti Lα peak simply overlaps with the Kα peak of N. Thus, this ratio was discounted. However, the method is more suited to a comparative analysis, e.g. for evaluating the homogeneity of the coating. Within one sample, less than 1% variation in the N/Ti ratio was measured. The rather high oxygen content in the EDS spectrum may partly originate from the oxidation of Ti(N), but mostly it is assumed to originate from the underlying glass substrate, which is composed of various oxides.

Table 1. Deposition parameters tested during IBAD TiN process optimization and AFM characterization results for each sample.

Sample #	Set anode voltage [V]	N_2 flow [sccm]	Ar flow [sccm]	Deposition rate [Å/s]	Color	Surface area ratio [%]	Notes
1	225	13.2	3.3	1	gold-brown	5.4	
2	225	13.2	3.3	2	purple-bronze	13.1	
3	225	13.2	3.3	3.5	light gold	5.1	
4	225	13.2	3.3	5	gray	3.4	
5	225	10.8	1.2	2	brown	4.3	
6	225	9.9	6.6	1	gold	6.0	Unstable deposition.
7	140	8.3	8.3	2	gray	4.5	One AFM measurement only.
8	225	16.8	4.2	1	gold	4.4	Ion beam pulsed 8 s ON, 7 s OFF.

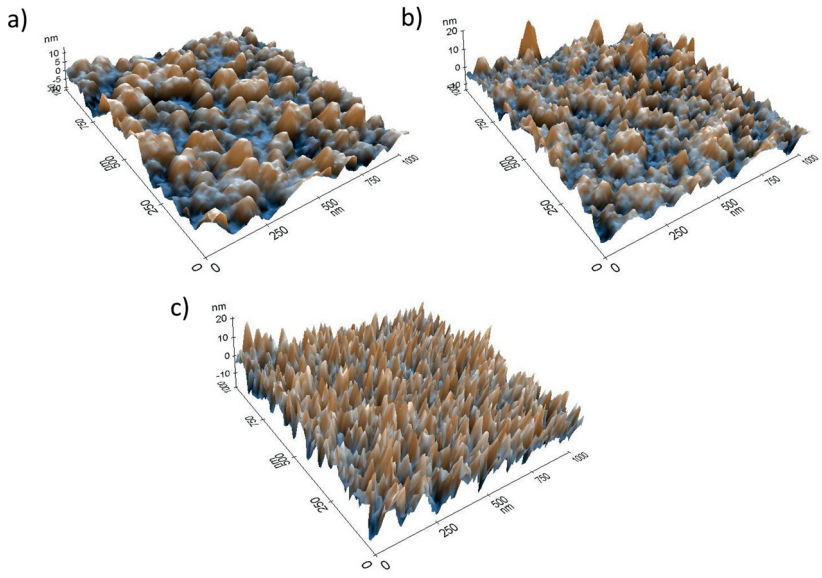

Figure 12. AFM images of 100 nm thick IBAD TiN thin films. Deposition rate was **a**) 5 Å/s (Sample #4 in Table 1), **b)** 3.5 Å/s (#3) and **c)** 2 Å/s (#2).

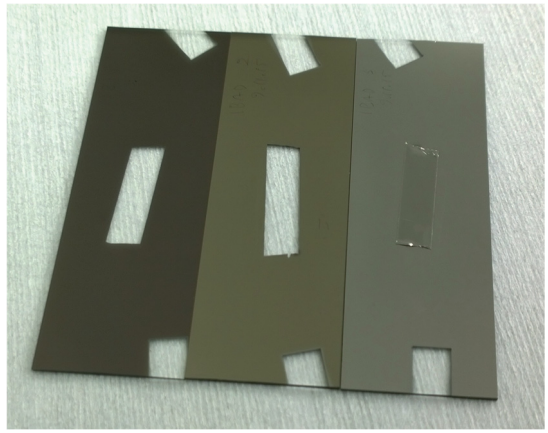

Figure 13. The color of IBAD TiN samples varied from brown or “purple-bronze” (Sample #1, left) to gold (Sample #3, center) and gray (Sample #4, right) depending on the process parameters.

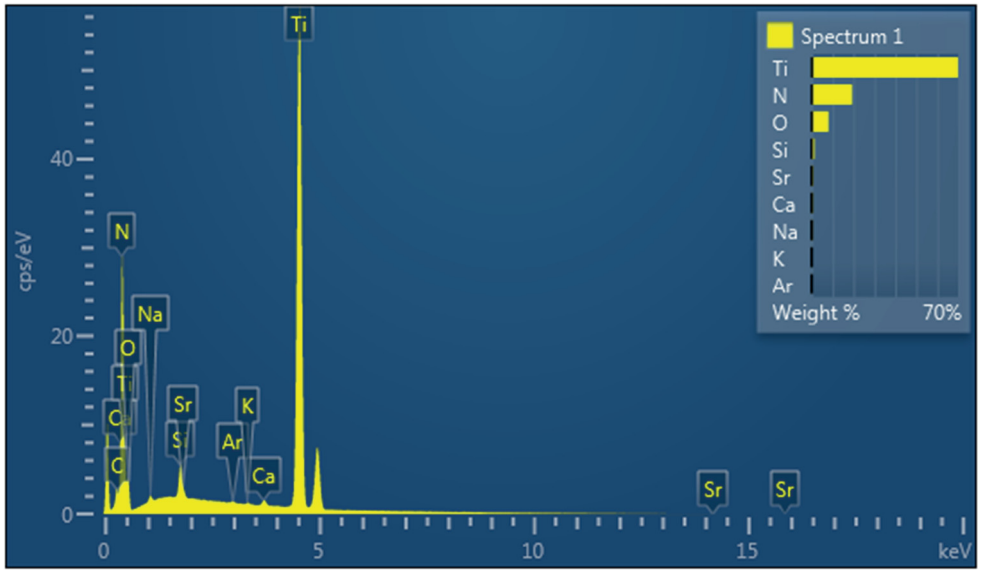

Figure 14. EDS spectrum measured from an IBAD TiN microelectrode confirms the electrode material to be titanium nitride as Ti and N dominate in the spectrum.

3.2.2 Impedance and noise

In Publication I, the root mean square (RMS) noise voltage level of 30 μm Ti electrodes was found to be somewhat higher (7.1 μV vs. 4.9 μV) than it was in commercial TiN electrodes, but it did not seem to result in a significantly worse signal-to-noise ratio. In addition to the larger noise, the signal peaks also seemed to be higher when recorded using Ti electrodes, at least in the sample data presented in Publication I. The impedance at 1 kHz of 30 μm Ti electrodes was measured to be only about double (126.5 kΩ vs. 54.8 kΩ) that of commercial TiN electrodes for new MEAs, and even closer (68.0 kΩ vs. 42.5 kΩ) for used ones. These impedance results, however, must have been faulty, as in all the later studies, e.g. Publication II, the impedance of Ti electrodes has been reported to be much higher, in the region of >1700 kΩ. The possible reasons for the initial faulty results in Publication 1 are presented in the discussion.

Table 2 summarizes the impedance and noise results of ALD IrOx and IBAD TiN electrodes from Publications II and III and also reviews the impedance values for some other common MEA microelectrode materials. If Pt black and sputtered TiN are taken as the reference points, the impedance of ALD IrOx is over 10 times higher than the references, but at the same time only (less than) half the impedances of common non-porous electrode materials such as Au and Pt. Similarly, the impedance of IBAD TiN is 2-4 higher than the references, but being in the same decade (tens of kΩ), it can be regarded as belonging to the same class as Pt black and sputtered TiN. In terms of noise, both ALD IrOx and IBAD TiN compete well with sputtered TiN, whereas pure Ti falls behind both in noise and impedance, as expected.

Figures 15 and 16 show the signal quality in cardiac and neuronal cell measurements using different electrode types. Ti electrodes detect the strong cardiac cell signal very well; maturation of the cells is seen as a strengthening of the signal (Fig. 15a) and the effect of the channel blocker is also visible (Fig. 15b). With neuronal cells the effect of the electrode material can be seen very clearly, but despite the fact that there is more noise in the Ti MEA (Fig. 16a) than there is in the ALD IrOx MEA (Fig. 16b), and certainly more than with the sputtered TiN MEA (Fig. 16c), the peaks can be separated from the noise almost equally well in each. Of course, the weaker peaks might be hidden more easily by the noise in the Ti MEAs. Finally, Figure 17 shows that there is no practical difference in the noise level or peak

amplitudes between IBAD TiN and sputtered TiN MEAs, nor any effect from using two different cell culturing media.

Publication III also produced the interesting observation that the impedance of the TiN electrodes does not remain constant, as after only 2-3 rounds of cell experiments the impedance had increased to above 100 kΩ both for sputtered and IBAD TiN. This is most likely due to the partial oxidation of the TiN surface (Birkholz et al. 2010; Hämmerle et al. 2002).

Table 2. Impedance of common microelectrodes (diameter 30 µm).

Material	**Impedance @ 1 kHz [kΩ]**	**RMS noise [µV]**	**References**
Ti	>1700	12.4**	Publication II
IBAD TiN	~90	~3-4	Publication III
Sputtered TiN	30-50	3.5-5.9**	Publications II and III, MCS
Unactivated ALD IrOx	450	5.2**	Publication II
Unactivated sputtered IrOx	~450		Gawad et al. 2009
Activated sputtered IrOx	~23		Gawad et al. 2009
Pt black	20-30		Axion Biosystems, Qwane Biosciences
ITO	>1000		Hammack et al. 2018
Pt	800-1100		Qwane Biosciences
Au	1000-1300*		Qwane Biosciences
Pedot-CNT	~20		MCS

*Values approximated from data given for 40 µm electrodes

** After Publication II was published an error was found in the Matlab code used to analyze the noise data. These are the corrected values.

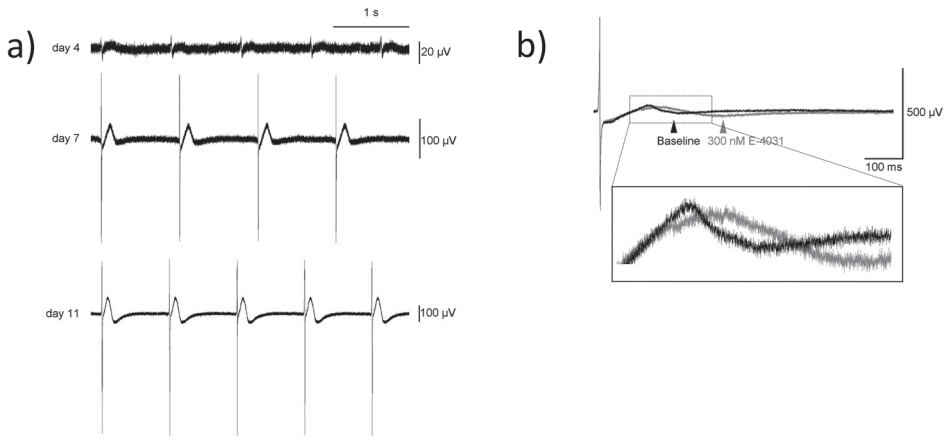

Figure 15. Examples of beating of cardiomyocytes recorded by a Ti MEA. **a)** Signal is hardly visible after only 4 days on the MEA, but strengthens after 7 and 11 days on it. **b)** Prolonged field potential duration by channel blocker.

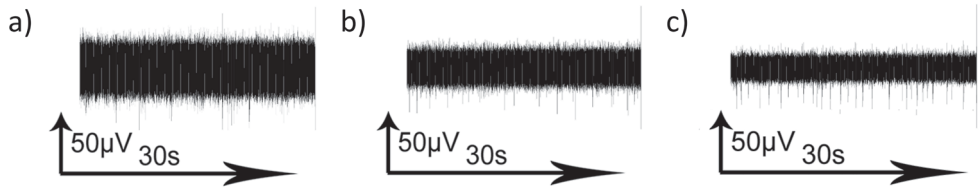

Figure 16. Neuronal cell signals recorded by **a)** a Ti MEA, **b)** an ALD IrOx MEA, and **c)** a sputtered TiN MEA (MCS). A smooth Ti electrode has the highest noisel level and the columnar/porous TiN the lowest.

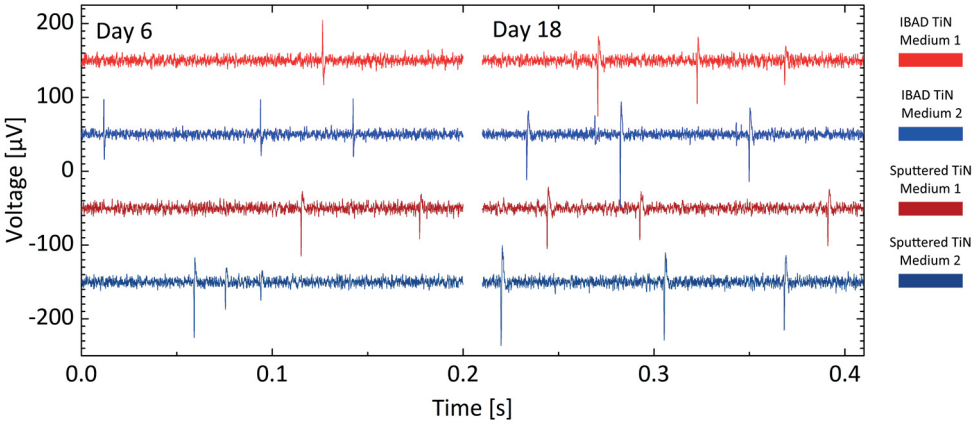

Figure 17. Neuronal cell signals recorded in two different cell culturing media by IBAD TiN and sputtered TiN (MCS) MEAs. The signals are equally well detectable on each from the noise.

The scanning electron microscope (SEM) images in Figure 18 show that the assumption about higher SAR leading to lower impedance makes sense. At lower magnifications, the Ti (Fig. 18a) and ALD IrOx (Fig. 18c) electrodes look completely smooth. However, with the IBAD TiN (Fig. 18g) and especially the sputtered TiN (Fig.18e), although they are not definitely porous, the non-smooth surfaces of the electrodes are clearly visible. With higher magnification, one can see that the Ti (Fig. 18b) and ALD IrOx (Fig. 18d) electrodes are not completely smooth either, but the surface roughness is more likely due to anomalies from the evaporation procedure rather than the column-like crystal structure visible in the TiN (Fig. 18f and 18h). In the low magnification images, the difference in the lithography quality between the film mask (Ti [Fig. 18a] and ALD IrOx [Fig. 18c]) and the chrome mask (TiN [Fig. 18g]) is also clearly visible.

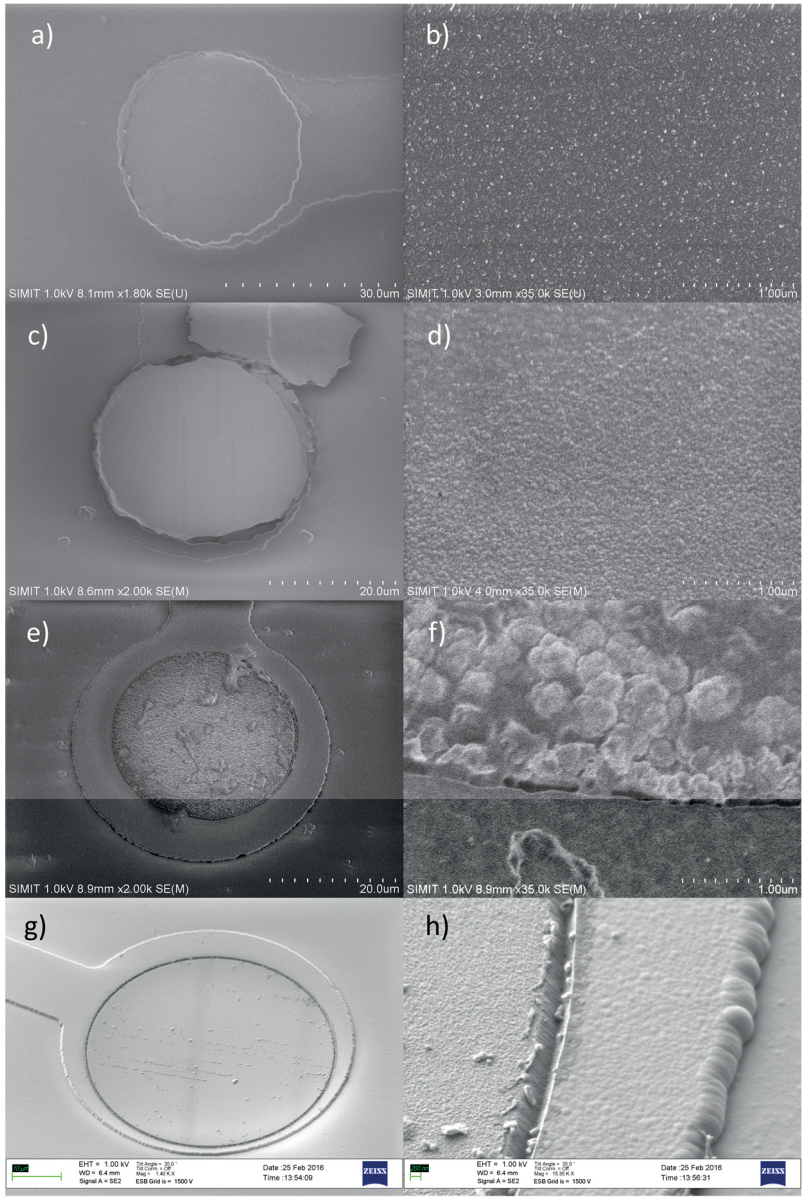

Figure 18. SEM images of microelectrodes. In each pair of images, the whole electrode is on the left and a magnification visualizing the surface topography is on the right. The electrode materials are, **a)-b)** Ti, **c)-d)** ALD IrOx, **e)-f)** sputtered TiN (MCS), and **g)-h)** IBAD TiN. The big flake above the electrode in c) is some lift-off residual and in h) the electrode surface is on the left third of the image.

3.3 Discussion

For any new electrode material, naturally the big question is how well they compare with the existing electrode materials. With the faulty impedance of only double (or less) that of TiN measured in Publication I, initially Ti seemed to be a perfect electrode material, at least in terms of impedance vs. ease of processing. However, when later research showed that the impedance of Ti electrodes is actually >1700 kΩ, the material immediately became less attractive than Au, Pt, and ITO as an electrode material (at least from impedance point of view). This is because the latter materials are all known to have impedances of about only 1000 kΩ for 30 μm electrodes. The reason for the relatively high impedance of Ti, in addition to its being a non-porous material, is its tendency to form native oxide on top. The oxide not only increases the impedance, but it also causes instability in the contacts. In Publication I, it was in fact speculated that this could be one cause for the high deviation in RMS noise levels. Nevertheless, it is no longer a mystery why there had been no Ti MEA papers published earlier. Since then, only Viitanen et al. (2011) have published an *in vitro* MEA paper where Ti has been used as the electrode material. So, what went wrong with the impedance in Publication I? In a discussion presented by Tanskanen et al. (2010) in a paper describing the impedance measurements for Publication I in more detail, a seed of doubt was planted about the impedance measurement arrangement when it was argued that it must have been at fault in some way. Other explanations for the too low values for Ti impedance include, for example, human error in interpreting the measurement data, or that the MEA insulator layer was completely degraded, a phenomenon later also observed in Publication III. This may be one partial explanation for the far too low impedance values reported for the old (many times used) MEAs studied in Publication I. However, it does not explain the low values for the new (previously unused) MEAs that were studied as well.

Despite the fact that Ti electrodes have higher impedance and noise than Au, Pt and ITO electrodes, let alone TiN or Pt black-type low impedance ones, Publications I and IV and Figure 15 showed that it is still possible to get a fully useable signal both from neuronal and cardiac cells with Ti electrodes. Thus, it can justifiably be regarded as a viable candidate for MEA prototyping. Compared to Au, Pt, or ITO, it is fully biocompatible and relatively easy to process. For example, it does not require an adhesion layer, which makes etching simple, and it is also very stable to

deposit by e-beam with only a moderate power requirement. Perhaps most importantly, it is much cheaper than Au or Pt. For example, the last time the author checked the commercial prices quoted for e-beam pellets were about 40 € for 100 g of pure Ti (99.995% purity), whereas the same amount of gold (99.99% purity) cost a hundred times more than that, i.e. about 4000 €! In brief, using Ti instead of Au or Pt when optimizing an MEA layout can easily save hundreds, or even thousands, of euros in the form of cheaper pellets or targets, and in the reduced hours of work required by the simpler processing. In prototyping, once the perfect layout has been found, then the final MEAs can be fabricated with a higher-performance and more reliable electrode material. As Ti is a good track material anyway, often all that needs to be changed for the final process is to have another deposition round to apply an additional electrode coating on the Ti after the openings in the insulator layer have been made and the native oxide has been removed.

Even though the impedance of ALD IrOx is clearly lower than the impedance of the intermediate performance electrode materials like Au and Pt, it is still more than ten times higher than the impedance of Pt black and sputtered TiN. This poses the question, is ALD IrOx a low impedance material at all? Based on the work of Comstock et al. (2010), who managed to do an electrochemical activation of ALD IrOx to make the electrode porous, the answer is yes, ALD IrOx has the potential to be a low impedance material. Even if (unactivated) ALD IrOx were not regarded as a low impedance electrode material, one should note that unactivated ALD IrOx, together with unactivated sputtered IrOx (Gawad et al. 2009) are still the lowest-impedance non-porous electrode materials, a feature which might well be of use in the future. For example, it has often been observed that porous materials can get clogged up with proteins used for surface modification in a cell culture (Brüggemann et al. 2011). The reason why IrOx already performs better as an unactivated material than other non-porous materials could originate from the transfer of electrons across the electrode-electrolyte interface by reversible Faradaic reactions that occur between Ir^{+3}/Ir^{+4} oxidation states. These thus provide additional current flow in addition to the capacitive current flow in the electrode-electrolyte double layer, which is the dominating mechanism in other electrode materials (Li et al. 2011). However, the greatest hope for ALD IrOx to be recognized as a useful MEA material will be if somebody is looking for an MEA design which includes step or cavity structures which cannot be coated with line-of-sight deposition methods like an (IBAD) e-beam; and in some sense also sputtering. ALD may also have lower

initial material costs than sputtering as there is no need to invest in a big and expensive Ir target to get started. Otherwise the choice between whether to use ALD or some other method mainly depends on availability. The potential future motivation for applying ALD IrOx, or actually any IrOx, on MEA is related to IrOx's pH sensitivity (Ryynänen et al. 2010). If the calibration issues for long-term measurements can be solved, it would be a great benefit to be able to use the same electrodes both as MEA electrodes and pH electrodes.

The ALD IrOx deposition process has not yet been fully optimized within the scope of this thesis. Deposition temperature and layer thickness would be the first parameters to study further. If ALD IrOx, or some other low impedance electrode material, is added on top of titanium tracks, it could also be worth studying how much the native oxide (or in the case of ALD the oxide generated by the ozone used in the ALD process) affects the impedance of the electrodes, and what would be the easiest way to remove the oxides without making the process too complex. The issue of complexity is also related to the electrochemical activation option with ALD IrOx. If Pt black can be deposited simply, using only an electrochemical process, and TiN with deposition + lift-off, then activated ALD IrOx, which requires all three steps, is not really a competitive method from the manufacturing point of view. However, if the application requires such high stimulation performance from the electrodes that only IrOx will do, or if there are deep structures that can only be coated by ALD, then the more complex fabrication process needed for activated ALD IrOx might well become viable.

One more discussion topic related to the ALD IrOx MEA process is the lift-off. In theory, the excellent step coverage makes ALD lift-off incompatible. Nevertheless, Publication II did demonstrate a successful lift-off process. This was somewhat overlooked when writing up that publication, but the key factor seems to have been the use of ultrasound in the lift-off. This means that the commonly held belief of lift-off incompatibility would also have applied in this case, but the "brutal force" of the ultrasound bath enabled the process in this particular case, in which only bulk electrode and contact pad patterns had to be created. However, it is unlikely that this method would work with finer and more complex patterns, e.g. long, twisted narrow tracks.

Likewise, although IBAD TiN may not be the lowest impedance microelectrode material in the history of MEAs, the difference between it and sputtered TiN is relatively small, especially after the MEAs have been used for a while. Due to this,

and the fact that the IBAD TiN process has by no means been fully optimized yet, it can fairly be stated that IBAD TiN can certainly be considered as a low impedance material. The most obvious advantage that IBAD TiN may have over sputtered TiN is related to the deposition system that the researcher can use. If a sputtering system with sufficient capacity is available, there is no reason to go for IBAD. But, if you don't have easy access to a sputtering device, then IBAD might be a valid option, especially if an e-beam system with an ion source is more readily available. Another scenario is if there is an e-beam coater available, but no ion-source. Upgrading the system with an ion source is cheaper than installing a sputtering source, beside the e-gun. In the final analysis, it is the aims and resources of the institution or company doing the work which will determine what kind of system or upgrade best supports MEA fabrication, and any other microfabrication activities.

So, it is clear that IBAD TiN has many parameters that could be optimized further, some of which have hardly been touched on in this work. One parameter that has been totally ignored in this study, but has sometimes been studied with IBAD, is the angle between the ion source and the substrate during deposition. The substrate temperature, which may also affect the properties of the thin film, was not actively controlled in the IBAD depositions made for this thesis. However, the very first thing to do in the future development of the process would be to check whether the chosen deposition parameters really do give the lowest impedance. Or, despite the lower SAR, could some other already-tried parameters give lower impedance. Based on that, one could choose which parameter combination should be taken as the starting point for fine-tuning the process. Both for ALD IrOx and IBAD TiN, one possible future approach could be studying the exact elemental composition of the layers, e.g. with ERDA (elastic recoil detection analysis) and trying to find its contribution to the impedance.

Engineers tend to place their trust in numerical values when characterising electrical devices. However, when comparing different microelectrode materials, one should not stick too closely just to numbers. Even though lower impedance and RMS noise readings usually mean better performance, the effect of small or even quite large differences in the numerical characteristics of the electrical qualities of an MEA may have a surprisingly minor effect on signal quality in practice. This was shown especially well in the comparison of two different TiN fabrication methods and two different cell culturing media in Publication III. Even though the numerical values showed what seemed to be a statistically significant difference in the noise

levels, it was nevertheless almost impossible to see any difference in the signal-to-noise ratio between the different electrode materials and medium combinations in practice. It is important to remember this, especially when prototyping and iterating new MEA designs. An adequate signal for prototyping purposes can probably be achieved with almost any common electrode material. It is only once the initial design has been fixed that it is time to think about whether some other material would bring any added value compared to the extra cost and effort. In general, the numerical evaluation of MEA characteristics, like impedance and noise level, should be made with caution. For example, calculating and comparing signal-to-noise ratio from MEA data is somewhat questionable, as the peak heights are not solely dependent on the electrode material. This is because the cells (or some other biological signal source) are never identical and neither are they identically located for each MEA. As discussed in Ryynänen & Lekkala (2018), there might be also external factors, such as the temperature, which affect the noise level even more than the electrode material itself. Similarly Brüggemann et al. (2011) questioned the direct impedance measurements in an MEA environment. As the electrode size is so small, the capacitive influence of the tracks under the thin insulator layer, as well as possible passivation defects on the electrodes and the contact pads may well make a significant contribution to the total impedance.

Another characterization method worth discussing is AFM. In Publication I, it was posited that AFM couldn't measure the real SAR of TiN electrodes because the SAR difference between Ti and TiN electrodes was found to be only about 10%, which is rather negligible in terms of what might be expected in the difference between impedances. For example, with electrochemical impedance spectroscopy, EIS, hundreds of times more effective area increases have been reported for bulk TiN samples (Norlin et al. 2002). If the sputtered TiN structure really is as columnar as is visualized in Figure 18f, or especially in Figure 19 (Egert et al. 1998), it is clear that the purely geometric SAR cannot be measured with AFM. An AFM tip simply does not fit in between the columns. This is supported by the fact that even though the IBAD TiN (Fig. 18h) does not look as columnar as the sputtered TiN, the SAR given for the IBAD TiN in Publication III is about the same as that measured for the sputtered TiN in Publication I. The surface areas not reachable by the AFM tip may thus explain the impedance difference between the two TiN types, at least partly. However only partly, as one could also speculate, how much of the cell culturing

medium eventually penetrates between the columns to translate the larger geometric area "under the surface" into a larger electrically active area.

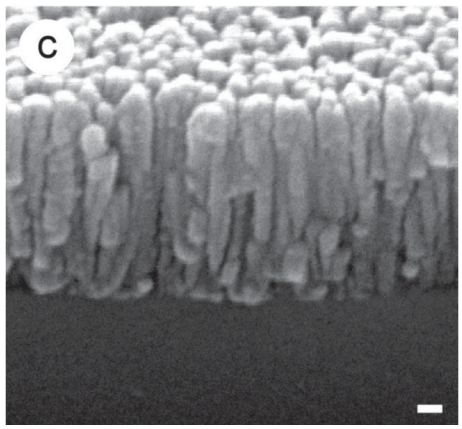

Figure 19. SEM image illustrating the highly columnar structure of sputtered TiN. The scale bar size is 0.1 μm. (Egert et al. 1998)

4 A SINGLE-CELL MEA FOR CARDIOMYOCYTES

4.1 Introduction

Heart cells, or cardiomyocytes, are one of the most common cell types that have been studied with MEA measurements (Mandenius et al. 2011; Pekkanen-Mattila et al. 2009). Cardiomyocyte clusters or monolayers can be used to answer many research questions. The fact is, however, that these larger cell populations are rather heterogeneous as they may contain several types of cardiac cells, and other cell types, too. For this reason, the response of such a heterogeneous cell population to certain drugs, for example, may not necessarily correspond to the response of a specific cell type as it is a sum of the responses from all the cell types. This makes the interpretation of the results challenging. Thus, in some research questions it would be better if one could perform the measurements at the single-cell level.

As previously stated, the patch clamp is the gold standard method for single cell studies, but it is a very laborious and time consuming method, and being such an invasive method, it also destroys the cells, which makes long-term studies impossible. MEA does not have either of these problems, so would seem to be an ideal candidate for single cardiac cell measurements. However, in typical MEA layouts the electrodes are smaller than the cardiomyocytes, and the electrode pitch in these layouts is relatively large. These facts make it highly problematic to get a single cardiomyocyte pipetted on an MEA electrode. This led to the commonly-held belief that using MEAs for single cardiac cell measurements is not possible. The importance of the study presented in Publication IV, therefore, is in showing that this belief is wrong, i.e. that a custom-designed electrode layout could enable MEA measurements to be taken at the single-cell level. Briefly, the challenges in single-cell level measurements are 1) how to get the cells on the electrodes, and 2) how to optimize the electrode size for an acceptable SNR. As already discussed in the theory section of this thesis, the noise level is inversely dependent on the electrode area. Thus, too small electrodes suffer from increased noise precisely because of their small area. On the other hand, if the electrode is too large compared to the cell, then the cell's

contribution gets lost in the noise arising from that area of the electrode that is not covered by the cell, as it picks up additional noise from its surroundings.

4.2 Materials and methods

The fabrication of the so-called single-cell MEAs was mainly based on the processes developed in Publications I, II, and III and also presented here in Chapter 2.4.1, so no detailed description of the fabrication process is required here. From a technical point of view, the only "novelties" (for the author) were the use of MLS as a patterning tool and ITO as the electrode material for some of the single-cell MEAs. For this work, three different single-cell MEA layouts were designed and fabricated. The conducting layer of a few of the very first Layout-1 MEAs was patterned with MLS in a direct writing mode. This means that for these MEAs, the chrome mask was used only to expose the openings in the insulator layer. The layout consisted of long, narrow parallel lines of electrodes all over the cell culture area (Fig. 20a). The idea was simply to maximize the probability of getting a cell on the electrode, and also to orientate the cardiomyocytes along the electrodes. In the next two layouts, the narrow lines of electrodes were abandoned, and larger than normal 30 μm round or oval electrodes were evaluated. Some of the electrodes were cut into halves or quarters (see insert in Fig. 22 for a 100 μm-electrode cut into four quarters) to evaluate the possibility of taking measurements at sub-cellular resolution, should the cell happen to land on one of these split electrodes. Alternatively, by measuring between two quarters one could study the effect of changing the lead field direction (Malmivuo and Plonsey 1995) over the cell. In addition, some of the electrodes contained grooves or pits, whose purpose was to attract the cells to attach themselves to the electrode, or even to orientate the cells, as cardiomyocytes are known to favor a non-smooth topography (Santoro et al. 2013). For Layout 3 (Fig. 20c) the major difference compared with Layout 2 (Fig. 20b) was that the electrodes were placed on the perimeter of the cell culture area and the electrode diameter was fixed at 80 μm, instead of using several different sizes. In the case of Layouts 2 and 3, the direct writing mode of MLS was no longer used because it was too time-consuming for the number of MEAs which had to be fabricated. Instead, all the MEAs were patterned by conventional photolithography, albeit by using chrome masks fabricated by MLS in-house. Two versions of Layout-3 MEAs were fabricated, one with opaque Ti

electrodes and the other with transparent ITO electrodes. This was because the objective was not only to evaluate the MEA measurement capability, but also to take video-based measurements (Ahola et al. 2014) at the same time. Once the MEAs were ready, specially designed PDMS rings were attached to each of them to limit the cell culturing area to about the size of the electrode array area.

The biological procedures are described in more detail in Publication IV, but are presented here in brief. Just before plating the human stem cell-derived cardiomyocytes (hPS-CMs), the MEA surface was hydrophilized with fetal bovine serum (FBS) and coated with 0.1% gelatin type A. Then, 50 µl of cell suspension including approximately 200–300 dissociated hPS-CMs cells was pipetted into the electrode area. After the cells had been allowed to attach for one hour in an incubator, 1 ml of cell culturing medium was added. The medium was changed every three days, always followed by MEA measurements the next day.

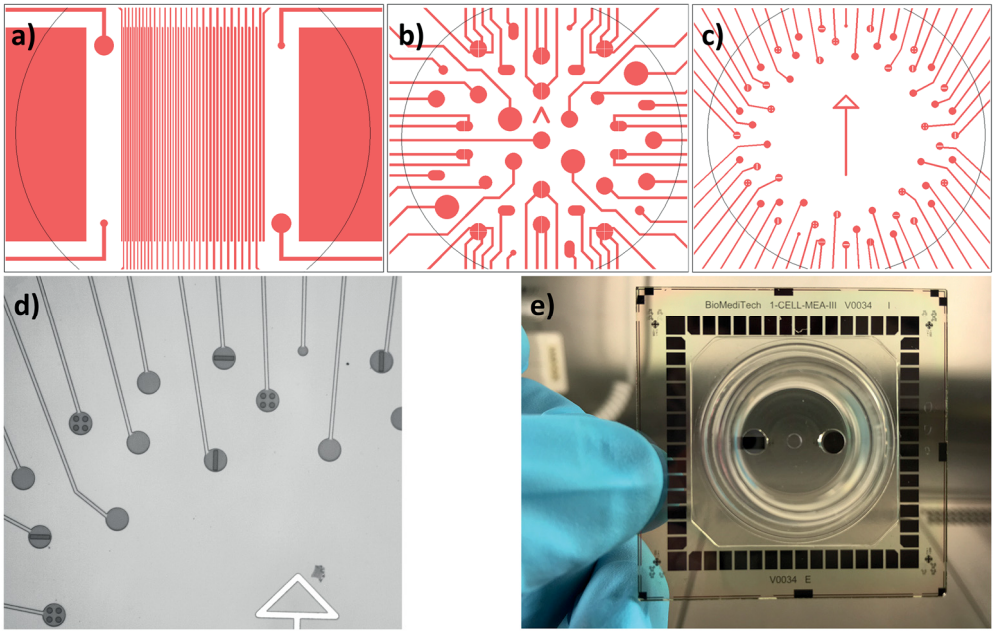

Figure 20. Single-cell MEA electrode layouts. **a)** Layout 1, **b)** Layout 2, and **c)** Layout 3. The black circles represent the central opening in the PDMS ring; diameter 2 mm in Layouts 1 and 2, and 3.5 mm in Layout 3. **d)** Microscope image of MEA with Layout 3. **e)** Layout-3 MEA with PDMS ring.

4.3 Results

In the case of Layout 1, it turned out that the area over which the cell crosses the electrode compared to the total electrode size was too small. Therefore, the long, narrow line electrodes only showed noise. Fortunately, the layout also included some round electrodes, originally intended for process characterization purposes, and some of the cells attached to these 100 μm electrodes. This was the first proof of an MEA being capable of measuring a signal from a single cardiomyocyte (Fig. 21).

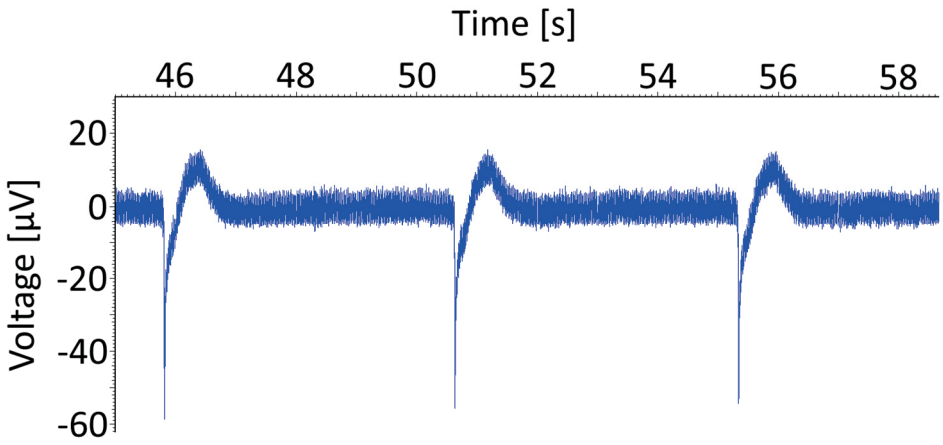

Figure 21. The very first single-cell signal measured by one of the bigger, round electrodes of a Layout- 1 MEA.

Yet more cells were measured successfully during the experiments with Layout 2, which confirmed that MEA measurements at the single-cell level really are possible. However, the number of cells that landed and attached themselves to the electrodes was so small that no effect of different electrode patternings could be observed. Neither were the split electrodes able to measure the subcellular propagation of the field potential, but all the electrodes under the same cell showed the signal to be in the same phase (Fig. 22). Therefore, based on the experience with the first two layouts, an 80 μm electrode was taken to be the "optimal" size to be used in Layout 3. The 80 μm electrode was large enough to house the cell, but not too big compared to the cell size. Another, even more important observation made with Layout 2 was that most of the cells tended to attach themselves to the perimeter of the cell

culturing area, near the edge of the PDMS ring that delimited the cell culturing area. So, in Layout 3 the electrodes were placed at the perimeter to increase the probability of the cells becoming attached to the electrodes.

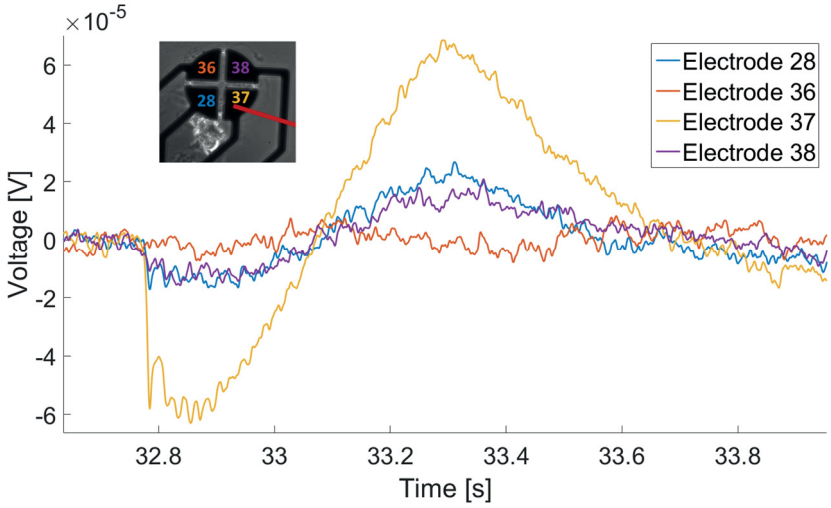

Figure 22. Signal from a single cardiomyocyte (grey clump in the insert) recorded by four quarter electrodes (an equivalent round electrode would have a diameter of 100 μm) of a Layout-2 MEA. No difference in the signal phase is observable. The somewhat out-of-phase signal by electrode 36 is basically just noise.

As expected, with Layout 3 more cells attached to the electrodes (Fig. 23a-f) and were thus measurable more often than in the case of Layout 2. The electrode size was also found to be suitable because the field potential signals were easy to separate from the noise and, for example, the effect of the E-4031 channel blocker drug can be clearly identified (Fig. 23g-h). In addition, transparent ITO electrodes enabled simultaneous video-based measurement to be taken along with the MEA measurements (Fig. 23g). As the electrode materials, Ti and ITO, are not regarded as low impedance materials, the impedance levels of 250 kΩ and 190 kΩ respectively, were still higher than the 30-50 kΩ of the commercially-produced normal 30 μm size TiN electrodes, despite their much bigger electrode size. The average baseline RMS noise level of 5.4±0.9 μV measured both for the ITO and Ti electrodes, however, is at about the same level as given for the 30 μm TiN electrodes in Table 2, and less than half what is given for the 30 μm Ti electrodes.

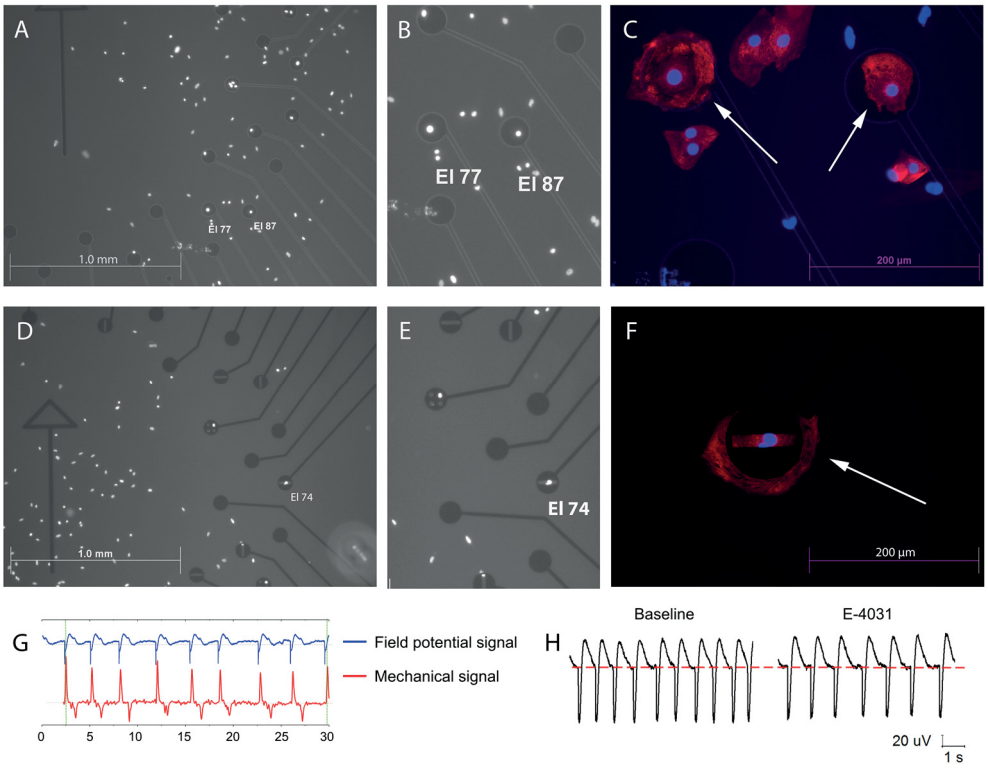

Figure 23. Single cardiomyocytes on Layout-3 MEAs. **a)** MEA with transparent 80 µm ITO electrodes and with dapi staining indicating cell nuclei. **b)** Insert of a), shows that electrodes 77 and 87 have one cell on each. **d)** MEA with opaque Ti electrodes. **e)** Dapi-stained nuclei are visible through the Ti electrodes with the inverted microscope only when there are holes in the electrode (el. 74). **c)**, **f)** The immunocytochemical staining with cardiac-specific Troponin T reveals that the cells on the electrodes shown with arrows are cardiomyocytes. **g)** Signal measured both with MEA and video analysis. **h)** Effect of E-4031 channel blocker on the field potential.

4.4 Discussion

This single-cell-MEA project is an excellent example of MEA customisation in a number of ways. In the beginning, there was only the biologists' need to measure single cells with MEA, but as the first trials with standard MEAs failed, the question became whether single-cell level MEA measurements were possible at all, or could they be with some custom-made electrode design. After the success of Layout 3,

with the benefit of hindsight, it is easy to say that the solution to the problem was actually much more straightforward than was first thought. Basically, all that was needed were slightly bigger than normal electrodes placed in a new configuration. MLS was a good tool for this project as it allowed several layouts to be tested without the burden of huge mask costs.

It is easy to compare this single-cell MEA method with other studies as only one single-cell MEA paper had been published before Publication IV, by Kaneko et al. (2018). However, the experiments for Publication IV had already been done before Kaneko et al.'s paper was published. By chance, they had opted for a totally different approach. They had custom made MEAs with ITO tracks and tiny 8 μm electrodes having three different thicknesses (1.45, 1.88, and 3.01 μm) of Pt black on top of ITO. The impedance of the thickest version was 123 kΩ. Each electrode was surrounded by an agarose chamber (diameter 20 μm, height 5 μm) into which they pipetted a single cardiomyocyte using a special micropipette and micromanipulator system. Although the MEAs with the two thinnest Pt black layers could not detect the FP changes properly, with the thickest version they succeeded in recording FPs. However, in that version there was not much left of the chamber walls because of the almost equally thick Pt black layer, and this largely negated the improved cell handling which the chamber structure was meant to provide. What can be concluded from both Kaneko's and the author's results is that for recording FPs from single cardiomyocytes, low impedance and low noise level are very essential factors. Kaneko et al. chose tiny electrodes and tried to manipulate the impedance down as far as they could by increasing the thickness of the electrode material. Our study had a ten times larger (80 μm) electrode diameter. This leaves more room for improving the impedance in the future and also enables the use of transparent (high impedance) ITO electrodes. The latter enables video analysis, which would not be possible with Kaneko et al's thick and opaque electrodes. The Kaneko approach to cell handling can be considered active, whereas the author relied on a passive approach. The active method, of course, provides better accuracy and repeatability, but it is more laborious and requires more expensive, specialised tools than the passive method, where the cells are expected to do the job of finding their way to the electrodes unaided. The optimal single-cell MEA will probably be found somewhere between these two contrasting approaches.

To return to Publication IV, even if the current electrodes were capable of recording FPs with acceptable SNR ratios, the impedance levels were relatively high

for such big electrodes. The next optimization target from the MEA technology point of view could well be lowering the noise and impedance. If opaque electrodes are acceptable, then the obvious solution is just to coat the Ti electrodes with TiN or some other low impedance electrode material. However, Figure 22 clearly demonstrates the problem with opaque electrodes in single cell measurements, no matter what the impedance of the electrode. Judging by the insert, the cell looks as if it is mostly on electrode 28, but based on the measured signal, it seems more likely that it is on electrode 37. With transparent electrodes, this problem would not arise as one would be able to see the whole cell. Of course, in this example it is always possible that electrode 28 was faulty in some way, which would also account for the weaker than expected signal. Or perhaps the lead field direction and propagation direction of the activation front just matched better with electrode 37 than they did with 28. This could have been studied in more detail by performing measurements where each of the quarters would have been used in turn as a reference electrode to change the lead field direction. On the other hand, it is easy to explain why no subcellular propagation of the field potential was seen by the split electrodes. Given that the conduction velocity in a cardiomyocyte is >40 mm/s (Zhu et al. 2017), it should take around 1 ms or even less for the field potential to go through an approximately 50 μm sized cell. Such a fast effect is simply beyond the resolution of the measurement system.

Naturally, transparent electrodes are a necessity for video analysis. Even though the cell in Figure 23f is partly visible both around the electrode and through the hole in the electrode, no video analysis was possible. The next challenging task is to find out how to decrease the impedance if transparency is an absolute requirement. MCS's (Mierzejewski et al. 2018) and the author's (Ryynänen et al. 2019) demonstrations with very thin TiN electrodes may be the best idea presented so far. Otherwise, one could start thinking about completely new electrode materials, or the possibility of somehow making the ITO porous or its surface very rough, thus increasing its SAR. Although there is undoubtedly still room for improving the electrode size and layout, and also in other materials than just the electrode material, the bottleneck in single-cell level measurements is not the MEA itself, but how to get the cells onto the electrodes in a reliable and repeatable way. In this study, placing the electrodes on the perimeter of the cell culturing area partly solved the problem, but the explanation for this is still unclear. Perhaps the gelatin coating layer applied to the cell culturing area was uneven, which for some reason made the area near the

PDMS ring more cell-favorable, or maybe fluid forces simply drive the cells away from the center during the pipetting procedure. Whatever the case, a more reliable method is still needed. In addition to Kaneko's rather heavy combination of a special pipetting system and agarose chambers, there are many other avenues still to be explored, such as dielectrophoresis (Zhou et al. 2015), 3D-bioprinting (Ong et al. 2017), microstamping (Wang et al. 2013), suction via perforated substrate (Stett et al. 2005), some microfluidic tunnels, optimized accurate pipetting techniques, the mechanical structures, and the list goes on. There is still one common denominator, single-cell level measurement requires a custom-designed MEA rather than the commercially available standard layouts.

In addition to contributing to the topic of single-cell MEAs, the research for this thesis has also contributed knowledge to other biological research questions in which custom-designed MEAs are deemed a necessity, particularly with regard to neuronal cells. One of these lines of enquiry has already led to a patent application (Narkilahti et al. 2014), while others are as yet unpublished. The common thread through all these projects is the aim of guiding the cell growth either by microstamped protein patterns (Tay et al. 2010) or by restriction tunnels made of PDMS (Toivanen et al. 2017). Even if the MEAs made for these purposes have mainly been only non-optimized first prototypes, the MEA has not been (at least so far) the bottleneck for the progress of the projects, rather it has been the functionality of the cells vs. the guiding structures. However, the MEA engineers' readiness to design and fabricate MEAs with almost any conceivable electrode layout has made the work of the restriction channel developers and biologists much easier. They have largely been able to ignore the limitations set by a particular fixed electrode layout, and have been able to focus on making the tunnels work with the cells instead. This in itself already requires a huge amount of work and iteration of the structures and the cell-culturing protocols.

5 CONCLUSIONS AND FUTURE PROSPECTS

The conclusions of this thesis can be summarized as follows:

- In prototyping new MEA layouts, costs and processing time can be saved if titanium is used as the conducting material instead of noble metals. Also, additional low impedance electrode coatings like Pt black or TiN are often unnecessary during the prototyping because, despite the higher noise level, bare Ti electrodes may still be capable of recording cell signals at a useable signal-to-noise ratio.

- ALD IrOx and IBAD TiN were found to be good alternatives for the industry standards, Pt black and sputtered TiN, and are comparable low-noise and low-impedance electrode materials. One of the major benefits of ALD IrOx is its step coverage capability and another is the option to decrease the impedance and improve the stimulation capability even further by electrochemical activation. IBAD TiN, on the other hand, is a feasible alternative for sputtered TiN if, for example, no sputter coater is available.

- Noninvasive single-cell level MEA measurements of cardiomyocytes can be achieved by modifying the size and location of the electrodes compared with standard MEA layouts. Improving the success rate of getting the cells on the electrodes, however, is still a major challenge.

For the future, it is worth considering what could be the next alternative microelectrode materials and fabrication methods to study. The hype related to CNTs and graphene will no doubt keep the scientific community looking at their applications in MEAs. However, no step change in MEA performance is currently expected from these materials, and it might be more worthwhile for the MEA research community to focus on materials which are easier to manufacture and process, as well as on gaining a better understanding of the more common materials

already in use. For example, there may well be ways to avoid the change in the impedance of TiN electrodes, which was observed in Publication III and had also been reported previously by, for example, Hämmerle et al. (2002). Another approach could be that instead of trying to get the last few kΩ out of the impedance by developing new electrode materials, a more fruitful approach to improving the overall MEA performance might be to focus on the insulator layer. This could affect both the durability of MEAs and the well-being of the cells, and might well lower the impedance and noise level of the signals. Finally, the current trends towards HTP and mass-produced disposable MEAs may direct researchers towards which layer of an MEA requires the most urgent attention in order to hasten the development of these platforms. As a technology, ALD may well be the key to solving problems in more than one layer of the MEA. The above-mentioned novel platforms accompanied by the rise of CMOS MEAs will undoubtedly reduce the need for glass substrate-integrated normal MEAs in the future, but at least the academic world will still find a use for them, and for the findings presented in this thesis, at least for another decade or two while they are developing their novel cell models.

REFERENCES

Ahola, A., Kiviaho, A.L., Larsson, K., Honkanen, M., Aalto-Setälä, K., Hyttinen, J., 2014. Video image-based analysis of single human induced pluripotent stem cell derived cardiomyocyte beating dynamics using digital image correlation. Biomed. Eng. Online 13:39.

Ariano, P., Lo Giudice, A., Marcantoni, A., Vittone, E., Carbone, E., Lovisolo, D., 2009. A diamond-based biosensor for the recording of neuronal activity. Biosens. Bioelectron. 24, 2046–2050.

Aryan, N.P., Asad, M.I.H. Bin, Brendler, C., Kibbel, S., Heusel, G., Rothermel, A., 2011. In vitro study of titanium nitride electrodes for neural stimulation. Proc. Annu. Int. Conf. IEEE Eng. Med. Biol. Soc. EMBS 2866–2869.

Aryan, N.P., Kaim, H., Rothermel, A., 2015. Electrode Materials: State-of-the-Art and Experiments, in: Stimulation and Recording Electrodes for Neural Prostheses. Springer International Publishing, Cham, pp. 45–64.

Bachmann, B., Adly, N.Y., Schnitker, J., Yakushenko, A., Rinklin, P., Offenhäusser, A., Wolfrum, B., 2017. All-inkjet-printed gold microelectrode arrays for extracellular recording of action potentials. Flex. Print. Electron. 2, 035003.

Berdondini, L., Chiappalone, M., Van Der Wal, P.D., Imfeld, K., De Rooij, N.F., Koudelka-Hep, M., Tedesco, M., Martinoia, S., Van Pelt, J., Le Masson, G., Garenne, A., 2006. A microelectrode array (MEA) integrated with clustering structures for investigating in vitro neurodynamics in confined interconnected sub-populations of neurons. Sensors Actuators, B Chem. 114, 530–541.

Bertotti, G., Velychko, D., Dodel, N., Keil, S., Wolansky, D., Tillak, B., Schreiter, M., Grall, A., Jesinger, P., Rohler, S., Eickenscheidt, M., Stett, A., Moller, A., Boven, K.H., Zeck, G., Thewes, R., 2014. A CMOS-based sensor array for in-vitro neural tissue interfacing with 4225 recording sites and 1024 stimulation sites. IEEE 2014 Biomed. Circuits Syst. Conf. BioCAS 2014 - Proc. 304–307.

Birkholz, M., Ehwald, K.E., Wolansky, D., Costina, I., Baristiran-Kaynak, C., Fröhlich, M., Beyer, H., Kapp, A., Lisdat, F., 2010. Corrosion-resistant metal layers from a CMOS process for bioelectronic applications. Surf. Coatings Technol. 204, 2055–2059.

Blau, A., 2013. Cell adhesion promotion strategies for signal transduction enhancement in microelectrode array in vitro electrophysiology : An introductory overview and critical discussion. Curr. Opin. Colloid Interface Sci. 18, 481–492.

Blau, A., Murr, A., Trellenkamp, S., Dautermann, C., Wolff, S., Heuschkel, M., Wuesten, J., Ziegler, C., Benfenati, F., 2009. Prototyping all-polymer bioelectrical signal transducers. IFMBE Proc. 25, 327–330.

Blau, A., Murr, A., Wolff, S., Sernagor, E., Medini, P., Iurilli, G., Ziegler, C., Benfenati, F., 2011. Flexible, all-polymer microelectrode arrays for the capture of cardiac and neuronal signals. Biomaterials 32, 1778–1786.

Blum, R.A., Ross, J.D., Simon, C.M., Brown, E.A., Harrison, R.R., DeWeerth, S.P., 2003. A custom multielectrode array with integrated low-noise preamplifiers. Eng. Med. Biol. Soc.

2003. Proc. 25th Annu. Int. Conf. IEEE 4, 3396–3399.
Boppart, S.A., Wheeler, B.C., Wallace, C.S., 1992. A flexible perforated microelectrode array for extended neural recordings. IEEE Trans. Biomed. Eng. 39, 37–42.
Borkholder, D.A., Bao, J., Maluf, N.I., Perl, E.R., Kovacs, G.T.A., 1997. Microelectrode arrays for stimulation of neural slice preparations. J. Neurosci. Methods 77, 61–66.
Brüggemann, D., Wolfrum, B., Maybeck, V., Mourzina, Y., Jansen, M., Offenhäusser, A., 2011. Nanostructured gold microelectrodes for extracellular recording from electrogenic cells. Nanotechnology 22, 265104.
Bucher, V., Brunner, B., Leibrock, C., Schubert, M., Nisch, W., 2001. Electrical properties of a light-addressable microelectrode chip with high electrode density for extracellular stimulation and recording of excitable cells. Biosens. Bioelectron. 16, 205–210.
Bucher, V., Graf, M., Stelzle, M., Nisch, W., 1999. Low-impedance thin-film polycrystalline silicon microelectrodes for extracellular stimulation and recording. Biosens. Bioelectron. 14, 639–649.
Buehler, S., Stubbe, M., Bonk, S., Nissen, M., Titipornpun, K., Klinkenberg, E.-D., Baumann, W., Gimsa, J., 2016. Cell Monitoring and Manipulation Systems (CMMSs) based on Glass Cell-Culture Chips (GC3s). Micromachines 7, 106.
Buitenweg, J.R., Rutten, W.L., Willems, W.P., van Nieuwkasteele, J.W., 1998. Measurement of sealing resistance of cell-electrode interfaces in neuronal cultures using impedance spectroscopy. Med. Biol. Eng. Comput. 36, 630–637.
Charkhkar, H., Arreaga-Salas, D.E., Tran, T., Hammack, A., Voit, W.E., Pancrazio, J.J., Gnade, B.E., 2016. Novel disposable microelectrode array for cultured neuronal network recording exhibiting equivalent performance to commercially available arrays. Sensors Actuators, B Chem. 226, 232–238.
Charkhkar, H., Frewin, C., Nezafati, M., Knaack, G.L., Peixoto, N., Saddow, S.E., Pancrazio, J.J., 2014. Use of cortical neuronal networks for in vitro material biocompatibility testing. Biosens. Bioelectron. 53, 316–323.
Charkhkar, H., Knaack, G.L., Gnade, B.E., Keefer, E.W., Pancrazio, J.J., 2012. Development and demonstration of a disposable low-cost microelectrode array for cultured neuronal network recording. Sensors Actuators, B Chem. 161, 655–660.
Comstock, D.J., Christensen, S.T., Elam, J.W., Pellin, M.J., Hersam, M.C., 2010. Synthesis of nanoporous activated iridium oxide films by anodized aluminum oxide templated atomic layer deposition. Electrochem. commun. 12, 1543–1546.
Dragas, J., Viswam, V., Shadmani, A., Chen, Y., Bounik, R., Stettler, A., Radivojevic, M., Geissler, S., Obien, M.E.J., Müller, J., Hierlemann, A., 2017. In Vitro Multi-Functional Microelectrode Array Featuring 59 760 Electrodes, 2048 Electrophysiology Channels, Stimulation, Impedance Measurement, and Neurotransmitter Detection Channels. IEEE J. Solid-State Circuits 52, 1576–1590.
Du, X., Wu, L., Cheng, J., Huang, S., Cai, Q., Jin, Q., Zhao, J., 2015. Graphene microelectrode arrays for neural activity detection. J. Biol. Phys. 41, 339–347.
Egert, U., Schlosshauer, B., Fennrich, S., Nisch, W., Fejtl, M., Knott, T., Müller, T., Hämmerle, H., 1998. A novel organotypic long-term culture of the rat hippocampus on substrate-integrated multielectrode arrays. Brain Res. Protoc. 2, 229–242.
Egert, U, Schlosshauer, B., Fennrich, S., Nisch, W., Fejtl, M., Knott, T., Müller, T., Hämmerle, H., 1998. A novel organotypic long-term culture of the rat hippocampus on substrate-integrated multielectrode arrays. Brain Res. Brain Res. Protoc. 2, 229–242.
Eggermann, E., Heuschkel, M., Fischler, G., Stoppini, L., 2016. Stand-alone MEA device for

medium-throughput testing of 3D engineered neural tissue, in: Front. Neurosci. Conference Abstract: MEA Meeting 2016 | 10th International Meeting on Substrate-Integrated Electrode Arrays, Reutlingen, Germany, 28 Jun - 1 Jul, 2016.

Eichler, M., Jahnke, H.G., Krinke, D., Müller, A., Schmidt, S., Azendorf, R., Robitzki, A.A., 2015. A novel 96-well multielectrode array based impedimetric monitoring platform for comparative drug efficacy analysis on 2D and 3D brain tumor cultures. Biosens. Bioelectron. 67, 582–589.

Eick, S., Wallys, J., Hofmann, B., van Ooyen, A., Schnakenberg, U., Ingebrandt, S., Offenhäusser, A., 2009. Iridium oxide microelectrode arrays for in vitro stimulation of individual rat neurons from dissociated cultures. Front. Neuroeng. 2:16, 1–12.

Fang, S.-P., Jao, P.F., Franca, E., DeMarse, T.B., Wheeler, B.C., Yoon, Y.-K., 2016. A carbon nanofiber (CNF) based 3-D microelectrode array for in-vitro neural proliferation and signal recording, in: 2016 IEEE 29th International Conference on Micro Electro Mechanical Systems (MEMS), Shanghai, 2016. pp. 423–426.

Fejtl, M., Stett, A., Nisch, W., Boven, K.-H., Möller, A., 2006. On Micro-Electrode Array Revival : Its Development , Sophistication of Recording , and Stimulation, in: Taketani, M., Baudry, M. (Eds.), Advances in Network Electrophysiology - Using Multi-Electrode Arrays. Springer Science+Business Media, Inc., New York, pp. 24–37.

Fofonoff, T.A., Martel, S.M., Hatsopoulos, N.G., Donoghue, J.P., Hunter, I.W., 2004. Microelectrode array fabrication by electrical discharge machining and chemical etching. IEEE Trans. Biomed. Eng. 51, 890–895.

Franks, W., Schenker, I., Schmutz, P., Hierlemann, A., 2005. Impedance characterization and modeling of electrodes for biomedical applications. IEEE Trans. Biomed. Eng. 52, 1295–1302.

Fromherz, P., Offenhausser, A., Vetter, T., Weis, J., 1991. A neuron-silicon junction: a Retzius cell of the leech on an insulated-gate field-effect transistor. Science 252, 1290–1293.

Furukawa, Y., Shimada, A., Kato, K., Iwata, H., Torimitsu, K., 2013. Monitoring neural stem cell differentiation using PEDOT-PSS based MEA. Biochim. Biophys. Acta - Gen. Subj. 1830, 4329–4333.

Gabay, T., Ben-David, M., Kalifa, I., Sorkin, R., Abrams, Z.R., Ben-Jacob, E., Hanein, Y., 2007. Electro-chemical and biological properties of carbon nanotube based multi-electrode arrays. Nanotechnology 18, 035201.

Gabay, T., Jakobs, E., Ben-Jacob, E., Hanein, Y., 2005. Engineered self-organization of neural networks using carbon nanotube clusters. Phys. A Stat. Mech. its Appl. 350, 611–621.

Gaio, N., Silvestri, C., Van Meer, B., Vollebregt, S., Mummery, C.L., Dekker, R., 2016. Fabrication and Characterization of an Upside-Down Carbon Nanotube Microelectrode Array. IEEE Sens. J. 16, 8685–8691.

Gawad, S., Giugliano, M., Heuschkel, M., Wessling, B., Markram, H., Schnakenberg, U., Renaud, P., Morgan, H., 2009. Substrate arrays of iridium oxide microelectrodes for in vitro neuronal interfacing. Front. Neuroeng. 2:1, 1–7.

Gerwig, R., Fuchsberger, K., Schroeppel, B., Link, G.S., Heusel, G., Kraushaar, U., Schuhmann, W., Stett, A., Stelzle, M., 2012. PEDOT–CNT Composite Microelectrodes for Recording and Electrostimulation Applications: Fabrication, Morphology, and Electrical Properties. Front. Neuroeng. 5:8, 1–11.

Giovangrandi, L., Gilchrist, K., Whittington, R., Takovacs, G., 2006. Low-cost microelectrode array with integrated heater for extracellular recording of cardiomyocyte cultures using commercial flexible printed circuit technology. Sensors Actuators B Chem. 113, 545–554.

Graham, A.H.D., Robbins, J., Bowen, C.R., Taylor, J., 2011. Commercialisation of CMOS integrated circuit technology in multi-electrode arrays for neuroscience and cell-based biosensors. Sensors 11, 4943–4971.

Granado, T.C., Neusser, G., Kranz, C., Filho, J.B.D., Carabelli, V., Carbone, E., Pasquarelli, A., 2015. Progress in transparent diamond microelectrode arrays. Phys. Status Solidi A 212, 2445–2453.

Green, R.A., Lovell, N.H., Wallace, G.G., Poole-Warren, L.A., 2008. Conducting polymers for neural interfaces: Challenges in developing an effective long-term implant. Biomaterials 29, 3393–3399.

Gross, G.W., 1979. Simultaneous Single Unit Recording in vitro with a Photoetched Laser Deinsulated Gold Multimicroelectrode Surface. IEEE Trans. Biomed. Eng. BME-26, 273–279.

Gross, G.W., Wen, W.Y., Lin, J.W., 1985. Transparent indium-tin oxide electrode patterns for extracellular, multisite recording in neuronal cultures. J. Neurosci. Methods 15, 243–252.

Guenther, E., Tro, B., Schlosshauer, B., Zrenner, E., 1999. Long-term survival of retinal cell cultures on retinal implant materials 39, 3988–3994.

Guo, J., Yuan, J., Chan, M., 2012. Modeling of the Cell-Electrode Interface Noise for Microelectrode Arrays. IEEE Trans. Biomed. Circuits Syst. 6, 605–613.

Guzman, L., Bonelli, M., Miotello, A., Kothari, D.C., 1998. Process parameters optimization for TiN and TiC formation using reactive ion beam assisted deposition. Surf. Coatings Technol. 100–101, 500–502.

Hämäläinen, J., Kemell, M., Munnik, F., Kreissig, U., Ritala, M., 2008. Atomic Layer Deposition of Iridium Oxide Thin Films from $Ir(acac)_3$ and Ozone. Thin Film. 2903–2907.

Hamill, O.P., Marty, A., Neher, E., Sakmann, B., Sigworth, F.J., 1981. Improved patch-clamp techniques for high-resolution current recording from cells and cell-free membrane patches. Pflügers Arch. Eur. J. Physiol. 391, 85–100.

Hammack, A., Rihani, R.T., Black, B.J., Pancrazio, J.J., Gnade, B.E., 2018. A patterned polystyrene-based microelectrode array for in vitro neuronal recordings. Biomed. Microdevices 20: 48.

Hämmerle, H., Kobuch, K., Kohler, K., Nisch, W., Sachs, H., Stelzle, M., 2002. Biostability of micro-photodiode arrays for subretinal implantation. Biomaterials 23, 797–804.

Heer, F., Franks, W., Blau, A., Taschini, S., Ziegler, C., Hierlemann, A., Baltes, H., 2004. CMOS microelectrode array for the monitoring of electrogenic cells. Biosens. Bioelectron. 20, 358–366.

Heim, M., Yvert, B., Kuhn, A., 2012. Nanostructuration strategies to enhance microelectrode array (MEA) performance for neuronal recording and stimulation. J. Physiol. Paris 106, 137–145.

Herrera Morales, J.M., 2015. Selecting and evaluating biocompatible barrier films for protecting medical micro devices. Université Grenoble Alpes.

Heuschkel, M.O., 2001. Fabrication of Multi-Electrode Array Devices for Electrophysiological Monitoring of in-vitro cell/tissue cultures. Ecole Polytechnique Fédérale de Lausanne.

Heuschkel, M.O., Wirth, C., Steidl, E.-M., Buisson, B., 2006. Development of 3-D Multi-Electrode Arrays for Use with Acute Tissue Slices, in: Taketani, M., Baudry, M. (Eds.), Advances in Network Electrophysiology - Using Multi-Electrode Arrays. Springer Science+Business Media, Inc., New York, pp. 69–111.

Hu, X., Cook, S., Wang, P., Hwang, H., Liu, X., Williams, Q.L., 2010. In vitro evaluation of cytotoxicity of engineered carbon nanotubes in selected human cell lines. Sci. Total

Environ. 408, 1812–1817.
Hubler, G.K., Vanvechten, D., Donovan, E.P., Kant, R.A., 1988. Ion Beam assisted Deposition of Titanium Nitride. MRS Proc. 128, 55–60.
Huigen, E., Peper, A., Grimbergen, C.A., 2002. Investigation into the origin of the noise of surface electrodes. Med. Biol. Eng. Comput. 40, 332–338.
Jaber, F.T., Labeed, F.H., Hughes, M.P., 2009. Action potential recording from dielectrophoretically positioned neurons inside micro-wells of a planar microelectrode array. J. Neurosci. Methods 182, 225–235.
James, C., Spence, A., Dowell, N., Hussein, R., Smith, K., Craighead, H., Isaacson, M., Shain, W., Turner, J., 2004. Extracellular Recordings from Constructed Neuronal Networks using Planar Microelectrode Arrays. IEEE Trans Biomed Eng 51, 1640–1648.
Janders, M., Egert, U., Stelzle, M., Nisch, W., 1996. Novel thin film titanium nitride micro-electrodes with excellent charge transfer capability for cell stimulation and sensing applications, in: Proceedings of 18th Annual International Conference of the IEEE Engineering in Medicine and Biology Society (1996). pp. 245–247.
Jao, P.F., Franca, E., Fang, S., Yoon, J., Cho, K., Senior, D.E., Kim, G., Wheeler, B., Yoon, Y., 2014. Fabrication of carbon nanofibrous microelectrode array (CNF-MEA) using nanofiber immersion photolithography, in: 2014 IEEE 27th International Conference on Micro Electro Mechanical Systems (MEMS). IEEE, San Francisco, pp. 498–501.
Jiang, N., Zhang, H.J., Bao, S.N., Shen, Y.G., Zhou, Z.F., 2004. XPS study for reactively sputtered titanium nitride thin films deposited under different substrate bias. Phys. B Condens. Matter 352, 118–126.
Jimbo, Y., Kasai, N., Torimitsu, K., Tateno, T., Robinson, H.P.C., 2003. A system for MEA-based multisite stimulation. IEEE Trans. Biomed. Eng. 50, 241–248.
Jing, G., Yao, Y., Gnerlich, M., Perry, S., Tatic-Lucic, S., 2009. Towards a multi-electrode array (MEA) system for patterned neural networks. Procedia Chem. 1, 329–332.
Johnstone, A.F.M., Gross, G.W., Weiss, D.G., Schroeder, O.H.-U., Gramowski, A., Shafer, T.J., 2010. Microelectrode arrays: a physiologically based neurotoxicity testing platform for the 21st century. Neurotoxicology 31, 331–350.
Jun, S.B., Hynd, M.R., Dowell-Mesfin, N., Smith, K.L., Turner, J.N., Shain, W., Kim, S.J., 2007. Low-density neuronal networks cultured using patterned poly-l-lysine on microelectrode arrays. J. Neurosci. Methods 160, 317–326.
Kaneko, T., Toriumi, H., Shimada, J., Nomura, F., 2018. Extracellular field potential recording of single cardiomyocytes in agarose microchambers using microelectrode array. Jpn. J. Appl. Phys. 57, 03EB03.
Kang, G., Lee, J.-H., Lee, C.-S., Nam, Y., 2009. Agarose microwell based neuronal micro-circuit arrays on microelectrode arrays for high throughput drug testing. Lab Chip 9, 3236–3242.
Kang, H., Kim, J.-Y., Choi, Y.-K., Nam, Y., 2017. Feasibility Study of Extended-Gate-Type Silicon Nanowire Field-Effect Transistors for Neural Recording. Sensors 17, 705.
Keefer, E.W., Botterman, B.R., Romero, M.I., Rossi, A.F., Gross, G.W., 2008. Carbon nanotube coating improves neuronal recordings. Nat. Nanotechnol. 3, 434–439.
Khoshfetrat Pakazad, S., Savov, A.M., Van De Stolpe, A., Braam, S., Van Meer, B., Dekker, R., 2011. A stretchable micro-electrode array for in vitro electrophysiology. Proc. IEEE Int. Conf. Micro Electro Mech. Syst. 829–832.
Kim, R., Nam, Y., 2015. Electrochemical layer-by-layer approach to fabricate mechanically stable platinum black microelectrodes using a mussel-inspired polydopamine adhesive. J. Neural Eng. 12, 026010.

Kim, Y.H., Kim, G.H., Baek, N.S., Han, Y.H., Kim, A.-Y., Chung, M.-A., Jung, S.-D., 2013. Fabrication of multi-electrode array platforms for neuronal interfacing with bi-layer lift-off resist sputter deposition. J. Micromechanics Microengineering 23, 097001.

Kiran, R., Rousseau, L., Lissorgues, G., Scorsone, E., Bongrain, A., Yvert, B., Picaud, S., Mailley, P., Bergonzo, P., 2012. Multichannel Boron Doped Nanocrystalline Diamond ultramicroelectrode arrays: Design, fabrication and characterization. Sensors 12, 7669–7681.

Kireev, D., Seyock, S., Ernst, M., Maybeck, V., Wolfrum, B., Offenhäusser, A., 2016. Versatile flexible graphene multielectrode arrays. Biosensors 7, 1–9.

Kireev, D., Seyock, S., Lewen, J., Maybeck, V., Wolfrum, B., Offenhäusser, A., 2017. Graphene Multielectrode Arrays as a Versatile Tool for Extracellular Measurements. Adv. Healthc. Mater. 6, 1601433.

Koerbitzer, B., Krauss, P., Nick, C., Yadav, S., Schneider, J.J., Thielemann, C., 2016. Graphene electrodes for stimulation of neuronal cells. 2D Mater. 3, 024004.

Koester, P.J., Tautorat, C., Reimer, T., Zwanzig, M., Baumann, W., Gimsa, J., 2010. Gold Shark Teeth Structures on MEAs - Electroplating of Nano-Structures on Metallic Microelectrodes, in: Stett, A. (Ed.), 7th Int. Meeting on Substrate-Integrated Microelectrode Arrays, June 29 - July 2, 2010. BIOPRO Baden-Württemberg GmbH, Reutlingen, pp. 289–290.

Krause, M., 2000. Extended gate electrode arrays for extracellular signal recordings. Sensors Actuators B Chem. 70, 101–107.

Kreutzer, J., Ylä-Outinen, L., Kärnä, P., Kaarela, T., Mikkonen, J., Skottman, H., Narkilahti, S., Kallio, P., 2012. Structured PDMS Chambers for Enhanced Human Neuronal Cell Activity on MEA Platforms. J. Bionic Eng. 9, 1–10.

Kshirsagar, P., Burkhardt, C., Mierzejewski, M., Chassé, T., Fleischer, M., Jones, P.D., 2018. Graphene-based transparent microelectrode arrays for optical access to the recording site, in: Front. Cell. Neurosci. Conference Abstract: MEA Meeting 2018 | 11th International Meeting on Substrate Integrated Microelectrode Arrays.

Lacour, S.P., Benmerah, S., Tarte, E., Fitzgerald, J., Serra, J., McMahon, S., Fawcett, J., Graudejus, O., Yu, Z., Morrison, B., 2010. Flexible and stretchable micro-electrodes for in vitro and in vivo neural interfaces. Med. Biol. Eng. Comput. 48, 945–954.

Lei, N., Ramakrishnan, S., Shi, P., Orcutt, J.S., Yuste, R., Kam, L.C., Shepard, K.L., 2011. High-resolution extracellular stimulation of dispersed hippocampal culture with high-density CMOS multielectrode array based on non-Faradaic electrodes. J. Neural Eng. 8, 044003.

Li, X., Pei, W., Tang, R., Gui, Q., Guo, K., Wang, Y., Chen, H., 2011. Investigation of flexible electrodes modified by TiN, Pt black and IrO x. Sci. China Technol. Sci. 54, 2305–2309.

López, J.M., Gordillo-Vázquez, F.J., Böhme, O., Albella, J.M., 2001. Low grain size TiN thin films obtained by low energy ion beam assisted deposition. Appl. Surf. Sci. 173, 290–295.

MacCarthy, N., Burke, M., Alderman, J., 2008. A Low Cost High Resolution Fabrication Process for Disposable MEAs, in: Conference Proceedings of the 6th International Meeting on Substrate-Integrated Micro Electrode Arrays July 8-11, 2008, Reutlingen, Germany.

Malmivuo, J., Plonsey, R., 1995. Bioelectromagnetism - Principles and Applications of Bioelectric and Biomagnetic Fields. Oxford University Press, New York.

Mandenius, C.F., Steel, D., Noor, F., Meyer, T., Heinzle, E., Asp, J., Arain, S., Kraushaar, U., Bremer, S., Class, R., Sartipy, P., 2011. Cardiotoxicity testing using pluripotent stem cell-derived human cardiomyocytes and state-of-the-art bioanalytics: A review. J. Appl. Toxicol. 31, 191–205.

Márton, G., Bakos, I., Fekete, Z., Ulbert, I., Pongrácz, A., 2014. Durability of high surface area platinum deposits on microelectrode arrays for acute neural recordings. J. Mater. Sci. Mater. Med. 25, 931–940.

Maybeck, V., Edgington, R., Bongrain, A., Welch, J.O., Scorsone, E., Bergonzo, P., Jackman, R.B., Offenhäusser, A., 2014. Boron-doped nanocrystalline diamond microelectrode arrays monitor cardiac action potentials. Adv. Healthc. Mater. 3, 283–289.

McConnell, E.R., McClain, M.A., Ross, J., LeFew, W.R., Shafer, T.J., 2012. Evaluation of multi-well microelectrode arrays for neurotoxicity screening using a chemical training set. Neurotoxicology 33, 1048–1057.

MCS, 2011. Microelectrode Array (MEA) Manual, 16.03.2011. ed. Multi Channel Systems MCS GmbH, Reutlingen.

Mierzejewski, M., Kshirsagar, P., Kraushaar, U., Heusel, G., Samba, R., Jones, P.D., 2018. Bringing transparent microelectrodes to market : Evaluation for production and real-world applications, in: Front. Cell. Neurosci. Conference Abstract: MEA Meeting 2018 | 11th International Meeting on Substrate Integrated Microelectrode Arrays.

Mohr, A., Finger, K.J., Göpel, W., Hämmerle, H., Nisch, W., 1996. Performance of a thin film microelectrode array for monitoring electrogenic cells in vitro. Sensors Actuators B Chem. 34, 265–269.

Morin, F., Nishimura, N., Griscom, L., LePioufle, B., Fujita, H., Takamura, Y., Tamiya, E., 2006. Constraining the connectivity of neuronal networks cultured on microelectrode arrays with microfluidic techniques: A step towards neuron-based functional chips. Biosens. Bioelectron. 21, 1093–1100.

Müller, J., Ballini, M., Livi, P., Chen, Y., Radivojevic, M., Shadmani, A., Viswam, V., Jones, I.L., Fiscella, M., Diggelmann, R., Stettler, A., Frey, U., Bakkum, D.J., Hierlemann, A., 2015. High-resolution CMOS MEA platform to study neurons at subcellular, cellular, and network levels. Lab Chip 15, 2767–2780.

Myers, F.B., Abilez, O.J., Zarins, C.K., Lee, L.P., 2011. Stimulation and artifact-free extracellular electrophysiological recording of cells in suspension. Proc. Annu. Int. Conf. IEEE Eng. Med. Biol. Soc. EMBS 4030–4033.

Nagarah, J.M., Stowasser, A., Parker, R.L., Asari, H., Wagenaar, D.A., 2015. Optically transparent multi-suction electrode arrays. Front. Neurosci. 9:384, 1–12.

Nam, Y., Musick, K., Wheeler, B.C., 2006. Application of a PDMS microstencil as a replaceable insulator toward a single-use planar microelectrode array. Biomed. Microdevices 8, 375–381.

Narkilahti, S., Ylä-Outinen, L., Sukki, L., Ryynänen, T., Mäkinen, M., Hyysalo, A., Kreutzer, J., 2014. A cell culturing platform, a cell culture system, and a method for modeling myelination in vitro. Patent application WO2015092141 (A1).

Nick, C., Thielemann, C., 2014. Are Carbon Nanotube Microelectrodes Manufactured from Dispersion Stable Enough for Neural Interfaces? Bionanoscience 4, 216–225.

Nisch, W., Böck, J., Egert, U., Hämmerle, H., Mohr, A., 1994. A thin film microelectrode array for monitoring extracellular neuronal activity in vitro. Biosens. Bioelectron. 9, 737–741.

Norlin, A., Pan, J., Leygraf, C., 2002. Investigation of interfacial capacitance of Pt, Ti and TiN coated electrodes by electrochemical impedance spectroscopy. Biomol. Eng. 19, 67–71.

Novak, J.L., Wheeler, B.C., 1986. Recording from the Aplysia abdominal ganglion with a planar microelectrode array. IEEE Trans. Biomed. Eng. 33, 196–202.

Nyberg, T., Shimada, A., Torimitsu, K., 2007. Ion conducting polymer microelectrodes for interfacing with neural networks. J. Neurosci. Methods 160, 16–25.

Oka, H., Shimono, K., Ogawa, R., Sugihara, H., Taketani, M., 1999. A new planar multielectrode array for extracellular recording: application to hippocampal acute slice. J. Neurosci. Methods 93, 61–67.

Ong, C.S., Fukunishi, T., Zhang, H., Huang, C.Y., Nashed, A., Blazeski, A., DiSilvestre, D., Vricella, L., Conte, J., Tung, L., Tomaselli, G.F., Hibino, N., 2017. Biomaterial-Free Three-Dimensional Bioprinting of Cardiac Tissue using Human Induced Pluripotent Stem Cell Derived Cardiomyocytes. Sci. Rep. 7, 4566.

Pancrazio, J.J., Bey, P.P., Loloee, A., Manne, S., Chao, H.C., Howard, L.L., Gosney, W.M., Borkholder, D.A., Kovacs, G.T.A., Manos, P., Cuttino, D.S., Stenger, D.A., 1998. Description and demonstration of a CMOS amplifier-based-system with measurement and stimulation capability for bioelectrical signal transduction. Biosens. Bioelectron. 13, 971–979.

Park, S., Song, Y.J., Boo, H., Chung, T.D., 2010. Nanoporous Pt microelectrode for neural stimulation and recording: In vitro characterization. J. Phys. Chem. C 114, 8721–8726.

Pekkanen-Mattila, M., Kerkelä, E., Tanskanen, J.M.A., Pietilä, M., Pelto-Huikko, M., Hyttinen, J., Skottman, H., Suuronen, R., Aalto-Setälä, K., 2009. Substantial variation in the cardiac differentiation of human embryonic stem cell lines derived and propagated under the same conditions—a comparison of multiple cell lines. Ann. Med. 41, 360–370.

Picollo, F., Battiato, A., Bernardi, E., Plaitano, M., Franchino, C., Gosso, S., Pasquarelli, A., Carbone, E., Olivero, P., Carabelli, V., 2016. All-carbon multi-electrode array for real-time in vitro measurements of oxidizable neurotransmitters. Sci. Rep. 6, 20682.

Pine, J., 1980. Recording action potentials from cultured neurons with extracellular microcircuit electrodes. J. Neurosci. Methods 2, 19–31.

Puurunen, R.L., 2014. A short history of atomic layer deposition: Tuomo Suntola's atomic layer epitaxy. Chem. Vap. Depos. 20, 332–344.

Ren, Y., Huang, S.H., Mosser, S., Heuschkel, M.O., Bertsch, A., Fraering, P.C., Chen, J.J.J., Renaud, P., 2015. A Simple and Reliable PDMS and SU-8 Irreversible Bonding Method and Its Application on a Microfluidic-MEA Device for Neuroscience Research. Micromachines 6, 1923–1934.

Ryynänen, T., Kujala, V., Ylä-Outinen, L., Kerkelä, E., Narkilahti, S., Lekkala, J., 2010a. Polystyrene coated MEA, in: Stett, A. (Ed.), 7th Int. Meeting on Substrate-Integrated Microelectrode Arrays. BIOPRO Baden-Württemberg GmbH, Reutlingen, pp. 265–266.

Ryynänen, T., Lekkala, J., 2018. Temperature effect on the baseline noise in MEA measurements, in: Eskola, H., Väisänen, O., Viik, J., Hyttinen, J. (Eds.), EMBEC 2017, NBC 2017, IFMBE Proceedings, IFMBE Proceedings. Springer Singapore, Singapore, pp. 5–8.

Ryynänen, T., Nurminen, K., Hämäläinen, J., Leskelä, M., Lekkala, J., 2010b. pH electrode based on ALD deposited iridium oxide. Procedia Eng. 5, 548–551.

Ryynänen, T., Pelkonen, A., Grigoras, K., Ylivaara, O.M.E., Hyvärinen, T., Ahopelto, J., Prunnila, M., Narkilahti, S., Lekkala, J., 2019. Microelectrode Array With Transparent ALD TiN Electrodes. Front. Neurosci. 13:226.

Samba, R., Fuchsberger, K., Matiychyn, I., Epple, S., Kiesel, L., Stett, A., Schuhmann, W., Stelzle, M., 2014. Application of PEDOT-CNT Microelectrodes for Neurotransmitter Sensing. Electroanalysis 26, 548–555.

Santoro, F., Schnitker, J., Panaitov, G., Offenhäusser, A., 2013. On chip guidance and recording of cardiomyocytes with 3D mushroom-shaped electrodes. Nano Lett. 13, 5379–5384.

Schmitt, G., Schultze, J.W., Faßbender, F., Buß, G., Lüth, H., Schöning, M.J., 2000. Passivation and corrosion of microelectrode arrays. Mater. Corros. 51, 20–25.

Schuettler, M., Doerge, T., Wien, S., Becker, S., 2005. Cytotoxicity of platinum black, in: Proceedings of the 10th Annual Conference of the International FES Society. Montreal, pp. 4–6.

Seidel, D., Jahnke, H.-G., Englich, B., Girard, M., Robitzki, A.A., 2017. In vitro field potential monitoring on a multi-microelectrode array for the electrophysiological long-term screening of neural stem cell maturation. Analyst 1929–1937.

Selvakumaran, J., Hughes, M.P., Keddie, J.L., Ewins, D.J., 2002. Assessing biocompatibility of materials for implantable microelectrodes using cytotoxicity and protein adsorption studies. 2nd Annu. Int. IEEE-EMBS Spec. Top. Conf. Microtechnologies Med. Biol. Proc. 261–264.

Sessolo, M., Khodagholy, D., Rivnay, J., Maddalena, F., Gleyzes, M., Steidl, E., Buisson, B., Malliaras, G.G., 2013. Easy-to-fabricate conducting polymer microelectrode arrays. Adv. Mater. 25, 2135–2139.

Smart, S.K., Cassady, A.I., Lu, G.Q., Martin, D.J., 2006. The biocompatibility of carbon nanotubes. Carbon N. Y. 44, 1034–1047.

Stein, B., George, M., Gaub, H.E., Parak, W.J., 2004. Extracellular measurements of averaged ionic currents with the light-addressable potentiometric sensor (LAPS). Sensors Actuators, B Chem. 98, 299–304.

Stett, A., Rudorf, R., Stein, B., Egert, U., Boven, K.-H., Gottschlich, N., Nisch, W., 2005. Perforated polyimide microelectrode arrays for single-cell and tissue recording, in: Mikrosystemtechnik Kongress 2005, 10.-12.10.2005. VDA Verlag GmbH, Freiburg, pp. 427–430.

Suchaneck, G., Norkus, V., Gerlach, G., 2001. Low-temperature PECVD-deposited silicon nitride thin films for sensor applications. Surf. Coatings Technol. 142–144, 808–812.

Suzuki, I., Fukuda, M., Shirakawa, K., Jiko, H., Gotoh, M., 2013. Carbon nanotube multi-electrode array chips for noninvasive real-time measurement of dopamine, action potentials, and postsynaptic potentials. Biosens. Bioelectron. 49, 1–6.

Suzuki, I., Sugio, Y., Jimbo, Y., Yasuda, K., 2005. Stepwise pattern modification of neuronal network in photo-thermally-etched agarose architecture on multi-electrode array chip for individual-cell-based electrophysiological measurement. Lab Chip 5, 241–247.

Takahashi, K., Yamanaka, S., 2006. Induction of Pluripotent Stem Cells from Mouse Embryonic and Adult Fibroblast Cultures by Defined Factors. Cell 126, 663–676.

Tang, C.S., Dusseiller, M., Makohliso, S., Heuschkel, M., Sharma, S., Keller, B., Vrs, J., Vo, J., 2006. Dynamic, Electronically Switchable Surfaces for Membrane Protein Microarrays. Anal Chem 78, 711–717.

Tang, R.Y., Pei, W.H., Chen, S.Y., Zhao, H., Chen, Y.F., Han, Y., Wang, C.L., Chen, H.D., 2014. Fabrication of strongly adherent platinum black coatings on microelectrodes array. Sci. China Inf. Sci. 57, 1–10.

Tanskanen, J.M.A., Kauppinen, P., Ryynänen, T., Lekkala, J., Hyttinen, J.A.K., 2010. On Microelectrode Impedance Measurements, in: Stett, A. (Ed.), 7th Int. Meeting on Substrate-Integrated Microelectrode Arrays. BIOPRO Baden-Württemberg GmbH, Reutlingen, pp. 243–244.

Tay, C.Y., Yu, H., Pal, M., Leong, W.S., Tan, N.S., Ng, K.W., Leong, D.T., Tan, L.P., 2010. Micropatterned matrix directs differentiation of human mesenchymal stem cells towards myocardial lineage. Exp. Cell Res. 316, 1159–1168.

Thiébaud, P., Beuret, C., Koudelka-Hep, M., Bove, M., Martinoia, S., Grattarola, M., Jahnsen, H., Rebaudo, R., Balestrino, M., Zimmer, J., Dupont, Y., 1999. An array of Pt-tip

microelectrodes for extracellular monitoring of activity of brain slices. Biosens. Bioelectron. 14, 61–65.
Thomas, C.A., Springer, P.A., Loeb, G.E., Berwald-Netter, Y., Okun, L.M., 1972. A miniature microelectrode array to monitor the bioelectric activity of cultured cells. Exp. Cell Res. 74, 61–66.
Toivanen, M., Pelkonen, A., Mäkinen, M., Ylä-Outinen, L., Sukki, L., Kallio, P., Ristola, M., Narkilahti, S., 2017. Optimised PDMS Tunnel Devices on MEAs Increase the Probability of Detecting Electrical Activity from Human Stem Cell-Derived Neuronal Networks. Front. Neurosci. 11:606, 1–12.
Tonomura, W., Moriguchi, H., Jimbo, Y., Konishi, S., 2010. Parallel multipoint recording of aligned and cultured neurons on micro channel array toward cellular network analysis. Biomed. Microdevices 12, 737–43.
Trantidou, T., 2014. Application of Parylene C thin films in cardiac cell culturing. Imperial College of Science, Technology and Medicine University of London.
Tyler, P.E., Rajaraman, S., 2016. A 48-well transparent microelectrode array fabricated utilizing a flexible, "wrapped around" interconnect technology, in: 2016 IEEE SENSORS. IEEE, pp. 1–3.
Urbanová, V., Li, Y., Vytřas, K., Yvert, B., Kuhn, A., 2011. Macroporous microelectrode arrays for measurements with reduced noise. J. Electroanal. Chem. 656, 91–95.
Van Pelt, J., Wolters, P.S., Corner, M.A., Rutten, W.L.C., Ramakers, G.J.A., 2004. Long-Term Characterization of Firing Dynamics of Spontaneous Bursts in Cultured Neural Networks. Ieee Trans. Biomed. Eng. 51, 2051–2062.
Viitanen, J., Heimala, P., Hokkanen, A., Iljin, K., Kerkelä, E., Kolari, K., Kattelus, H., 2011. Stimulation of human embryonic stem cell-derived cardiomyocytes on thin-film microelectrodes. Biotechnol. J. 6, 600–603.
Wang, K., Fishman, H. a., Dai, H., Harris, J.S., 2006. Neural stimulation with a carbon nanotube microelectrode array. Nano Lett. 6, 2043–2048.
Wang, L., Liu, L., Li, X., Magome, N., Agladze, K., Chen, Y., 2013. Microelectronic Engineering Multi-electrode monitoring of guided excitation in patterned cardiomyocytes. Microelectron. Eng. 111, 267–271.
Weiland, J.D., Anderson, D.J., Humayun, M.S., 2002. In vitro electrical properties for iridium oxide versus titanium nitride stimulating electrodes. IEEE Trans. Biomed. Eng. 49, 1574–1579.
Wesche, M., Hüske, M., Yakushenko, A., Brüggemann, D., Mayer, D., Offenhäusser, A., Wolfrum, B., 2012. A nanoporous alumina microelectrode array for functional cell-chip coupling. Nanotechnology 23, 495303.
Whittington, R.H., Giovangrandi, L., Kovacs, G.T.A., 2005. A Closed-Loop Electrical Stimulation System for Cardiac Cell Cultures 52, 1261–1270.
Xiang, G., Pan, L., Huang, L., Yu, Z., Song, X., Cheng, J., Xing, W., Zhou, Y., 2007. Microelectrode array-based system for neuropharmacological applications with cortical neurons cultured in vitro. Biosens. Bioelectron. 22, 2478–2484.
Xiao, L., Chen, Q., Liu, Q., Wang, P., 2010. Microelectrode Array (MEA) as Cell-Based Biosensors, Cell-Based Biosensors - Principles and Application. Artech House, Norwood, MA.
Yamanaka, S., 2009. A Fresh Look at iPS Cells. Cell 137, 13–17.
Yeung, C.K., Sommerhage, F., Wrobel, G., Offenhäusser, A., Chan, M., Ingebrandt, S., 2007. Drug profiling using planar microelectrode arrays. Anal. Bioanal. Chem. 387, 2673–2680.

Zhang, W.Y., Labukas, J.P., Tatic-Lucic, S., Larson, L., Bannuru, T., Vinci, R.P., Ferguson, G.S., 2005. Novel room-temperature first-level packaging process for microscale devices. Sensors Actuators, A Phys. 123–124, 646–654.

Zhao, Y., Inayat, S., Dikin, D.A., Singer, J.H., Ruoff, R.S., Troy, J.B., 2008. Patch clamp technique: Review of the current state of the art and potential contributions from nanoengineering. Proc. Inst. Mech. Eng. Part N J. Nanoeng. Nanosyst. 222, 1–11.

Zhou, T., Perry, S.F., Berdichevsky, Y., Petryna, S., Fluck, V., Tatic-Lucic, S., 2015. Multi-electrode array capable of supporting precisely patterned hippocampal neuronal networks. Biomed. Microdevices 17, 1–12.

Zhu, H., Scharnhorst, K.S., Stieg, A.Z., Gimzewski, J.K., Minami, I., Nakatsuji, N., Nakano, H., Nakano, A., 2017. Two dimensional electrophysiological characterization of human pluripotent stem cell-derived cardiomyocyte system. Sci. Rep. 7, 43210.

PUBLICATIONS

PUBLICATION I

All Titanium Microelectrode Array for Field Potential Measurements from Neurons and Cardiomyocytes–A Feasibility Study

Ryynänen, T., Kujala, V., Ylä-Outinen, L., Korhonen, I., Tanskanen, J.M.A., Kauppinen, P., Aalto-Setälä, K., Hyttinen, J., Kerkelä, E., Narkilahti, S., Lekkala, J.

Micromachines (2011), 2(4), 394–409
https://doi.org/10.3390/mi2040394

Micromachines **2011**, *2*, 394-409; doi:10.3390/mi2040394

OPEN ACCESS

micromachines

ISSN 2072-666X

www.mdpi.com/journal/micromachines

Article

All Titanium Microelectrode Array for Field Potential Measurements from Neurons and Cardiomyocytes—A Feasibility Study

Tomi Ryynänen [1,*], Ville Kujala [2], Laura Ylä-Outinen [2], Ismo Korhonen [2], Jarno M.A. Tanskanen [3], Pasi Kauppinen [3], Katriina Aalto-Setälä [2,4], Jari Hyttinen [3], Erja Kerkelä [2,†], Susanna Narkilahti [2] and Jukka Lekkala [1]

[1] Department of Automation Science and Engineering, Tampere University of Technology, Korkeakoulunkatu 3, FI-33720 Tampere, Finland; E-Mail: jukka.lekkala@tut.fi (J.L.)

[2] Institute for Biomedical Technology, University of Tampere, Biokatu 12, FI-33520 Tampere, Finland; E-Mails: ville.kujala@uta.fi (V.K.); laura.yla-outinen@uta.fi (L.Y.-O.); ismo.korhonen@tut.fi (I.K.); katriina.aalto-setala@uta.fi (K.A.-S.); erja.kerkela@veripalvelu.fi (E.K.); susanna.narkilahti@uta.fi (S.N.)

[3] Department of Biomedical Engineering, Tampere University of Technology, Biokatu 6, FI-33520 Tampere, Finland; E-Mails: jarno.m.tanskanen@tut.fi (J.M.A.T.); pasi.kauppinen@tut.fi (P.K.); jari.hyttinen@tut.fi (J.H.)

[4] Heart Center, Tampere University Hospital, Biokatu 6, FI-33520 Tampere, Finland

† Current address: Finnish Red Cross Blood Service, Kivihaantie 7, FI-00310 Helsinki, Finland

* Author to whom correspondence should be addressed; E-Mail: tomi.ryynanen@tut.fi; Tel.: +358-3-3115-11; Fax: +358-4219-198-1189.

Received: 19 September 2011; in revised form: 19 October 2011 / Accepted: 20 October 2011 / Published: 28 October 2011

Abstract: In this paper, we describe our all-titanium microelectrode array (tMEA) fabrication process and show that uncoated titanium microelectrodes are fully applicable to measuring field potentials (FPs) from neurons and cardiomyocytes. Many novel research questions require custom designed microelectrode configurations different from the few commercially available ones. As several different configurations may be needed especially in a prototyping phase, considerable time and cost savings in MEA fabrication can be achieved by omitting the additional low impedance microelectrode coating, usually made of titanium nitride (TiN) or platinum black, and have a simplified and easily processable

MEA structure instead. Noise, impedance, and atomic force microscopy (AFM) characterization were performed to our uncoated titanium microelectrodes and commercial TiN coated microelectrodes and were supplemented by FP measurements from neurons and cardiomyocytes on both platforms. Despite the increased noise levels compared to commercial MEAs our tMEAs produced good FP measurements from neurons and cardiomyocytes. Thus, tMEAs offer a cost effective platform to develop custom designed electrode configurations and more complex monitoring environments.

Keywords: microelectrode array (MEA); measurement noise; impedance; stem cell; field potential measurement; titanium

1. Introduction

In this paper, we introduce a relatively inexpensive method to fabricate custom microelectrode arrays (MEAs). Since the early 1970s, MEAs have been used [1], now for almost four decades, as powerful tools to measure field potentials (FPs) from various kinds of tissues and cell cultures, including neurons and cardiomyocytes. With MEAs it is possible to study the electrical activity on cell population level instead of single cells measured using patch clamp analysis.

MEA platforms have been widely used in neuroscience research. Acute tissue slices, primary cells as well as cell lines can be cultured on different types of MEAs and their neuronal electrical activities can be measured [2-5]. MEAs offer useful, non-invasive, repeatable, and long term setups for neuronal network activity measurements that can be used to study spontaneous activity, effects of electrical and chemical stimuli, and plasticity [6-9]. Additionally, they can be used for drug screening purposes and for toxicological studies [10,11]. Nevertheless, only a few MEA studies have been conducted with human-derived neurons. Especially for drug screening or tissue engineering purposes, the use of human-derived neurons [6,12] would be important.

MEAs serve also as a valuable tool in studying the basic electrophysiology of cardiomyocytes [13]. MEAs have been used in conduction studies of cardiomyocytes derived from human embryonic stem cells (hESCs) [14], for analyzing cardiomyocytes derived from different hESC lines [15] and for studying *in vitro* pharmacology of the hESC-derived cardiomyocytes [15-18]. The field potential duration (FPD) on MEAs has been shown to correspond to the QT prolongation potential of different drugs indicating that the platform may be useful in safety assays [19].

Most of the current *in vitro* research can well be performed using the commercially available MEAs. Novel research questions including controlled growth of cell networks, complex and sensor controlled cell culturing environments for long term measurements, or just new material trials are, however, constantly increasing demand for custom designed MEAs. Especially the prototyping phase of new ideas would benefit from MEA platforms enabling fast and low cost customization.

When fabrication costs of a set of MEAs with several custom designed electrode configurations is considered, there are practically two ways to cut the costs. The first one is cutting the lithography mask costs, which can be achieved for example by reducing the area of the microlithographically patterned part [20,21], direct writing the custom patterns [22], or utilizing inexpensive film masks, which have

been applied, even though not discussed, also in this paper. Another way to cut the fabrication costs and also time, is to keep the MEA structure as simple as possible. It is clear that substrate, metal layer including electrodes, contact pads, and tracks, and an insulator layer are needed. The necessity of one more common part in the MEA structure, the additional microelectrode coating, however, can be questioned.

Throughout MEA history, engineers have tried to improve the measurement and stimulation capabilities of the microelectrodes by applying an additional coating on a microelectrode base material. The coating is usually aimed to reduce noise and improve the impedance characteristics and charge transfer capacity of the microelectrodes, which affect the probability of detecting cellular activity and the stimulation capability. Wide availability and sufficiently good electrical characteristics have made platinum black (Pt black) probably the most commonly used microelectrode surface coating throughout MEA history [1,4,23,24], even if it suffers from adhesion and reproducibility problems [25,26]. TiN is the microelectrode surface material favored by one of the leading commercial MEA manufacturers (Multi Channel Systems (MCS), Reutlingen, Germany) [27-29]. Iridium oxide (IrOx) is widely studied, even though not yet commercialized, microelectrode coating that has excellent charge transfer capacity and high long term stability, but suffers from need for electrochemical (re)activation [25,26,30]. There is no common opinion whether TiN or IrOx has better characteristics [26,28,31]. Recently several groups have reported microelectrodes coated with carbon nanotubes (CNTs) [32-35] which have not only superior electrical properties but also support cell adhesion via extremely rough surface [34]. There are, however, general concerns related to the biocompatibility [36] and mechanical stability [26,35] of the CNT coatings. Expensive materials and in some cases necessary special devices and special expertise for reactive or otherwise complex processes make the additional coating often the most expensive, time consuming, and error prone phase in the MEA fabrication—an issue which can be ignored at most by very experienced and well equipped organizations. Thus if the sufficient MEA performance level can be reached without the additional coating, it may lead to significant cost and time savings in MEA fabrication.

MEAs with gold, platinum, or indium tin oxide (ITO) microelectrodes without additional coating are commercially available [20], but certain aspects, e.g., material costs and processing difficulties, make those materials less attractive for simple and low cost fabrication schemes. Titanium, on the other hand, is a common, easy to process, and highly biocompatible electrode material. Titanium has not, however, been employed as sole MEA microelectrode material, but always either only as thin adhesion layer for some other metal [2,3,24,30] or coated with titanium nitride (TiN) [27]. The rationale against using titanium microelectrodes without additional coating may be the existence of a few nanometers thick dielectric native oxide (TiO_2) layer which always forms on a titanium surface in air. However, direct tunneling through the thin dielectric layer [37], existence of conducting suboxides [37-39], and impurities originating from the glass surface prior to titanium deposition [38] have been proposed to account for local electron transfer through the native oxide layer, thus giving rise to sufficient conductivity.

The aim of this study is to show that the FP measurement capabilities of titanium microelectrodes without any additional surface coating are well comparable to standard microelectrodes used today. As shown in this paper, with our in-house MEAs (later referred to as tMEAs), such microelectrodes are

fully capable for FP measurements from neurons and cardiomyocytes, yielding signal quality well sufficient for the intended analysis purposes.

2. Methods

2.1. tMEA Fabrication

Our in-house built tMEAs have 58 microelectrodes in 8 × 8 square matrix format, with one microelectrode missing from each corner and two microelectrodes missing from both sides close to the central line. There are two large electrodes on both sides of the matrix which can be used as measurement reference, ground, and stimulation electrodes. In the first batch of tMEAs (later referred to as old tMEAs, because of being used in biological measurements before noise and impedance measurements), all the microelectrodes were square shaped and approximately 30 × 30 µm in size. The second batch of tMEAs (later referred to as new tMEAs, because not used in biological measurements before other measurements) suffered from certain processing condition failures causing microelectrode size variation and rounding of the intended square shape with the average microelectrode diameter of 23 µm. To verify noise performance vs. electrode area dependence, some of the microelectrodes were made larger (55 µm in diameter). The inter-electrode distance was 200 µm in all tMEAs.

The fabrication process of tMEAs is illustrated in Figure 1. Briefly, a 0.9 mm thick Schott Desag D263 glass (Schott, Mainz, Germany) was chosen for the substrate material due to its high mechanical durability. The glass was cut into 49 × 49 mm size wafers, cleaned with dishwashing liquid, water and ethanol, and e-beam coated with 300 nm layer of titanium at Oplatek Oy (Leppävirta, Finland). Before proceeding to the next lithographic steps, the glass wafers were cleaned with acetone, 2-propanol, and de-ionized water. Spin coated hexamethyldisilazane (HMDS, Acros Organics, Geel, Belgium) was used as photoresist adhesion promoter followed with immediate spin coating of ma-P 1225 positive photoresist (micro resist technology, Berlin, Germany) to ~2.2 µm thickness that was further baked on the wafers. Next, the microelectrode pattern from laser photoplotted mask was UV-exposed, developed, and hardbaked on photoresist.

Figure 1. Fabrication process of tMEAs: **(a)** Bulk glass wafer; **(b)** Titanium coating; **(c)** Photoresist coating; **(d)** UV-exposure and development; **(e)** Wet etching and resist removal; **(f)** PECVD deposition of Si_3N_4; **(g)** Photoresist coating; **(h)** UV-exposure and development; and **(i)** Dry etching and resist removal. Images are not to scale.

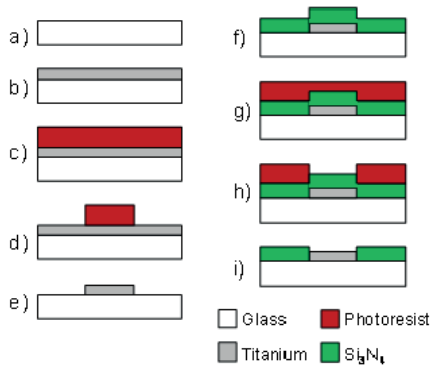

Wet etching (20 H_2O:1 H_2O_2 (30%):1 HF) was used to transfer the microelectrode pattern from the photoresist layer to titanium. After cleaning the wafer from remaining photoresist, a 500 nm layer of silicon nitride (Si_3N_4) was PECVD deposited as dielectric insulating layer at Optoelectronics Research Centre (ORC, Tampere University of Technology, Tampere, Finland). Lithographic steps for making openings for electrodes and contact pads in the insulator layer were performed with the same procedures as the patterning of titanium described above. After the hardbake step, however, reactive ion etching with SF_6 and O_2 gases [40] was applied instead of wet etching. In final fabrication step, a short oxygen plasma treatment (O_2 30 sccm, RF power 30 W, pressure 30 mTorr), was run in reactive ion etcher (RIE, Advanced Vacuum Vision 320, Advanced Vacuum, Lomma, Sweden) to make the surface hydrophilic.

2.2. Commercial MEAs Used for Comparison

The commercial MEAs (later referred to as cMEAs) used in the study were standard MEAs of type 200/30iR-Ti (MCS). The 59 round microelectrodes in 8 × 8 square format had the diameter of 30 µm and the inter-electrode distance of 200 µm. Titanium was used as a conductor base material and, unlike in tMEAs, both the electrodes and the contact pads were coated with TiN. Alike in tMEAs, 500 nm PECVD silicon nitride was used as an insulator layer [27]

2.3. Noise Measurements

Noise and biological FP measurements were performed with MEA1060-Inv-BC amplifier and MC_Rack software, both from MCS. The noise signal was recorded from MEAs filled with cardiomyocyte cell culture medium (EB-medium) without cells, at first for three minutes immediately after filling the MEAs, and after one and two hours to see how the noise behaves as a function of time. The measurement sampling frequency was 20 kHz. Total of three new and three old tMEAs and three new and three old cMEAs were measured.

From each MEA, 6 microelectrodes from the second row were chosen for noise analysis. From the data, we calculated root mean square (RMS) noise for each microelectrode by using the following formula:

$$RMS = \sqrt{\frac{1}{n}\sum_{i=1}^{n} x_i^2} \tag{1}$$

where n is the number of samples in the measured signal and x_i is the voltage sample measured at time i. For each MEA, an average RMS noise was calculated. Thereafter, average RMS noise for each MEA type was calculated from the average RMS noises of individual MEAs. As it has been shown that the noise of microelectrodes is inversely related to the square root of the electrode area [41], for fair comparisons between tMEAs and cMEAs, the RMS noise levels of tMEA microelectrodes were normalized to correspond to the RMS noise level of a microelectrode with the area equal to the area of a cMEA microelectrode.

Noise voltage spectra over the frequency range from 0.3 Hz to 10 kHz were plotted using the Welch estimate method [42] with the 50% overlapping and window length of 60615 samples. Estimates were calculated with a Measurement Signal Processing (MSP) toolbox [43] for Matlab. Also noise voltage histograms with 200 bins of width 20 µV were calculated for the microelectrodes.

2.4. Impedance Measurements

Impedances of the tMEA and cMEA microelectrodes were measured using Solartron Analytical 1260A Impedance/Gain-phase Analyzer (Solartron Analytical, Hampshire, UK) connected to Solartron 1294A Impedance Interface, whose four-terminal non-human interface was utilized, and connected according to the two-terminal impedance measurement configuration described in [44]. 1294A was connected to a MEA via MEA1060-Inv contacting adapter (MCS). The MEAs were let stabilize at least over night at room temperature in isotonic saline (sodium chloride 9 mg/mL, Baxter, Lessines, Belgium), rinsed with distilled water, and let stabilize for at least one hour filled with the cardiac cell culture medium (described in detail in Section 2.6) prior to impedance measurement. The contact pins of the contacting adapter and the MEA contact pads were cleaned with 70% ethanol. The temperature of a MEA was allowed to stabilize to approximately 37 °C for at least three minutes in the contacting adapter. Impedance measurement current was set to 10 μA. Current driven measurement setup was selected to ensure that the current density remained sufficiently low (approx. 14 mA/mm^2 for a microelectrode diameter of 30 μm) regardless of microelectrode impedances.

Impedances were measured at 1 kHz, which is the common practice also in commercial MEA datasheets, and data was recorded using SMaRT software (Solartron Analytical). With tMEAs, the ground electrode on the same side of the MEA as in the cMEAs was used. For fair comparison between tMEAs and cMEAs, the impedance magnitudes of the tMEA microelectrodes were normalized by the microelectrode surface areas so that all impedance magnitudes are presented for microelectrodes with the surface area of cMEA microelectrodes. In the sequel, this is referred to as area-normalization.

As one potential source for lower impedance is the bigger effective surface area, we also performed atomic force microscopy (AFM) measurements (XE-100 AFM, Park Systems, Suwon, Korea) to assess effective surface area difference between titanium and TiN surfaces. For each MEA type 1 μm × 1 μm scans including 256 × 256 pixels were performed in a tapping mode.

2.5. Assessment of Neuronal Cell FP Measurement Capabilities

The neural differentiation of hESCs was performed as reported [45,46] and MEA preparation and measurements were performed as described earlier [6]. Prior to cell seeding, the MEAs were coated with two step coating procedure with 0.05%(w/v) polyethylenimine (PEI) and mouse laminin, 20 μg/mL (both from Sigma-Aldrich, St. Louis, MO, USA). Thereafter, neurospheres, predifferentiated from hESCs for 8 weeks, were cut into small aggregates (∅ ~100 μm) and seeded onto coated MEA plates. Neuronal culture consisted of 1:1 DMEM/F12 and Neurobasal media supplemented with 2 mM GlutaMax, 1 × B27, 1 × N2 (all from Invitrogen, Carlsbad, CA, USA), and 25 U/mL penicillin/streptomycin (Lonza, Basel, Switzerland). The medium was changed 3 times per week. The cells were cultured for 21 days *in vitro* (DIV) on three tMEAs and on three cMEAs. Spontaneous activities of neuronal networks were measured for five minutes once a week. Neuronal action potential spike detection was performed based on an amplitude threshold at five times the signal standard deviation from the mean of the signal. Also, phase contrast microscope images were taken weekly.

2.6. Assessment of Cardiomyocyte FP Measurement Capabilities

Differentiation of hESC line H7 was performed as described earlier [47]. The MEAs were coated as follows: 30 minutes with fetal bovine serum (Gibco, Invitrogen) after which they were washed twice with sterile water and one hour with 0.1% gelatine type A (Sigma-Aldrich). After coating the MEAs, the spontaneously beating cardiomyocyte aggregates, excised from cell cultures mechanically, were plated onto the electrode areas in cell culture medium consisting of KO-DMEM (Invitrogen) supplemented with 20% FBS (Invitrogen), 1% NEAA (Lonza), 1% Glutamax (Invitrogen), and 50 U/mL penicillin/streptomycin (Lonza). The cells were cultured for 14 days *in vitro* on four tMEAs and on three cMEAs. After 14 days in culture on MEA, baseline electrical signal was recorded and the effect of E-4031 (Alomone Labs, Jerusalem, Israel), a known blocker of human ether-a-go-go potassium current at the concentration of 300 nM was analyzed in order to test whether tMEAs were sensitive enough to detect changes in the cardiac repolarization current.

3. Results and Discussion

3.1. tMEA Fabrication

By omitting additional microelectrode coating we were able to save at least one deposition step compared to Pt black coated microelectrodes [24] and one deposition and one lift-off process step, compared to TiN coating [29]. Depending on the selected fabrication method, CNT and IrOx coatings might need even more process steps. Cutting process steps does not only save time and money, but decreases the risk of process failures and increases the repeatability of the fabrication process. In the case of integrating sensors or cell growth guiding structures on MEAs or replacing chemically and thermally durable glass substrate or silicon nitride insulator layer by some polymer based materials [48,49], each additional process step might be even fatal for the most sensitive layers or force to make unpractical changes in the fabrication process chain.

3.2. Noise Analysis

Even if precise statistical analysis was omitted due to difficulty of defining the exact area of each individual arbitrary shaped microelectrode, a rough comparison of RMS noise levels between the normal approximately 23 μm microelectrodes and 55 μm control microelectrodes of new tMEAs allowed us to conclude that at least on average, the tMEAs follow the theory of the noise of electrodes being inversely related to the square root of the electrode area [41]. Thus, we were able to normalize the RMS noise data of tMEAs to correspond the electrode size of cMEAs, *i.e.*, 30 μm in diameter.

The average measured RMS noises both from three new and three old tMEAs and cMEAs with average deviations along with the area normalized average RMS noises of tMEAs are all shown in Table 1. The results indicate roughly 33% higher noise for the new tMEAs compared to new cMEAs and roughly 90% higher noise for the old tMEAs compared to old cMEAs. The lower noise of old MEAs compared to new MEAs is probably mainly due to electrode surface modifications caused by long term exposure to cell and culture medium. At least for tMEAs, but possibly also for cMEAs, the batch to batch variations partly explain the noise variations. The uncontrolled long term natural

oxidation of titanium may partly explain the ten times larger deviation in average RMS noise from MEA to MEA observed in tMEAs compared to cMEAs. Another explanation for the larger deviation is tMEAs' presumably bigger deviation also on microelectrode sizes and other MEA structure dimensions compared to cMEAs.

Table 1. Average RMS noise and impedance magnitudes (area-normalized) comparison of three new (unused) and three old (previously used in biological measurements) tMEAs and cMEAs at three different times after filling the MEAs with medium.

Time (h)	Average measured RMS noise (µV)	Average noise deviation (µV)	Average normalized RMS noise (µV)	Average normalized impedance magnitude at 1 kHz (kΩ)	Average normalized impedance magnitude deviation (kΩ)	Average measured RMS noise (µV)	Average noise deviation (µV)	Average normalized impedance magnitude at 1 kHz (kΩ)	Average normalized impedance magnitude deviation (kΩ)
	New tMEA					**New cMEA**			
0	8.3	3.7	7.5	-	-	5.7	0.3	-	-
1	7.1	1.1	6.4	126.6	39.1	4.9	0.3	54.8	1.0
2	7.1	2.1	6.3	-	-	4.7	0.3	-	-
	Old tMEA					**Old cMEA**			
0	5.1	1.6	5.8	-	-	2.7	0.2	-	-
1	4.3	2.7	4.8	68.0	20.4	2.7	0.1	42.5	2.5
2	4.3	1.7	4.8	-	-	2.7	0.1	-	-

Figure 2. (a) Typical noise voltage density spectra of old tMEA and cMEA microelectrodes at times of 0 h, 1 h, and 2 h after filling the MEAs with medium. Noise voltage histograms (200 bins of width 0.2 µV) at the time of 1 h time point are presented from the same **(b)** tMEA and **(c)** cMEA microelectrodes.

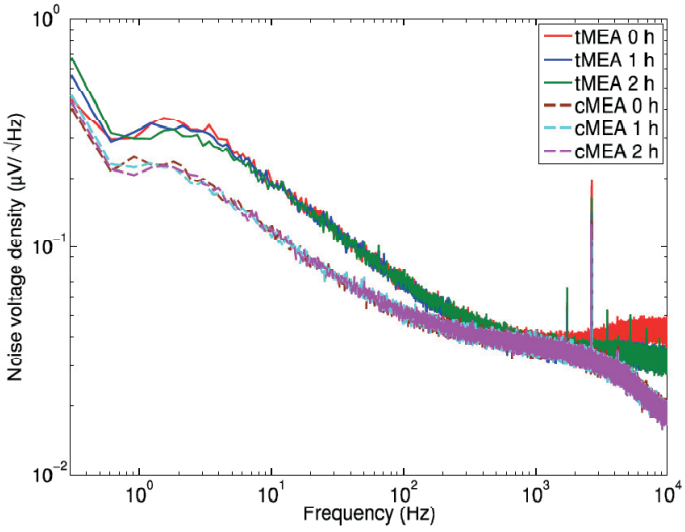

(a)

Figure 2. *Cont.*

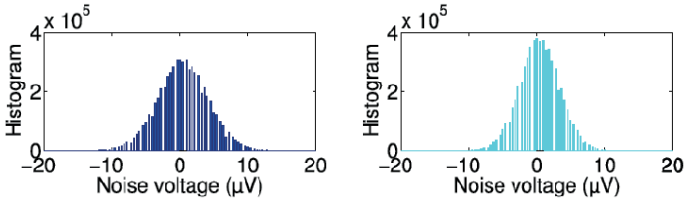

(b) **(c)**

Typical noise voltage spectra are shown in [Figure 2(a)] from one microelectrode of an old tMEA and an old cMEA 0, 1, and 2 h after filling the MEAs with medium. [Figure 2(b,c)] include 200 bin noise voltage histograms from the same microelectrodes at the 1 h time point. Both MEA types have quite constant spectrum behavior as a function of time over the full frequency range excluding the clear drop at very low frequency between 0 h and 1 h in tMEA's spectrum. At about 2,640 Hz, both MEA types exhibit a peak, which we assume to originate from the amplifier electronics. In general some microelectrodes of some MEAs of all types also exhibited other occasional peaks, induced by some random additional activity in the laboratory or some MEA or microelectrode specific defects. Observable of 50 Hz mains frequency peak was more common in tMEAs than cMEAs. The shape of the histograms resembles in both cases Gaussian, but as can be assumed, the distribution for the tMEAs is wider.

3.3. Impedance Magnitude Analysis

Average impedances measured at 1 kHz and normalized by the microelectrode area relative to that of the cMEA electrodes are given in Table 1 in conjunction with the corresponding average RMS noise values. The impedances of the tMEAs are on the average 60% higher for old MEAs and 130% higher for new MEAs than those of the corresponding cMEAs.

The impedance magnitude values measured for cMEAs are at the same level with the earlier reported values [27-29]. As no previous reports about titanium MEAs exist, there is no direct comparison to earlier results corresponding to tMEAs. However one order of magnitude difference in impedance has been reported for uncoated and TiN coated gold microelectrodes [28,29], and Pt and ITO microelectrodes of the corresponding size have been reported having impedances above 800 kΩ [20]. Even if different studies are not fully comparable due to obvious differences in impedance measurement arrangements and microelectrode sizes, still the impedance characteristics of titanium microelectrodes can be considered competitive to other single material microelectrodes.Typical AFM images of the microelectrode surface of tMEA and cMEA are presented in Figure 3. Due to the columnar morphology of the TiN coating [27,28] the AFM cantilever is able to measure only the very top surface of the TiN coating, giving no more than 10% increase in the effective surface area compared to the uncoated titanium. Thus, we suspect that our AFM has failed to convey full information of the fine surface structures, resulting in underestimating the effective surface area difference between tMEAs and cMEAs. The differences in noise and impedance values between tMEAs and cMEAs result from differences in effective surface areas due to different surface microstructures, and from different surface electrochemistries, including the natural oxidation of titanium.

Figure 3. AFM images from **(a)** all-titanium microelectrode of tMEA and **(b)** TiN coated microelectrode surface of cMEA. Note the different vertical z-axis scales.

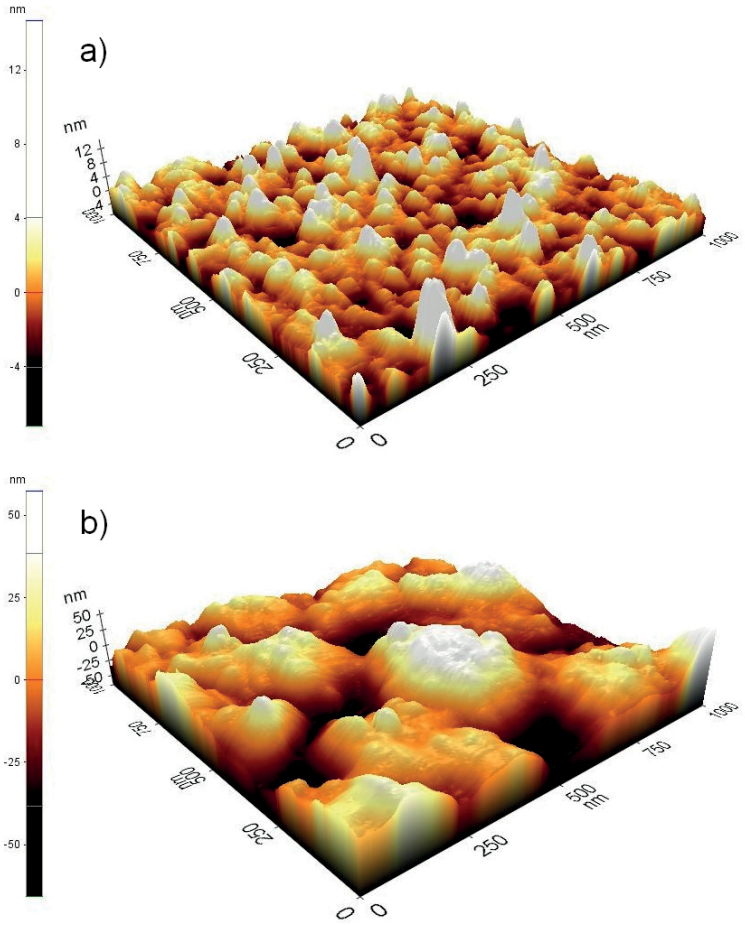

3.4. Viability and Electrical Signaling of Neurons on tMEAs

The neuronal aggregates attached successfully to all MEAs [Figure 4(a,c)]. The viability of the cells was similar on both tMEAs and cMEAs. Neurons started to grow processes and some cells migrated along these processes. In more detail, neuronal cells formed neural networks on tMEA surface and the spontaneous activity of the networks was measured with titanium microelectrodes [Figure 4(b)]. Corresponding spontaneous activity observed with cMEAs is presented in [Figure 4(d)]. Similarly, during the first week of culturing on MEA, the first individual spikes were detected on both MEA types. Further, the signaling developed as shown earlier [6] into more organized train-like activity [Figure 4(b,d)] and even burst activity. tMEAs had twice as high noise levels as the cMEAs, but the spikes were twice as high too. Thus tMEAs showed signal-to-noise (S/N) ratio comparable to cMEAs. The results support all-titanium MEAs' capability to function as an efficient and tunable tool for measuring neuronal activity and maturation with different electrode layouts.

Figure 4. Neuronal and cardiac electrical activities on old MEAs. Neuronal network formed **(a)** on tMEA and **(c)** on cMEA. Train-like activity **(b)** from tMEA and **(d)** from cMEA. Signals were measured after 2 weeks culturing on MEAs. Note the different y-axis scale in figures **(b)** and **(d)**; **(e)** Cardiac FP activity on tMEA over the two-week culture period. Note the increasing FP amplitudes; **(f)** 50% prolonged FPD by E-4031 hERG channel blocker, detected with tMEA. The arrows point out the ends of the repolarizations.

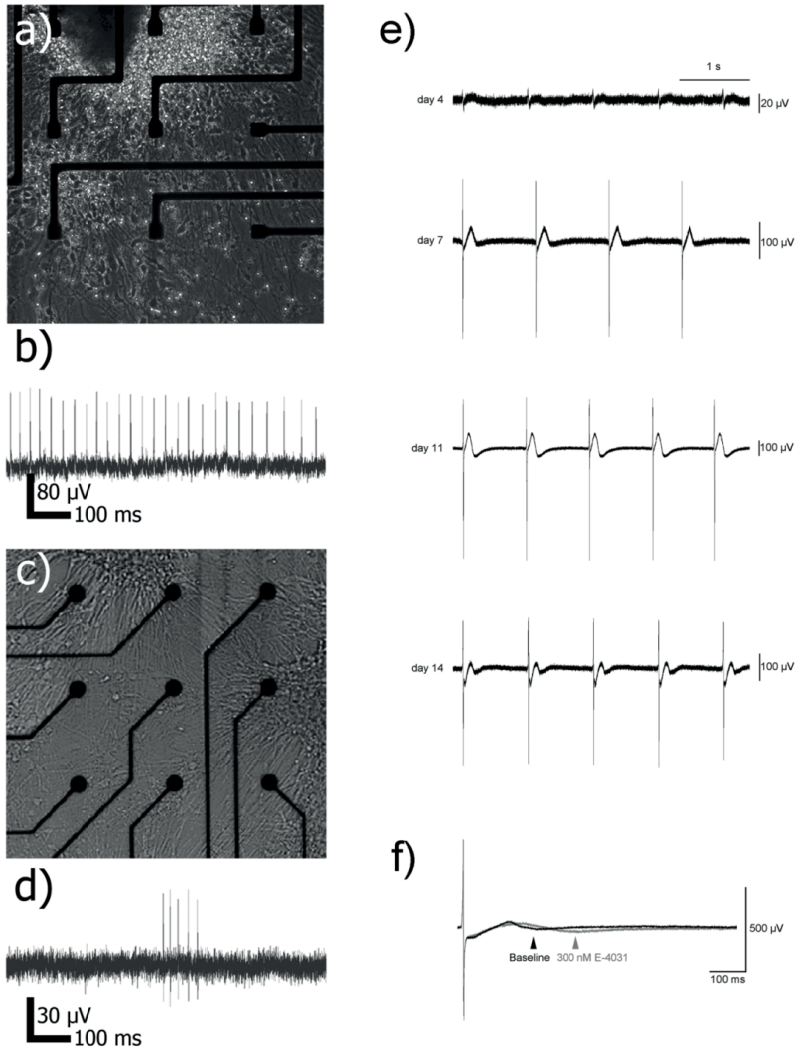

3.5. Viability and Electrical Signaling of Cardiomyocytes on tMEAs

The beating aggregates adhered well on tMEAs and no difference in adhesion property was detected compared to aggregates seeded on cMEAs. Upon inspection, the cardiomyocyte aggregates exhibited strong spontaneous contractility. We were able to record cardiac FP activity using tMEAs [Figure 4(e)]. The highest quality signals recorded were in the millivolt range. The FP signal generated by the spontaneously beating hESC-derived cardiomyocytes, was detected well with both tMEAs and cMEAs

from DIV 4 onward, which was the first day of recording. The signal amplitude grew larger over time reaching the peak value at DIV 7. The morphology of the signal was also better defined by that time, marked by a higher S/N ratio, which was a direct result of the larger systolic peak amplitude. This indicated stronger cell adhesion of the cardiomyocytes to the MEAs and better and more mature connection between cells. tMEAs tended to have greater variation in background noise levels between recordings of the same MEA than cMEAs. Also, a cardiac drug effect could be adequately and repeatedly recorded with tMEA. The hERG channel blocker E-4031, known to prolong QT time and FPD, prolonged FPD approximately 50% [Figure 4(f)]. All this indicates as a proof-of-concept that all-titanium MEAs can be used for drug testing and that the resolution of the signal generated is good enough to detect changes in FP morphology.

4. Conclusions

Our experiments with hESC-derived neurons and cardiomyocytes show that the performance of all-titanium MEA microelectrodes is comparable to MEAs with TiN coated microelectrodes when the recording of FP signals from neuronal cells or cardiomyocytes is considered. For certain type of applications requiring detection of very weak signals or exact signal morphology, all-titanium MEA, despite its comparable S/N ratio, may not be the optimal choice because of higher background noise and fluctuations. Furthermore, as the impedance measurement indicates, also the charge transfer capacity of titanium electrodes may have to be improved by some additional electrode surface coating for stimulation purposes, especially for cardiac cells—even though this was not fully evaluated in this paper. However, for many applications such as neuronal or cardiac activity, maturation, or drug testing where small additional noise is not an issue, the performance of all-titanium MEAs is adequate to detect neuronal spiking or changes in the cardiomyocyte FP morphology. The all-titanium technology presents us with several advantages in terms of modifying the MEA platform for future uses. These include being able to design and manufacture a variety of MEA layouts and microelectrode configurations in a cost and time effective manner e.g., for more complex experimental setups of neuronal network geometries or cardiomyocyte syncytium and connectivity studies.

Acknowledgements

This work was supported by the Academy of Finland (decision numbers 122947, 122959, 123233, 123359 and 123762), the Competitive Research Funding of the Tampere University Hospital, the Finnish Cultural Foundation, CHEMSEM graduate school, BioneXt Tampere, and Biosensing Competence Centre, BCC. The authors wish to thank all the current and past *Stemfunc* project members for the valuable comments and aid during the process towards this publication.

References

1. Thomas, C.A.; Springer, P.A.; Loeb, G.E.; Berwald-Netter, Y.; Okun, L.M. A miniature microelectrode array to monitor the bioelectric activity of cultured cells. *Exp. Cell. Res.* **1972**, *74*, 61-66.

2. Gross, G.W.; Reiske, E.; Kreutzberg, G.W.; Mayer, A. A new fixed-array multimicroelectrode system designed for long-term recording of extracellular single unit activity *in vitro*. *Neurosci. Lett.* **1977**, *6*, 101-105.
3. Gross, G.W. Simultaneous single unit recording *in vitro* with a photoetched laser deinsulated gold multi-microelectrode surface. *IEEE Trans. Biomed. Eng.* **1979**, *26*, 273-279.
4. Pine, J. Recording action potentials from cultured neurons with extracellular microcircuit electrodes. *J. Neurosci. Methods* **1980**, *2*, 19-31.
5. Johnstone, A.F.M.; Gross, G.W.; Weiss, D.G.; Schroeder, O.H.-U.; Gramowski, A.; Shafer, T.J. Microelectrode arrays: A physiologically based neurotoxicity testing platform for the 21st century. *Neurotoxicology* **2010**, *31*, 331-350.
6. Heikkilä, T.J.; Ylä-Outinen, L.; Tanskanen, J.M.; Lappalainen, R.S.; Skottman, H.; Suuronen, R.; Mikkonen, J.E.; Hyttinen, J.A.; Narkilahti, S. Human embryonic stem cell-derived neuronal cells form spontaneously active neuronal networks *in vitro*. *Exp. Neurol.* **2009**, *218*, 109-116.
7. Illes, S.; Fleischer, W.; Siebler, M.; Hartung, H.P.; Dihne, M. Development and pharmacological modulation of embryonic stem cell-derived neuronal network activity. *Exp. Neurol.* **2007**, *207*, 171-176.
8. Jimbo, Y.; Tateno, T.; Robinson, H.P. Simultaneous induction of pathway-specific potentiation and depression in networks of cortical neurons. *Biophys. J.* **1999**, *76*, 670-678.
9. Wagenaar, D.A.; Pine, J.; Potter, S.M. An extremely rich repertoire of bursting patterns during the development of cortical cultures. *BMC Neurosci.* **2006**, *7*, 11.
10. Bal-Price, A.K.; Hogberg, H.T.; Buzanska, L.; Lenas, P.; van Vliet, E.; Hartung, T. *In vitro* developmental neurotoxicity (DNT) testing: Relevant models and endpoints. *Neurotoxicology* **2010**, *31*, 545-554.
11. Ylä-Outinen, L.; Heikkilä, T.; Skottman, H.; Suuronen, R.; Äänismaa, R.; Narkilahti, S. Human cell-based micro electrode array platform for studying neurotoxicity. *Front. Neuroeng.* **2010**, *3*, 111.
12. Buzanska, L.; Zychowicz, M.; Ruiz, A.; Ceriotti, L.; Coecke, S.; Rauscher, H.; Sobanski, T.; Whelan, M.; Domanska-Janik, K.; Colpo, P.; *et al*. Neural stem cells from human cord blood on bioengineered surfaces—Novel approach to multiparameter bio-tests. *Toxicology* **2010**, *270*, 35-42.
13. Reppel, M.; Pillekamp, F.; Lu, Z.J.; Halbach, M.; Brockmeier, K.; Fleischmann, B.K.; Hescheler, J. Microelectrode arrays: A new tool to measure embryonic heart activity. *J. Electrocardiol.* **2004**, *37*, 104-109.
14. Kehat, I.; Gepstein, A.; Spira, A.; Itskovitz-Eldor, J.; Gepstein, L. High-resolution electrophysiological assessment of human embryonic stem cell-derived cardiomyocytes: A novel *in vitro* model for the study of conduction. *Circ. Res.* **2002**, *91*, 659-661.
15. Pekkanen-Mattila, M.; Kerkelä, E.; Tanskanen, J.M.A.; Pietilä, M.; Pelto-Huikko, M.; Hyttinen, J.; Skottman, H.; Suuronen, R.; Aalto-Setälä, K. Substantial variation in the cardiac differentiation of human embryonic stem cell lines derived and propagated under the same conditions—A comparison of multiple cell lines. *Ann. Med.* **2009**, *41*, 360-370.
16. Braam, S.R.; Tertoolen, L.; van de Stolpe, A.; Meyer, T.; Passier, R.; Mummery, C.L. Prediction of drug-induced cardiotoxicity using human embryonic stem cell-derived cardiomyocytes. *Stem Cell Res.* **2010**, *4*, 107-116.

17. Caspi, O.; Itzhaki, I.; Arbel, G.; Kehat, I.; Gepstien, A.; Huber, I.; Satin, J.; Gepstein, L. *In vitro* electrophysiological drug testing using human embryonic stem cell derived cardiomyocytes. *Stem Cells Dev.* **2009**, *18*, 161-172.
18. Reppel, M.; Pillekamp, F.; Brockmeier, K.; Matzkies, M.; Bekcioglu, A.; Lipke, T.; Nguemo, F.; Bonnemeier, H.; Hescheler, J. The electrocardiogram of human embryonic stem cell-derived cardiomyocytes. *J. Electrocardiol.* **2005**, *38*, 166-170.
19. Meyer, T.; Boven, K.H.; Gunther, E.; Fejtl, M. Micro-electrode arrays in cardiac safety pharmacology: A novel tool to study QT interval prolongation. *Drug Saf.* **2004**, *27*, 763-72.
20. Ayanda Biosystems SA. MEA Biochip Product Catalog. Available online: http://www.ayanda-biosys.com/Documents/MEA_Product_Catalog.pdf (accessed on 3 September 2010).
21. MacCarthy, N.; Burke, M.; Alderman, J. A Low Cost High Resolution Fabrication Process for Disposable MEAs. In *Proceedings of the 6th International Meeting on Substrate-Integrated Microelectrode Arrays*, Reutlingen, Germany, 8–11 July 2008; pp. 321-323.
22. Ryynänen, T.; Kattipparambil Rajan, D.; Lekkala, J. Concept for Low-Cost Rapid Prototyping of New MEA Designs. In *Proceedings of the 2009 Symposium on Microelectrode Arrays in Tissue Engineering (MEATE)*, Tampere, Finland, 4–5 June 2009.
23. Novak, J.L.; Wheeler, B.C. Recording from the Aplysia abdominal ganglion with a planar microelectrode array. *IEEE Trans. Biomed. Eng.* **1986**, *BME-33(February)*, 196-202.
24. Kim, J.S.; Lee, K.J.; Pak, J.J. The Effects of Pt Electroplating on the Multi-Electrode Array Surface in Measuring Neuronal Signal. Presented at *APCTP-KU Joint Conference on Bio-complexity*, Seoul, Republic of Korea, 2–5 November 2005; p. 10. Available online: http://mins.korea.ac.kr/bbs/?mid=conference&page=5&document_srl=1309 (accessed on 27 May 2011).
25. Gawad, S.; Giugliano, M.; Heuschkel, M.; Wessling, B.; Markram, H.; Schnakenberg, U.; Renaud, P.; Morgan, H. Substrate arrays of iridium oxide microelectrodes for *in vitro* neuronal intgerfacing. *Front. Neuroeng.* **2009**, *2*, 1.
26. Eick, S.; Wallys, J.; Hofmann, B.; van Ooyen, A.; Schnakenberg, U.; Ingebrandt, S.; Offenhäusser, A. Iridium oxide microelectrode arrays for in vitro stimulation of individual rat neurons from dissociated cultures. *Front. Neuroeng.* **2009**, *2*, 16.
27. Multi Channel Systems MCS GmbH. MEA Microelectrode (MEA) Manual. Available online: http://www.multichannelsystems.com/uploads/media/MEA_Manual.pdf (accessed on 23 May 2011).
28. Janders, M.; Egert, U.; Stelzle, M.; Nisch, W. Novel Thin Film Titanium Nitride Micro-Electrodes with Excellent Charge Transfer Capability for Cell Stimulation and Sensing Applications. In *Proceeding of the 18th Annual International Conference of the IEEE Engineering in Medicine and Biology Society*, Amsterdam, The Netherlands, 31 October–3 November 1996; pp. 245-247.
29. Egert, U.; Schlosshauer, B.; Fennrich, S.; Nisch, W.; Fejtl, M.; Knott, T.; Müller, T.; Hämmerle, H. A novel organotypic long-term culture of the rat hippocampus on substrate-integrated multielectrode arrays. *Brain Res. Protoc.* **1998**, *2*, 229-242.
30. Blau, A.; Ziegler, C.; Heyer, M.; Endres, F.; Schwitzgebel, G.; Matthies, T.; Stieglitz, T.; Meyer, J.U.; Gopel, W. Characterization and optimization of microelectrode arrays for *in vivo* nerve signal recording and stimulation. *Biosens. Bioelectron.* **1997**, *12*, 883-892.

31. Weiland, J.D.; Humayun, M.S.; Anderson, D.J. *In vitro* electrical properties for iridium oxide versus titanium nitride stimulating electrodes. *IEEE Trans. Biomed. Eng.* **2002**, *49*, 1574-1579.
32. Wang, K.; Fishman, H.A.; Dai, H.; Harris, J.S. Neural stimulation with a carbon nanotube microelectrode array. *Nano Lett.* **2006**, *6*, 2043-2048.
33. Keefer, E.W.; Botterman, B.R.; Romero, M.I.; Rossi, A.F.; Gross, G.W. Carbon nanotube coating improves neuronal recordings. *Nat. Nanotechnol.* **2008**, *3*, 434-439.
34. David-Pur, M.; Shein, M.; Hanein, Y. Carbon nanotube-based neurochips. *Meth. Mol. Biol.* **2010**, *625*, 171-177.
35. Fuchsberger, K.; Le Goff, A.; Gerwig, R.; Burkhardt, C.; Elit, J.; Li, Y.; Scheipers, A.; Stett, A.; Stelzle, M. Integration of Carbon Nanotubes in Microelectrode Arrays by Microcontact Printing and Electropolymerization for Neurostimulation and Biosensing Applications. In *Proceedings of the 7th International Meeting on Substrate-Integrated Microelectrode Arrays*, Reutlingen, Germany, 29 June–2 July 2010; pp. 267-268.
36. Smart, S.K.; Cassady, A.I.; Lu, G.Q.; Martin, D.J. The biocompatibility of carbon nanotubes. *Carbon* **2006**, *44*, 1034-1047.
37. Boxley, C.J.; White, H.S.; Gardner, C.E.; Macpherson, J.V. Nanoscale imaging of the electronic conductivity of the native oxide film on titanium using conducting atomic force microscopy. *J. Phys. Chem. B* **2003**, *107*, 9677-9680.
38. Cai, K.; Müller, M.; Bossert, J.; Rechtenbach, A.; Jandt, K.D. Surface structure and composition of flat titanium thin films as a function of film thickness and evaporation rate. *Appl. Surf. Sci.* **2003**, *250*, 252-267.
39. McCafferty, E.; Wightman, J.P. An X-ray photoelectron spectroscopy sputter profile study of the native air-formed oxide film on titanium. *Appl. Surf. Sci.***1999**, *143*, 92-100.
40. Williams, K.R.; Gupta, K.; Wasilik, M. Etch rates for micromachining processing—Part II. *J. Microelectromech. Syst.* **2003**, *12*, 761-778.
41. Huigen, E.; Peper, A.; Grimbergen, C.A. Investigation into the origin of the noise of surface electrodes. *Med. Biol. Eng. Comput.* **2002**, *40*, 332-338.
42. Welch, P.D. The use of fast Fourier transform for the estimation of power spectra: A method based on time averaging over short, modified periodograms. *IEEE Trans. Audio Electrocoust.* **1967**, *AU-15*, 70-78.
43. Ihalainen, H. *Matlab MSP Toolbox*; Tampere University of Technology: Tampere, Finland, 1987-2010.
44. Agilent Technologies. *Agilent Impedance Measurement Handbook: A Guide to Measurement Technology and Techniques*; Agilent Technologies, Inc: Santa Clara, CA, USA, 2009. Available online: http://cp.literature.agilent.com/litweb/pdf/5950-3000.pdf (accessed on 11 May 2010).
45. Lappalainen, R.S.; Salomäki, M.; Ylä-Outinen, L.; Heikkilä, T.J.; Hyttinen, J.A.K.; Pihlajamäki, H.; Suuronen, R.; Skottman, H.; Narkilahti, S. Similarly derived and cultured hESC lines show variation in their developmental potential towards neuronal cells in long-time culture. *Regen. Med.* **2010**, *5*, 749-762.

46. Sundberg, M.; Jansson, L.; Ketolainen, J.; Pihlajamäki, H.; Suuronen, R.; Skottman, H.; Inzunza, J.; Hovatta, O.; Narkilahti, S. CD marker expression profiles of human embryonic stem cells and their neural derivatives, determined using flow-cytometric analysis, reveal a novel CD marker for exclusion of pluripotent stem cells. *Stem Cell Res.* **2009**, *2*, 113-124.
47. Mummery, C.; Ward-van Oostwaard, D.; Doevendans, P.; Spijker, R.; van den Brink, S.; Hassink, R.; van der Heyden, M.; Opthof, T.; Pera, M.; de la Riviere, A.B.; *et al*. Differentiation of human embryonic stem cells to cardiomyocytes: Role of coculture with visceral endoderm-like cells. *Circulation* **2003**, *107*, 2733-2740.
48. Ryynänen, T.; Kujala, V.; Ylä-Outinen, L.; Kerkelä, E.; Narkilahti, S.; Lekkala, J. Polystyrene Coated MEA. In *Proceedings of the 7th International Meeting on Substrate-Integrated Microelectrode Arrays*, Reutlingen, Germany, 29 June–2 July 2010; pp. 265-266.
49. Blau, A.; Murr, A.; Trellenkamp, S.; Dautermann, C.; Wolff, S.; Heuschkel, M.; Wuesten, J.; Ziegler, C.; Benfenati, F. Prototyping All-Polymer Bioelectrical Signal Transducers. In *Proceedings of the World Congress on Medical Physics and Biomedical Engineering*, Munich, Germany, 7−12 September 2009; pp. 327-330.

PUBLICATION II

Atomic layer deposited iridium oxide thin film as microelectrode coating in stem cell applications

Ryynänen, T., Ylä-Outinen, L., Narkilahti, S., Tanskanen, J.M.A., Hyttinen, J., Hämäläinen, J., Leskelä, M., Lekkala, J.

Journal of Vacuum Science & Technology A (2012), 30(4), 1–5
https://doi.org/10.1116/1.4709447

Atomic layer deposited iridium oxide thin film as microelectrode coating in stem cell applications

Tomi Ryynänen[a)]
Department of Automation Science and Engineering, Tampere University of Technology, and BioMediTech, Korkeakoulunkatu 3, FI-33720 Tampere, Finland

Laura Ylä-Outinen and Susanna Narkilahti
Institute of Biomedical Technology, University of Tampere, and BioMediTech, Biokatu 12, FI-33520 Tampere, Finland

Jarno M. A. Tanskanen
Department of Biomedical Engineering, Tampere University of Technology, and BioMediTech, Finn-Medi 1 L 4, Biokatu 6, FI-33520 Tampere, Finland

Jari Hyttinen
Department of Biomedical Engineering, Tampere University of Technology, and BioMediTech, P.O.Box 692, FI-33101 Tampere, Finland

Jani Hämäläinen and Markku Leskelä
Department of Chemistry, University of Helsinki, P.O. Box 55, FI-00014, Helsinki, Finland

Jukka Lekkala
Department of Automation Science and Engineering, Tampere University of Technology, and BioMediTech, Korkeakoulunkatu 3, FI-33720 Tampere, Finland

(Received 25 January 2012; accepted 12 April 2012; published 27 April 2012)

Microelectrodes of microelectrode arrays (MEAs) used in cellular electrophysiology studies were coated with iridium oxide (IrOx) thin film using atomic layer deposition (ALD). This work was motivated by the need to find a practical alternative to commercially used titanium nitride (TiN) microelectrode coating. The advantages of ALD IrOx coating include decreased impedance and noise levels and improved stimulation capability of the microelectrodes compared to uncoated microelectrodes. The authors' process also takes advantage of ALD's exact process control and relatively low source material start costs compared to traditionally used sputtering and electrochemical methods. Biocompatibility and suitability of ALD IrOx microelectrodes for stem cell research applications were verified by culturing human embryonic stem cell derived neuronal cells for 28 days on ALD IrOx MEAs and successfully measuring electrical activity of the cell network. Electrode impedance of 450 kΩ at 1 kHz was achieved with ALD IrOx in the authors' 30 μm microelectrodes. This is better than that reported for any uncoated microelectrodes with equal size, even equal to that of inactivated sputtered IrOx coating. Also, stimulation capability was demonstrated. However, further development, including, e.g., applying electrochemical activation, is needed to achieve the performance of commercial TiN-coated microelectrodes. © *2012 American Vacuum Society*. [http://dx.doi.org/10.1116/1.4709447]

I. INTRODUCTION

Microelectrode arrays (MEAs)[1,2] are widely used in tissue engineering to study electrical activity of various types of cells and tissues, and to deliver electrical stimulation. MEA measurements are one important tool for neuronal stem cell researchers to study neuronal cells and networks and brain development, and in developing cell based therapies for currently incurable diseases and traumas like Parkinson's disease and spinal cord injury.[3–6] Stem cell based methods are also expected to in part replace animal experiments in drug research and toxicity tests.[7]

In their simplest form, microelectrodes, contact pads and their connecting tracks can be fabricated from a single conducting material like Au, Pt, Ti,[8] or indium tin oxide (ITO). Of these Au, Pt, and ITO MEAs are commercially available (from Qwane Biosciences in Lausanne, Switzerland, for example).[9] However, when low impedance and noise levels are desirable, or MEAs are used for stimulation purposes requiring high charge transfer capacity, the microelectrodes—and often also the contact pads—typically receive additional coating, like platinum black (Pt black),[1,2] titanium nitride (TiN),[10] iridium oxide (IrOx),[11–13] or carbon nanotubes (CNTs).[14,15] In all these, the nanostructured surface increases effective surface area, which again leads to lower impedance. Most of these additional microelectrode coatings unfortunately suffer from certain drawbacks. Widely used electrodeposited Pt black suffers from reproducibility and mechanical instability issues.[16] It has even been stated that the coating should be reapplied after each use of the MEAs.[11] IrOx is known for its large charge storage capacity (CSC) and the characteristics of IrOx coating, whether made by sputtering or electrochemical methods, are usually improved by electrochemical activation applied after the

[a)]Electronic mail: tomi.ryynanen@tut.fi

coating process. Activated electrodes, however, tend to lose most of their improved performance rather quickly in as short a time as in two days,[12] which is problematic for long-term cell experiments lasting several weeks. Another drawback particularly seen in sputter deposition of IrOx thin films is the requirement for a very expensive sputtering target. CNT coatings have been actively studied recently, but still have unresolved issues related to difficult fabrication processes and concerns about biocompatibility and long-term adhesion.[17] It is uncertain whether CNTs will ever reach commercial maturity as MEA electrode coating materials. Conversely, sputter deposited TiN coating is used by Multi Channel Systems MCS GmbH (MCS, Reutlingen, Germany), a leading commercial MEA manufacturer.[18] The obvious reason is that TiN coating has not been reported to suffer from any significant drawbacks, although its CSC has been considered low in some publications.[19,20] Finding the correct process parameters for a reactive sputtering process that ensures optimal pillarlike surface structure,[10] provides large effective surface area, and thus low impedance could be laborious, which may explain why TiN coating has rarely been used in noncommercial MEAs.

The motivation for the work presented here was to find a high-performance MEA microelectrode coating to serve as a practical alternative to TiN, preferably one with commercialization potential. Atomic layer deposition (ALD)[21] was chosen as the fabrication method for two reasons: (1) superior thin-film thickness control and repeatability compared to reactive sputtering or electrochemical methods, and (2) low source material investment needed for start-up compared to the big, expensive targets needed for sputtering. Although ALD also can be used to deposit TiN, IrOx was chosen because of its potential for improved CSC and lower impedance.[22] In this paper we compare the electric and surface characteristics of in-house uncoated, ALD IrOx coated, and commercial TiN coated microelectrode arrays. Further, the arrays' biological applicability was tested with cell cultures and electrophysiological assessment of the cell functions.

II. EXPERIMENT

A. MEA fabrication

Six in-house MEAs (later referred to as sMEAs) were produced and tested. They consisted of a glass substrate, titanium as the base conducting material for microelectrodes, contact pads and tracks between them, and Si_3N_4 as the insulator layer as described by Ryynänen *et al.*[8] Next, the sMEAs were spin coated with an approximately 2.5 μm thick photoresist layer (ma-P 1225, micro resist technology GmbH, Berlin, Germany). Openings were made above the leftmost 29 microelectrodes of the 58 microelectrodes, and above the two bigger electrodes and all the contact pads using normal lithographic procedures. Hard baked photoresist was left on sMEAs as a coating mask. In the ALD process, described in more detail by Hämäläinen *et al.*,[23] iridium oxide was deposited at 185 °C on the sMEAs. A total of 3000 cycles were grown using 2 s $Ir(acac)_3$ and 4 s ozone pulses separated by 2 s purges, which corresponds to an iridium oxide film thickness of approximately 120 nm. After the ALD process, lift-off in a heated RR4 resist remover (Futurrex, Inc., Franklin, NJ) concluded the MEA fabrication process. As a result, half of the microelectrodes were uncoated titanium and half were coated with ALD IrOx (Fig. 1).

As referenced earlier, we also used five commercial MEAs [later referred to as cMEAs, type 200/30iR-Ti from MCS (Ref. 18)], whose structure consisted of glass as a substrate, Ti as the base conducting material, and Si_3N_4 as the insulator layer, making them very similar to sMEAs, except that the microelectrodes were coated with reactively sputtered TiN and potential differences in layer thicknesses and linewidths. Unlike the sMEAs, the cMEAs had been used in cell experiments before this study. In all the MEAs the microelectrodes were round with diameters of 30 μm. In-house polydimethyl siloxane (PDMS) structures were attached to MEAs to form pools for liquids and cells on the microelectrodes.[24]

B. Measurements

For the first experiment, the surfaces of randomly selected Ti and IrOx microelectrodes from a randomly selected sMEA were studied with atomic force microscopy [(AFM), XE-100 AFM, Park Systems Corp., Suwon, Korea]. Using tapping mode, 256 × 256 pixel scans were taken over a 1 μm × 1 μm area, and surface area ratio and surface roughness [root mean square (rms)] were calculated with XEI software (Park Systems). Due to the small, pillarlike structure of the microelectrode surface of cMEAs, evaluating a TiN surface with AFM was found unreliable in our earlier study[8] and thus only sMEAs were evaluated using AFM for this experiment.

Following AFM, microelectrode impedances were measured with a 60 channel impedance testing device MEA-IT (MCS). MEA-IT measures the impedances of all the microelectrodes against an external Ag/AgCl pellet ground electrode using a 100 mV 1 kHz sinusoidal test signal. MEAs were filled with saline [Dulbecco's Phosphate Buffered Saline—0.0095 M (PO_4) without Ca and Mg, Lonza, Verviers,

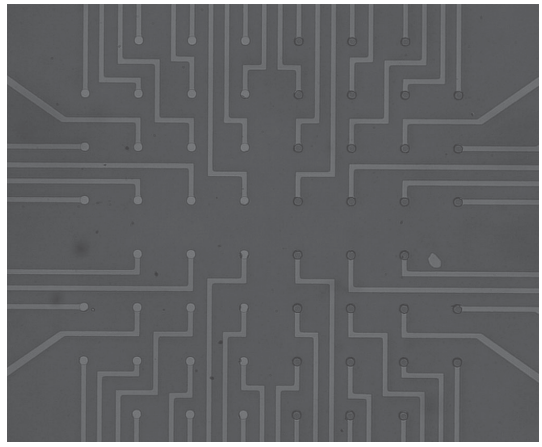

FIG. 1. In-house sMEA with 29 Ti microelectrodes (left half) and 29 ALD IrOx coated microelectrodes (right half). Microelectrode diameter is 30 μm.

Belgium] and kept at room temperature for 24 h before measuring the impedance. All 58 microelectrodes in sMEAs and 59 microelectrodes in cMEAs were measured three times in a row and averages of the measurements were calculated for each microelectrode. For each MEA, average impedance was calculated from the impedances of microelectrodes made of the same material. Finally, for each microelectrode material (Ti, IrOx, TiN), average impedances were calculated from the average values of corresponding MEAs.

Next, the stimulation capability of MEAs was established by a simple impulse measurement. Again, the MEAs were filled with saline a day before the measurements, and contact pads were wiped with 70% ethanol just before the measurement. In this case, the MEAs were placed in USB-MEA 1060 (MCS) and a stimulation pulse of 1 mV for 20 μs, -1 mV for 20 μs, and 0 mV for 10 ms from STG2004 (MCS) were applied repeatedly for 1000 times. Pulses were applied for one microelectrode at the bottom row and the second or the seventh column to apply stimulation via both Ti and ALD IrOx microelectrodes on the sMEAs, and TiN microelectrodes on cMEAs. The same Ag/AgCl pellet used in the impedance measurement was used as an external ground and reference. The pellet was located below the microelectrode array in a PDMS ring restricted pool. Response to the stimulation pulses was recorded from each microelectrode at a frequency of 50 kHz and stored to a personal computer using MC_RACK software (MCS). To alleviate otherwise excessive 50 Hz interference, the in-house sMEAs and the USB-MEA 1060 were covered with aluminum foil.

For impulse measurements, the responses were recorded for 15 s and the stimulation sequence (lasting a total of 10.04 s) was manually started within 1–2 s after starting the recording, so at least the last 3 s of the recordings contained nonstimulated data. This allowed us to evaluate noise levels. From the data, rms noise was calculated for each microelectrode by using the following formula:

$$\text{noise}_{\text{rms}} = \sqrt{\frac{1}{n}\sum_{i=1}^{n} x_i^2}, \tag{1}$$

where n is the number of samples in the measured signal and x_i is the voltage sample measured at time i. For each MEA or half MEA for the in-house sMEAs, average rms noise was calculated. Thereafter, average rms noise for each microelectrode coating type was calculated from the average rms noises of individual MEAs or array halves.

For impedance and noise measurements, the microelectrodes having impedance or noise levels that differed greatly from the common trend within the same MEA were excluded from the calculations, as those microelectrodes most likely suffered from fabrication defects or the measured signals were corrupted by amplifier saturation or contact pin problems. All measurements were performed at room temperature.

C. Cell experiments

In the cell experiments, the neural differentiation of human embryonic stem cells (hESCs), MEA preparation, and measurements were performed as described earlier.[3,25] The stem cell derived neuronal cells were plated on MEAs and cultivated on the MEAs for 28 days. Spontaneous activities of neuronal networks were recorded for 5 min once a week and the maturation of the neural network was followed for each MEA.

III. RESULTS AND DISCUSSION

AFM software was used to estimate a surface area ratio of 5.0 and surface roughness of 3.4 nm (rms) for Ti, and surface area ratio of 5.2 and surface roughness of 3.9 nm (rms) for ALD IrOx. Along with the visual images [Fig. 2(a) for Ti and Fig. 2(b) for ALD IrOx], these values confirm that the ALD IrOx process very much replicates the smoothness of the Ti surface. That is, of course, an expected result due to the conformal nature of ALD. This property of ALD IrOx could be utilized in the future in coating nanoporous structures[26] or otherwise nanopatterned surfaces in order to produce microelectrodes with increased surface areas and lower impedances. This could be done independently or with electrochemical activation, which in the case of sputtered IrOx has been reported to increase the surface roughness to 2–12 times higher than that reported previously in this paper, depending on the number of activation cycles.[11,13]

Impedance measurement results are summarized in Table I. The result of 450 kΩ for ALD IrOx is consistent with the

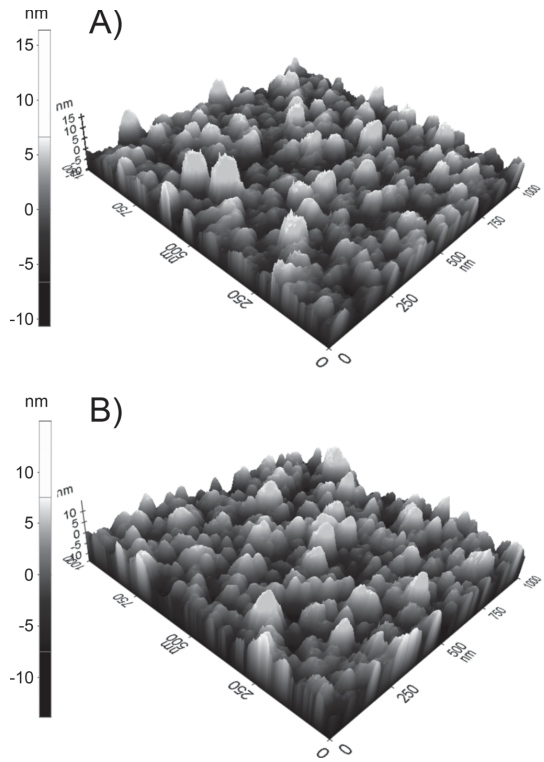

FIG. 2. AFM images of (a) Ti and (b) ALD IrOx surface.

TABLE I. Impedance magnitude measurement results and literature values for microelectrodes with different coatings. All impedance magnitudes have been normalized to correspond to those of corresponding microelectrodes of 30 μm in diameter.

Material	Average impedance at 1kHz (kΩ)	Average impedance deviation (kΩ)	Reference
Ti	>1700	>210	
ALD IrOx	450	40	
Unactivated sputtered IrOx	~450		12
Activated sputtered IrOx	~23		12
Sputtered TiN	30	3	
Sputtered TiN	30–50		18
Pt (not black)	800–1100		9
Au	1000–1300		9

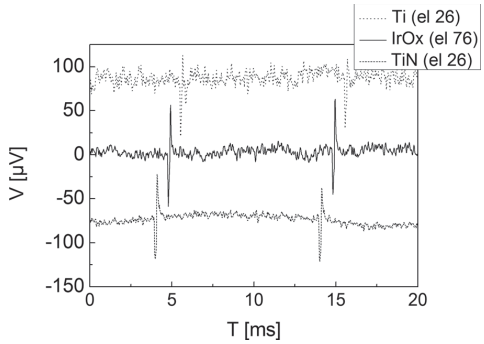

FIG. 3. Typical examples of response to voltage impulse stimulation applied in another electrode in MEA with different Ti, ALD IrOx, and TiN microelectrodes. Curves have been shifted horizontally and vertically for clarity.

impedance reported for inactivated sputtered IrOx in the literature,[12] which indicates that the coating method does not affect the impedance of IrOx. When compared to the impedances of uncoated microelectrodes, our result for ALD IrOx microelectrodes is two to three times less than what has been reported for commercial Pt and Au MEAs (Ref. 9) and at least four times less than our measurement for uncoated titanium microelectrodes. This comparison suggests that ALD IrOx provides a feasible method for moderate improvement of impedance in MEAs. However, without further increase of surface area in the MEA structure, ALD IrOx on a planar surface cannot compete with the 30 kΩ impedance reported by the manufacturer[18] and confirmed in our measurements for pillarlike surface structured TiN microelectrodes. This is also true for about 23 kΩ impedance reported for electrochemically activated sputtered IrOx thin film microelectrodes, in which the electrochemical activation leads to roughening of the surface and thus to increased surface area.[12] However, Comstock *et al.*[26] have shown that electrochemical activation can be successfully applied on ALD iridium thin films and thus, it can be expected that electrochemical activation could also decrease the impedance in the case of ALD IrOx. Whether the activated ALD IrOx has as short of a deactivation time as sputtered IrOx will be seen in future studies.

The average rms noise of ALD IrOx microelectrodes was measured to be 4.6 μV with an average standard deviation of 1.9 μV, or about half that measured for uncoated Ti microelectrodes (9.1 μV with a standard deviation of 6.1 μV). By comparison, the rms noise of TiN microelectrodes was 5.5 μV with a standard deviation of 1.4 μV. Note that cMEAs were not covered with aluminum foil when measuring, and thus the noise figures for TiN microelectrodes may not be exactly comparable to those of sMEA microelectrodes of either type. The lower noise results for TiN microelectrodes is supported by visual assessment of the cell experiment data shown in Fig. 4 and also by our earlier results,[8] where in specific noise measurements, the rms noise of TiN microelectrodes was measured to be just 2.7 μV with very little deviation.

Examples of typical responses to stimulus impulses measured for the different microelectrode types are shown in Fig. 3. The presented electrodes are located two electrodes up (toward the center of the array) from the stimulating microelectrode. At the minimum, the results show that at least ALD IrOx and TiN microelectrodes are conducive to stimulation and measurement. Both upwards and downwards peaks can be clearly separated from noise, which is not the case with Ti microelectrodes where the upper peak mostly disappears in noise. As can be expected, the peak amplitudes weaken as a function of the distance from the stimulating electrode. The attenuation is lowest with TiN microelectrodes and strongest with Ti microelectrodes. For example, the peak amplitude drop between the electrodes in Fig. 3 and the electrodes two rows above them (el 24 or 74) are 27% (Ti), 23% (ALD IrOx), and 4% (TiN). Due to varying stimulation electrode materials in each case and a lack of an aluminum shield in cMEA measurements, the results should be interpreted with caution. For more complete characterization of the differently coated microelectrodes, cyclic voltametry measurements and voltage transient measurements should be conducted in the future.

One obvious contributor for the modest performance of Ti microelectrodes is the possible interfering effect of the native oxide layer on the Ti. As the oxide layer is also present in ALD IrOx microelectrodes, it should be eliminated in future experiments. In the case of TiN coated microelectrodes, that is possible by etching the oxide away just before applying the coating, but in the case of ALD IrOx, the ozone used in the ALD process makes the etching useless. Therefore, the Ti base material should be replaced by another conductor like Au or Pt. Only after such a modification and future electrochemical activation experiments can the commercialization potential of ALD IrOx coating for microelectrodes be fully evaluated.

In the cell experiments, no differences were observed between cell behaviors on different kinds of electrodes. The cells attached and grew on ALD IrOx microelectrodes equally well as on uncoated Ti microelectrodes and on cMEAs. No biocompatibility related issues were observed. Figure 4 shows measurements taken from the human embryonic stem cell derived neuronal cell (hESC-N) cell networks at day 14. As expected, the noise level decreases from

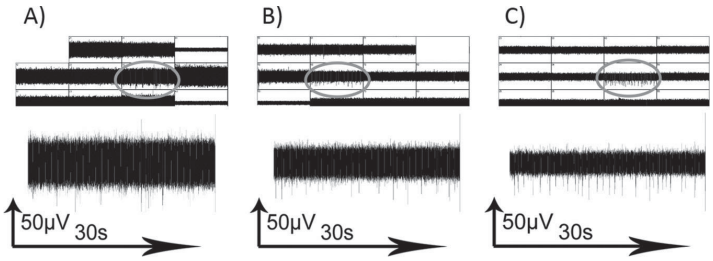

FIG. 4. Examples of measured hESC-N network activity at day 14 using MEAs with different kinds of microelectrodes, (a) Ti, (b) ALD IrOx, and (c) sputtered TiN. In each rectangle (upper panels) the signal from one microelectrode is shown, and the ovals indicate the magnified signals (lower panels).

uncoated Ti [Fig. 4(a)] to ALD IrOx coated [Fig. 4(b)] and finally to TiN coated [Fig. 4(c)] microelectrodes. However, as reported earlier,[8] neuronal signal strength increases along with increasing noise levels, so signaling is still easily observable for microelectrode types having higher noise levels.

IV. CONCLUSIONS

IrOx thin film was deposited on MEA titanium microelectrodes using an ALD method. Comparisons between the impedance values given by literature for Au and Pt microelectrodes and our results for Ti microelectrodes strongly indicate that ALD IrOx coating clearly improves noise, impedance, and stimulation characteristics of the microelectrodes, even without any further optimization. However, to compete with commercial TiN coated microelectrodes, ALD IrOx coating requires further optimization. Surface roughening by electrochemical activation is the obvious way to improve the microelectrode characteristics, but some improvement may also be achieved by optimizing the ALD process parameters like thin-film thickness and process temperature. In addition, the possible interfering effect of the native oxide on the underlaying Ti layer could be eliminated by using another electrode base material. To conclude, ALD IrOx was found to be a promising alternative for electrode coating cell culture MEAs. ALD IrOx coated microelectrodes were successfully used to measure field potentials from human embryonic stem cell derived neuronal cells, indicating good biocompatibility.

ACKNOWLEDGMENTS

This work was supported by the Academy of Finland (Decision Nos. 122947, 122959, 123359, and 123762, and the Finnish Centre of Excellence in Atomic Layer Deposition), Tekes (Decision Nos. 40345/11 and 40346/11), the Finnish Cultural Foundation and its Pirkanmaa Regional Fund, and CHEMSEM graduate school.

[1]C. A. Thomas, P. A. Springer, G. E. Loeb, Y. Berwald-Netter, and L. M. Okun, Exp. Cell. Res. **74**, 61 (1972).
[2]J. Pine, J. Neurosci. Methods **2**, 19 (1980).
[3]T. J. Heikkilä, L. Ylä-Outinen, J. M. A. Tanskanen, R. Lappalainen, H. Skottman, R. Suuronen, J. E. Mikkonen, J. A. K. Hyttinen, and S. Narkilahti, Exp. Neurol. **218**, 109 (2009).
[4]H. T. Hogberg, T. Sobanski, A. Novellino, M. Whelan, D. G. Weiss, and A. K. Bal-Price, Neurotoxicology **32**, 158 (2011).
[5]R. Pizzi, G. Cino, F. Gelain, D. Rossetti, and A. Vescovi, Biosystems **88**, 1 (2007).
[6]T. J. O'Shaughnessy, J. L. Liu, and W. Ma, Biosens. Bioelectron. **24**, 2365 (2009).
[7]A. F. M. Johnstone, G. W. Gross, D. G. Weiss, O. H.-U. Schroeder, A. Gramowski, and T. J. Shafer, Neurotoxicology **31**, 331 (2010).
[8]T. Ryynänen *et al.*, Micromachines **2**, 394 (2011).
[9]Qwane Biosciences SA, "MEA60 Biochips Product Catalog," http://www.qwane.com/Documents/MEA60_Product_Catalog.pdf (accessed 19 January 2012).
[10]M. Janders, U. Egert, M. Stelzle, and W. Nisch, *Proceedings of the 18th Annual International Conference of the IEEE Engineering in Medicine and Biology Society,* Amsterdam 1996, p. 245.
[11]S. Eick, J. Wallys, B. Hofmann, A. van Ooyen, U. Schnakenberg, S. Ingebrandt, and A. Offenhäusser, Front. Neuroeng. **2**, 16 (2009).
[12]S. Gawad, M. Giugliano, M. Heuschkel, B. Wessling, H. Markram, U. Schnakenberg, P. Renaud, and H. Morgan, Front. Neuroeng. **2**, 1 (2009).
[13]A. Blau, C. Ziegler, M. Heyer, F. Endres, G. Schwitzgebel, T. Matthies, T. Stieglitz, J. U. Meyer, and W. Gopel, Biosens. Bioelectron. **12**, 883 (1997).
[14]K. Wang, H. A. Fishman, H. Dai, and J. S. Harris, Nano Lett. **6**, 2043 (2006).
[15]K. Fuchsberger, A. L. Goff, L. Gambazzi, F. M. Toma, A. Goldoni, M. Giugliano, M. Stelzle, and M. Prato, Small **7**, 524 (2011).
[16]M. Heim, B. Yvert, and A. Kuhn, "Nanostructuration strategies to enhance microelectrode array (MEA) performance for neuronal recording and stimulation," J. Physiol. (Paris) (in press).
[17]S. K. Seidlits, J. Y. Lee, and C. E. Schmidt, Nanomedicine **3**, 183 (2008).
[18]Multi Channel Systems MCS GmbH, "MEA Microelectrode (MEA) Manual," http://www.multichannelsystems.com/uploads/media/MEA_Manual.pdf (accessed 23 May 2011).
[19]X. Q. Li, W. H. Pei, R. Y. Tang, Q. Gui, K. Guo, Y. Wang, and H. D. Chen, Sci. China Tech. Sci. **54**, 2305 (2011).
[20]S. F. Cogan, Annu. Rev. Biomed. Eng. **10**, 275 (2008).
[21]M. Leskelä and M. Ritala, Angew. Chem., Int. Ed. **42**, 5548 (2003).
[22]J. D. Weiland, M. S. Humayun, and D. J. Anderson, IEEE Trans. Biomed. Eng. **49**, 1574 (2002).
[23]J. Hämäläinen, M. Kemell, F. Munnik, U. Kreissig, M. Ritala, and M. Leskelä, Chem. Mater. **20**, 2903 (2008).
[24]J. Kreutzer, L. Ylä-Outinen, P. Kärnä, T. Kaarela, J. Mikkonen, H. Skottman, S. Narkilahti, and P. Kallio, J. Bionic Eng. **9**, 1 (2012).
[25]R. S. Lappalainen, M. Salomäki, L. Ylä-Outinen, T. J. Heikkilä, J. A. K. Hyttinen, H. Pihlajamäki, R. Suuronen, H. Skottman, and S. Narkilahti, Regen. Med. **5**, 749 (2010).
[26]D. J. Comstock, S. T. Christensen, J. W. Elam, M. J. Pellin, and M. C. Hersam, Electrochem. Commun. **12**, 1543 (2010).

PUBLICATION III

Ion Beam Assisted E-Beam Deposited TiN Microelectrodes–Applied to Neuronal Cell Culture Medium Evaluation

Ryynänen, T., Toivanen, M., Salminen, T., Ylä-Outinen, L.,
Narkilahti, S., Lekkala, J.

Frontiers in Neuroscience (2018), 12:882, 1–13
https://doi.org/10.3389/fnins.2018.00882

frontiers in Neuroscience

ORIGINAL RESEARCH
published: 04 December 2018
doi: 10.3389/fnins.2018.00882

Ion Beam Assisted E-Beam Deposited TiN Microelectrodes—Applied to Neuronal Cell Culture Medium Evaluation

Tomi Ryynänen[1], Maria Toivanen[2], Turkka Salminen[3], Laura Ylä-Outinen[2], Susanna Narkilahti[2] and Jukka Lekkala[1]*

[1] BioMediTech Institute and Faculty of Biomedical Sciences and Engineering, Tampere University of Technology, Tampere, Finland, [2] NeuroGroup, BioMediTech Institute and Faculty of Medicine and Life Sciences, University of Tampere, Tampere, Finland, [3] Laboratory of Photonics, Tampere University of Technology, Tampere, Finland

Microelectrode material and cell culture medium have significant roles in the signal-to-noise ratio and cell well-being in *in vitro* electrophysiological studies. Here, we report an ion beam assisted e-beam deposition (IBAD) based process as an alternative titanium nitride (TiN) deposition method for sputtering in the fabrication of state-of-the-art TiN microelectrode arrays (MEAs). The effects of evaporation and nitrogen flow rates were evaluated while developing the IBAD TiN deposition process. Moreover, the produced IBAD TiN microelectrodes were characterized by impedance, charge transfer capacity (CTC) and noise measurements for electrical properties, AFM and SEM for topological imaging, and EDS for material composition. The impedance (at 1 kHz) of brand new 30 μm IBAD TiN microelectrodes was found to be double but still below 100 kΩ compared with commercial reference MEAs with sputtered TiN microelectrodes of the same size. On the contrary, the noise level of IBAD TiN MEAs was lower compared with that of commercial sputtered TiN MEAs in equal conditions. In CTC IBAD TiN electrodes (3.3 mC/cm^2) also outperformed the sputtered counterparts (2.0 mC/cm^2). To verify the suitability of IBAD TiN microelectrodes for cell measurements, human pluripotent stem cell (hPSC)-derived neuronal networks were cultured on IBAD TiN MEAs and commercial sputtered TiN MEAs in two different media: neural differentiation medium (NDM) and BrainPhys (BPH). The effect of cell culture media to hPSC derived neuronal networks was evaluated to gain more stable and more active networks. Higher spontaneous activity levels were measured from the neuronal networks cultured in BPH compared with those in NDM in both MEA types. However, BPH caused more problems in cell survival in long-term cultures by inducing neuronal network retraction and clump formation after 1–2 weeks. In addition, BPH was found to corrode the Si_3N_4 insulator layer more than NDM medium. The developed IBAD TiN process gives MEA manufacturers more choices to choose which method to use to deposit TiN electrodes and the medium evaluation results remind that not only electrode material but also insulator layer and cell culturing medium have crucial role in successful long term MEA measurements.

Keywords: titanium nitride, microelectrode array, MEA, IBAD, cell culture medium

OPEN ACCESS

Edited by:
Ioan Opris,
University of Miami, United States

Reviewed by:
Ikuro Suzuki,
Tohoku Institute of Technology, Japan
Volker Bucher,
Furtwangen University, Germany

****Correspondence:***
Tomi Ryynänen
tomi.ryynanen@tut.fi

Specialty section:
This article was submitted to Neural Technology, a section of the journal Frontiers in Neuroscience

Received: *15 December 2017*
Accepted: *12 November 2018*
Published: *04 December 2018*

Citation:
Ryynänen T, Toivanen M, Salminen T, Ylä-Outinen L, Narkilahti S and Lekkala J (2018) Ion Beam Assisted E-Beam Deposited TiN Microelectrodes—Applied to Neuronal Cell Culture Medium Evaluation. Front. Neurosci. 12:882. doi: 10.3389/fnins.2018.00882

INTRODUCTION

A microelectrode array (MEA) is a common tool to measure the electrical activity of various cell types *in vitro* and to provide an electrical stimulus to the objects under study. The applications of MEAs vary from basic biological research to drug screening and toxicity testing. In neuroscience, it has been found to be applicable for *in vitro* drug screening and toxicity testing (Johnstone et al., 2010; Ylä-Outinen et al., 2010). Recently, the rise of human pluripotent stem cell (hPSC)-based technologies for human cell-based modeling, including disease modeling, has benefitted from MEA technology (Falk et al., 2016; Odawara et al., 2016).

In its simplest form, MEA consists of a glass substrate, a metal layer containing electrodes, tracks, and contact pads, and an insulator layer with openings on the electrodes and the contact pads. Even though metal electrodes such as Pt, Au, or Ti can be used, they have limitations in their performance. For this reason, metallic microelectrodes are usually coated with a porous material that increases the effective surface area ratio (SAR) and decreases the impedance, leading to a higher signal-to-noise ratio of the electrodes (Bauerdick et al., 2003). Since the early days of MEA (Thomas et al., 1972), platinum black (Pt black) has been one of the most commonly used coating materials for low impedance electrodes. It has excellent electrical characteristics, but in addition to obvious cost issues, a major drawback is that Pt black has been reported to have problems with mechanical stability during long-term use (Heim et al., 2012). Iridium oxide (IrOx), even as a rather common *in vivo* electrode material (Cogan, 2008), has not reached notable popularity for *in vitro* microelectrodes. This is likely to be at least partly due to its tendency to lose the low impedance state rather rapidly in a liquid environment (Gawad et al., 2009). Carbon nanotube-based solutions do exist (Gabay et al., 2007; Samba et al., 2014), and even though excellent performance has been reported, they are still more a topic of academic interest than a real choice for active use. The only commonly used substitute for Pt black has been titanium nitride (TiN) (Janders et al., 1996), especially in commercial solutions. Depending on the deposition parameters and methods, the morphology of a TiN thin film may vary a lot from plain to highly columnar. The latter is seen as increased SAR and decreased impedance. Although, some doubts about the performance of TiN exist (Weiland et al., 2002), it can generally be considered as the least problematic high-performance microelectrode coating developed to date. In addition to *in vitro* electrodes, TiN can be used also in *in vivo* applications (Stelzle et al., 2001).

There exists a wide range of methods for the fabrication of TiN coatings. Because TiN is applied as the last layer on MEAs in the fabrication process, finding an etching process that is not harmful for the MEA insulator layer, typically Si_3N_4, and underlying track material, commonly titanium, might be challenging and may require additional process steps for preparing the etch mask. Thus, a lift-off process is favored with TiN. Because photoresist is needed for lift-off and the melting temperature of the glass substrate set limits for the maximum allowed temperature during the TiN deposition process, certain common TiN deposition processes such as atomic layer deposition (ALD) (Xie et al., 2014), thermal chemical vapor deposition (CVD) (Wagner et al., 2008), and physical vapor deposition (PVD) (Gahlin et al., 1995; Peng et al., 2015) techniques must be ruled out when selecting the TiN deposition method for the MEAs. For this reason, reactive sputtering has been the only method used to deposit TiN on MEA electrodes (Egert et al., 1998; Cyster et al., 2002; Bauerdick et al., 2003; Gabay et al., 2007). However, there is also an alternative method for the low temperature deposition of TiN: ion beam assisted deposition (IBAD) in which the e-beam evaporated titanium is bombarded by a flux of low energy nitrogen and argon ions from the ion source to form TiN (**Figure 1**). The dominating mechanism in TiN formation is adsorption of ambient gaseous atoms on the growth surface (Hubler et al., 1988). Over the last three decades, several groups have reported their IBAD TiN experiments for hard coatings (Guzman et al., 1998; López et al., 2001) and more general materials science (Hubler et al., 1988; Huang et al., 2000; Yokota et al., 2004) applicable not only on hard coatings but also, for example, on decoration coatings and microelectronics diffusion barriers. By contrast, as far as we know, IBAD TiN has not been applied on MEAs previously.

In this paper, we evaluated different deposition parameters, including evaporation and nitrogen flow rates, for optimal IBAD TiN microelectrode coating. The coatings are characterized by impedance, charge transfer capacity (CTC) and noise measurements for electrical properties, AFM and SEM for topological imaging, and EDS for material composition. Comparison to sputtered TiN electrodes of commercial MEAs (Multi Channel Systems MCS GmbH) is also reported. To verify the biocompatibility and performance of these novel IBAD TiN microelectrodes, we cultured and measured hPSC-derived neuronal networks for 3 weeks. The neuronal networks were grown in two different cell culture media: neural differentiation medium (NDM) (Heikkilä et al., 2009) and BrainPhys (BPH)-supplemented medium recently introduced by Bardy et al. (2015)

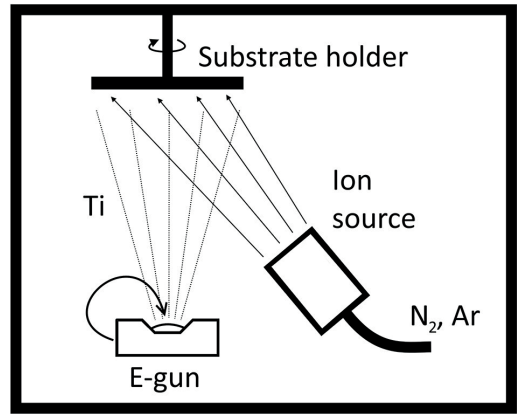

FIGURE 1 | Schematic of an ion beam assisted deposition system. Briefly, e-beam evaporated titanium is bombarded with nitrogen and argon ions to form a TiN thin film on substrates in a vacuum chamber.

to evaluate possible medium derived effects on MEA grown cultures.

MATERIALS AND METHODS

IBAD TiN Deposition Process Development

Microscope slides (76 mm × 26 mm × 1 mm; Gerhard Menzel GmbH) were used as substrates while optimizing the IBAD TiN deposition parameters. The slides were cleaned with acetone and isopropanol in an ultrasound bath, rinsed with DI water and dried with a nitrogen blow. Cleaned slides were placed in an Orion BC-3000 series box coater (System Control Technologies) equipped with a Telemark 246 e-beam source, Saintech Series III ST55 gridless ion source, Saintech ion current density monitor, and a Meissner trap for 100 nm IBAD TiN depositions. **Table 1** includes different parameter values tested during process development. In all depositions, a filament current of ∼20 A was used, and the vacuum during deposition was in the 10^{-5} Torr range (∼10^{-3} Pa). The substrate holder was rotated at 5 rpm during the deposition. The 99.995% purity Ti pellets used in both IBAD TiN depositions and later in Ti track depositions in the MEA fabrication were purchased from g-materials. Right after the deposition, the color of the thin films was evaluated visually.

AFM Measurements

While optimizing the IBAD TiN deposition process, an atomic force microscope (XE-100 AFM, Park Systems) equipped with an ACTA probe (AppNano; radius of curvature, 6 nm) was used for measuring the effective surface area ratio (SAR). An area of 1 μm × 1 μm was measured in intermittent mode for each sample. XEI analysis software (Park Systems) was used for calculating the SAR as per the formula

$$SAR = \frac{A_S - A_G}{A_G} * 100 \quad (1)$$

where A_G is the plain geometric area and A_S is the total surface area of the corresponding region. The result was finally given as a mean of two areas measured from the same sample. In addition, the software was used to calculate the root-mean-square roughness R_q.

IBAD TiN MEA Fabrication

Microscope slide grade glass plates (49 mm × 49 mm × 1 mm; Gerhard Menzel GmbH) were used as substrates for the MEAs. The slides were cleaned with acetone and isopropanol in an ultrasound bath and oxygen plasma before 400 nm of titanium was e-beam deposited at 5 Å/s on the slides. Electrode sites (30 μm in diameter), tracks and contact pads were patterned to the titanium layer in a wet etching [120 H_2O: 4 H_2O_2 (30%): 3 HF (50%)] process in which PR1-2000A positive photoresist (Futurrex, Inc.) was used as an etching mask. Next, 500 nm of silicon nitride was PECVD deposited as an insulator layer at 300°C. PR1-2000A was again used as an etching mask when reactive ion etching with SF_6 and O_2 gases was performed with Vision 320 RIE (Advanced Vacuum) to etch the openings on electrode sites and contact pads. The etching mask was not removed after the etching but was reused as a lift-off mask in the IBAD deposition of 400 nm of TiN. For comparison purposes, also MEA versions with 200 nm layer of IBAD TiN as well as MEAs without TiN were fabricated. Just prior to TiN deposition, a 10 min Ar sputter etch was run with the ion source to remove the native oxide layer on titanium electrode sites. IBAD TiN deposition parameters were as follows: anode voltage, 225 V; filament current, 20 A; N_2 flow, 13.2 sccm; Ar flow, 3.3 sccm; ion current density, 14 μA/cm^2; ion current density monitor bias, 35.0 V; deposition rate, 2 Å/s; and vacuum, 10^{-5} Torr range (∼10^{-3} Pa). The substrate holder was rotated at 5 rpm during the deposition. Finally, lift-off was performed in an acetone ultrasound bath. Either an in-house made PDMS ring or Spikebooster™ 6-well culture chamber (BioMediTech) (Kreutzer et al., 2012) was attached on MEAs to form a pool for Dulbecco's phosphate buffered saline (DPBS) or cell culture media. All of the photolithography masks used in this work were in-house fabricated with a μPG501 direct writing system (Heidelberg Instruments Mikrotechnik GmbH) on chrome mask blanks from Clean Surface Technology Co.

Impedance and Charge Transfer Capacity Characterization

The pools on the MEAs were filled with DPBS (PBS Dulbecco w/o Ca++, Mg^{2+}, Biochrom GmbH), and the MEAs were placed in a temperature chamber at 37°C inside petri dishes for at least 20 h. Subsequently, the MEAs were decreased to room temperature

TABLE 1 | Deposition parameters tested during IBAD TiN process optimization and AFM characterization results for each sample.

Sample	Set anode voltage [V]	N_2 flow [sccm]	Ar flow [sccm]	Deposition rate [Å/s]	Color	Surface area ratio [%]	Notes
1	225	13.2	3.3	1	gold-brown	5.4	
2	**225**	**13.2**	**3.3**	**2**	**purple-bronze**	**13.1**	
3	225	13.2	3.3	3.5	light gold	5.1	
4	225	13.2	3.3	5	gray	3.4	
5	225	10.8	1.2	2	brown	4.3	
6	225	9.9	6.6	1	gold	6.0	Unstable deposition
7	140	8.3	8.3	2	gray	4.5	1 AFM measurement only
8	225	16.8	4.2	1	gold	4.4	Ion beam pulsed 8 s ON, 7 s OFF

Parameters of sample 2 (bolded) were chosen to be used in the IBAD TiN MEA fabrication due to the highest surface area ratio.

for at least 1 h before the impedance measurement. MEA-IT60 from MCS, a dedicated device for measuring the impedances of all the microelectrodes of a MEA, was used as the measurement device. The measurement was performed at 1 kHz frequency with the sinusoidal test signal being 100 mV and an external Ag/AgCl pellet acting as a grounding electrode. Faulty electrodes existing both in commercial and in-house made MEAs were excluded before calculating mean values for each MEA. For a few randomly selected electrodes of in-house made IBAD TiN MEAs and, for comparison, also of pure Ti MEAs without TiN electrode coating an additional electrochemical analysis was performed. Frequency dependency of the impedance and CTC were measured with Iviumstat potentiostat (Ivium Technologies B.V.). The frequency range was from 1 to 100 kHz and a Pt wire (ALS-Japan) was used as the counter electrode in the impedance measurement. CTC was integrated from the third CV curve when the voltage was ramped between −0.9 and 0.9 V. The same Pt wire acted as the counter electrode as in the impedance measurements, and the reference electrode was DRIREF-2 (World Precision Instruments). Scan rate was 100 mV/s.

Noise Characterization

Noise characterization was performed as part of the cell culture experiments, where the cell culture medium acted as an electrically conducting solvent. After taking the MEAs from the incubator, they were at first left to stabilize in headstage for 3 min without recording the data. Then, the MEAs were measured for 10 min with the MEA2100 MEA system, MC_Rack software, and temperature controllers TC02 set at 37°C (all from MCS). The voltage signal was filtered (200–3,000 Hz bandpass), and the noise for each electrode of each MEA was calculated as an estimate of the standard deviation of background noise previously described in Quiroga et al. (2004). In calculating noise values for each MEA-medium combination, electrodes with a noise value above 7.0 μV were excluded as they were considered faulty electrodes. Mann-Whitney U-test was performed to indicate statistical significances: for each MEA type between the media at days 6 and 18, and for each medium type between the MEAs at days 6 and 18. $P < 0.05$ were considered significant.

SEM Imaging and EDS

Zeiss Crossbeam 540 FIB-SEM (Carl Zeiss Microscopy GmbH) with a Gemini II SEM column and Oxford Instruments X-Max^n 80 EDS detector was used in SEM imaging and EDS measurements. In the imaging, the acceleration voltage was 1 kV, and magnifications in **Figure 2b** were 1.16 and 15.35 kX. In the EDS measurements, acceleration voltages from 7 to 15 kV were used.

Neural Differentiation

The human embryonic stem cell (hESC) line Regea 08/023 was used in the experiments. BioMediTech has approval from the Finnish Medicines Agency (FIMEA) to perform research with human embryos (Dnro 1426/32/300/05). There are also supportive statements from the regional ethical committee of Pirkanmaa Hospital District for the derivation, culturing, and differentiation of hESCs (R05116). Neurons were differentiated from hESCs as previously described (Lappalainen et al., 2010). Neuronal differentiation medium (NDM) consisted of 1:1 DMEM/F12 and Neurobasal medium supplemented with 1 × B27, 1 × N2, 2 mM GlutaMax (all from Gibco Invitrogen), and 25 μ/mL penicillin/streptomycin (Lonza Group Ltd) and, during the differentiation stage, 20 ng/ml of basic fibroblast growth factor (bFGF) (R&D Systems) as previously described (Lappalainen et al., 2010) with or without low-dose naltrexone LDN193189 (100 nM; Stemcell Technologies, Inc.).

MEA Preparation and Adherent Culture

MEA preparations were performed as previously described (Heikkilä et al., 2009) with some modifications. MEAs (10 BMT MEAs and 9 60-6wellMEA200/30iR-Ti from MCS) were combined with SpikeBoosters^{TM} (BioMediTech) (Kreutzer et al., 2012) and coated with 0.05% (w/v) polyethylenimine (PEI) incubated overnight, washed with sterile H_2O, and coated with 20 μg/ml of mouse laminin (both from Sigma-Aldrich) and incubated overnight. A 48-well plate (Thermo Scientific) was coated with 20 μg/ml or 10 μg/ml of mouse laminin in wells with or without coverslips (Ø 9 mm, VWR).

The 8 week pre-differentiated neurospheres were dissected into small cell aggregates (ø∼50–200 μm), and 7–10 of them were plated onto the coated MEA wells and the control 48-well plate, which were filled with NDM. During the 1st week, the medium was gradually switched to BrainPhys medium (BPH) consisting of BPH Neuronal Medium supplemented with 1 × NeuroCult SM1 Neuronal Supplement, 1 × N2 Supplement-A (all from Stemcell Technologies), GlutaMax to 2 mM final concentration, and 25 μ/ml penicillin/streptomycin for half of the cells. Additionally, from 2 days in adherent culture 1 mM cyclic adenosine monophosphate (cAMP) and 200 nM ascorbic acid (AA, both from Sigma-Aldrich) were added to the media and from 7 days after plating 8 ng/ml of bFGF and 10 ng/ml of brain-derived neurotrophic factor (BDNF, Gibco Invitrogen) were added to the media. The cells were maintained in a humidified incubator at 37°C and 5% CO_2, and half of the medium was refreshed 3 times per week. The cells were imaged weekly using a phase contrast microscope (Eclipse Ts2R, Nikon). In addition, the control plate was maintained in Cell-IQ (Chip-Man Technologies) 10 days after plating for 26 h with a 1 h imaging interval (**Supplementary Videos 1–3**). Spontaneous activities of neuronal networks were measured for 10 min twice per week.

Immunocytochemistry

The control plate cells were fixed after 12 days in adherent culture, and immunocytochemical staining was performed as previously described (Lappalainen et al., 2010). Primary antibodies, rabbit polyclonal anti-Microtubule-Associated Protein 2 (MAP2) (1:400; Millipore), mouse anti-beta-III Tubulin (β-tub) (1:1000; Sigma-Aldrich), chicken anti-Glial Fibrillary Acidic Protein (GFAP) (1:4000; Abcam), mouse anti-Synaptophysin (1:500; Sigma-Aldrich), chicken MAP2 (1:4000; Novus), and chicken β-tub (1:4000; Abcam) were used together with secondary antibodies Alexa 488 donkey anti-rabbit, Alexa 568 donkey anti-mouse and Alexa 647 goat anti-chicken (all 1:400; Invitrogen). In addition, the nuclei of the cells were

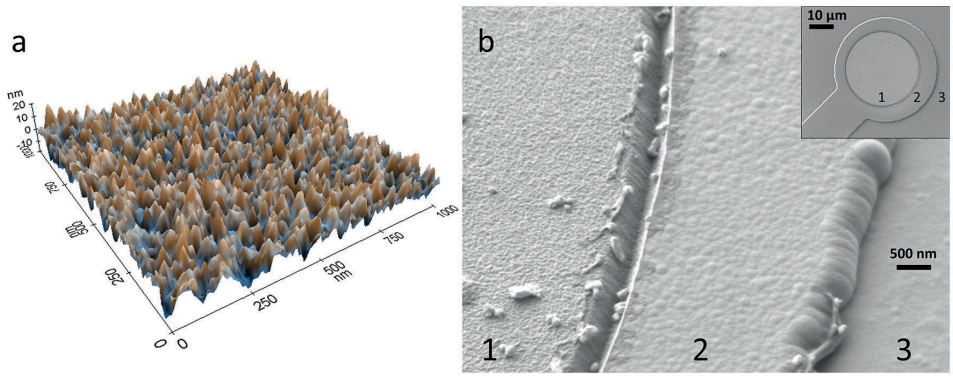

FIGURE 2 | Topological imaging of IBAD TiN. **(a)** AFM image of IBAD TiN surface of sample 2, and **(b)** SEM images of a 30 µm IBAD TiN microelectrode, where 1 is IBAD TiN on Ti, 2 is Si_3N_4 on Ti, and 3 is Si_3N_4.

stained with 4',6-diamidino-2 phenylindole (DAPI), which was included in the mounting medium (Prolong Gold, Molecular Probes). The cells were imaged with a fluorescence microscope (Olympus IX51, Olympus Corporation) and a laser scanning confocal microscope (LSM 780, Carl Zeiss).

MEA Signal Analysis and Statistics

Signal analysis from the MEA data was performed using MATLAB (The MathWorks, Inc.) with a custom-made analysis program based on work by Quiroga et al. (2004) in which the spike detection threshold was set to 5, and spikes larger than 500 times the standard deviation of noise were excluded as artifacts. An electrode was regarded as an active electrode if the spike frequency was more than 0.04 Hz. The threshold was determined by measuring spike rates from MEAs without cells and MEAs with TTX-silenced neuronal cultures (data not shown). For spike waveform analysis, 0.8 ms of voltage signal before and 1.76 ms after the largest absolute value of the spike from the filtered data were clipped. The detector dead time between two waveforms was 1.48 ms. Bursts were detected using a MATLAB code based on work by Kapucu et al. (2012) with additional conditions: burst detection was only applied to channels where the total spike frequency was at least 0.167 Hz (10/min). Thereafter, burst analysis criteria included a median of more than two spikes per burst and more than 1 burst per electrode. For each MEA type, Mann-Whitney U-test was performed to indicate statistical significances between the media at each measurement time point. $P < 0.05$ were considered significant.

RESULTS

IBAD TiN Process Development

With the assumption that the highest SAR would lead to the lowest microelectrode impedance, we focused on finding the IBAD deposition parameters that would give the highest SAR for the TiN thin film. Briefly, the purpose was to find deposition parameters for a thin film that we expect to give the lowest impedance, not necessarily the purest TiN from material science point of view. The deposition parameters tested while optimizing the IBAD TiN deposition process are presented in **Table 1**. The effect of changing deposition rates from 1 to 5 Å/s was tested for the same anode voltage and gas flow rate. In addition, some experiments with different anode voltages (sample 7), gas flow rates (samples 5–8) and pulsing of the ion beam (sample 8) were tested. Too high evaporation rate (sample 4) or a too low nitrogen flow rate (sample 7) led to gray thin films resembling pure Ti, which indicates that the conditions did not support the formation of TiN. Lower deposition rate (samples 1 and 2) and higher nitrogen content to argon (sample 5) were seen as brownish thin films, which more closely resembled the almost black thin film in MCS's sputtered TiN MEAs. The remainder (samples 3, 6, and 8) were goldish, which is considered to be the color of TiN hard coatings (Jiang et al., 2004).

In the AFM measurements, purple-bronze-colored sample 2 clearly had the highest SAR of 13.1%. The root-mean-square roughness (R_q) was 3.1 nm. The AFM image of sample 2 is shown in **Figure 2a**. According to the assumption of the highest SAR giving the lowest impedance and noise level, we chose the deposition parameters of sample 2 to be used as the deposition parameters in MEA fabrication. **Figure 2b** shows an SEM image of the IBAD TiN microelectrode. The slight pillar-like structure of TiN can be seen in the image. The EDS measurements showed <1% variation for the N/Ti ratio, indicating excellent homogeneity of the coating. However, as N is a light element and produces only the Kα peak that partly overlaps with the Ti Lα peak, EDS is better suited for comparative analysis than exact quantification of the N/Ti ratio.

MEA Performance Characterization

The experimental details are shown in **Table 2**. Once we had determined the optimal IBAD TiN deposition parameters, we fabricated a batch of IBAD TiN MEAs (hereafter referred to as BMT MEAs) in a 6-well layout mimicking MCS's 60-6wellMEA200/30iR-Ti-w/o array design. In this design, the

TABLE 2 | Experimental setup for MCS MEAs and BMT MEAs.

MEA type	Impedance measurement before use	Cell experiments	Impedance measurement after use
MCS MEA	**before E1**	E1*, E2*, **E3**	**after E2**
BMT MEA	**before E3**	**E3**	**after E3**

The impedance of each MEA was measured before and after the cell experiments. All the cell experiments (E1–E3) included both NMD and BPH medium tests.
**Results excluded due to incubator malfunction.*
Included measurements are bolded: impedance measurement results for MCS MEAs from before cell experiment E1 and after experiment E2 and for BMT MEA before and after cell experiment E3. Cell experiment results are presented from cell experiment E3.

microelectrodes are grouped in six 3 × 3 electrodes areas for a total of 6 areas with 9 electrodes / MEA. Both in IBAD TiN MEAs and MCS's MEAs the diameter of the electrodes is 30 μm. **Table 3** presents the impedance values for the included results, which are grouped by both MEA type and medium used in the cell experiments. Before the cell experiments, the BMT's IBAD TiN electrodes had ∼2× higher impedance compared with that of MCS's sputtered TiN electrodes, approximately 90 kΩ vs. 45 kΩ, respectively. However, as the impedances of Au, Pt or ITO MEAs, i.e., MEAs without a porous electrode coating are typically ∼10× higher (∼1 MΩ), the impedance of IBAD TiN is still comparable to sputtered TiN electrodes. After the cell experiments, the impedance of both IBAD and sputtered TiN electrodes increased >100 kΩ; thus, in this sense as well, the behaviors of the two electrode types were comparable. For IBAD TiN MEAs in BPH medium the after cell experiments impedance was significantly lower, only 35 kΩ, but this is because of severe insulator layer corrosion (**Figure 7c**). Thus, the result is not reliable, as the impedance in this case is not impedance of the electrodes only but rather impedance of both electrodes and tracks. IBAD TiN MEAs in NDM medium, on the contrary, suffered only minor corrosion (**Figure 7d**), indicating that we can consider their impedance values reliable enough for comparison. The insulator layer of MCS MEAs survived the cell experiments without visible corrosion in both media.

The measurement of impedance as a function of frequency show (**Figures 3A,B**) that the thickness of the IBAD TiN strongly affects to the impedance. Decreasing the thickness from 400 to 200 nm about doubles the impedance (at 1 kHz). As expected, compared with the Ti electrodes without the TiN coating the IBAD TiN coating significantly decreases the impedance and also improves the stability at low frequencies. Charge transfer capacity (CTC) integrated from the third CV curves (**Figure 3C**) was 3.3 ± 0.2 mC/cm^2 for IBAD TiN microelectrodes and about one tenth of that for Ti electrodes without TiN coating. For MCS MEAs CTC of 2.0 ± 0.2 mC/cm^2 was measured.

The noise level of each MEA type and medium combination was evaluated by calculating the estimate for standard deviation of background noise from 10 min cell measurement data (Quiroga et al., 2004). The results are summarized in **Figure 4A**. Briefly, the noise level of BMT MEAs was significantly lower from that of MCS's sputtered TiN MEAs under the same time point and condition ($p < 0.001$ for all). Moreover, BPH medium decreased the noise significantly compared with that of the NDM medium (at day 6 in BMT MEAs, $p \leq 0.001$, and at day 18 in both MEA plate versions, $p \leq 0.001$). However, typical examples of raw measurement data plotted in **Figure 4B** show well that, despite the differences in both numerical impedance and noise results, in practice there is no notable difference in the base noise levels and the signal peaks can be separated from the noise equally well with each MEA type and medium combination.

Effect of Cell Culture Medium

Neuronal Network Formation in NDM and BPH Media and BMT and MCS MEAs

Human pluripotent stem cell (hPSC)-derived neurons were cultured in neural differentiation medium (NDM) and BrainPhys medium (BPH) in control cell culture plastic wells. Both medium types supported the formation of MAP2 and β-tub-positive neuronal networks with expression of synaptophysin (**Figures 5a–f**) during a 12 days follow-up period. However, GFAP-positive astrocytes were only found in cultures supplemented with BPH medium (**Figure 5e**). Even though the network formation was good in both media, the organization of the networks differed between them. The neuronal networks were denser in BPH than those in NDM medium (**Figures 5c,f**). Neuronal cells migrated out of the cell aggregates in both media but more extensively in BPH. In NDM, neuronal cells remaining in the aggregates extended long neurites, which were less common in BPH.

Even though the networks grew well in both media in both MEA types at the beginning of the experiment (**Figures 5g,j,m,p**), after 1–2 weeks the neuronal networks started to retract and form clumps in BPH (**Figures 5k,q**). Network retraction also occurred in some NDM wells but typically later than in BPH (**Figures 5h,n,i,o** vs **Figures 5k,q,l,r**). The results were the same for both MEA types. The cultures were kept for 19–20 days on MEAs until the network retraction was too extensive, especially in BHP medium, for further measurements. Example videos of network growth on control plates after 10 days in adherent culture (**Supplementary videos 1–3**) show the typical behavior of the neuronal networks in both media over 26 h. At this point, the networks were not yet retracting in NDM or BPH on cell culture plastic (**Supplementary videos 1, 2**). However, network retraction in BHP on coverslips was substantial (**Supplementary video 3**). The cell culture experiments were repeated, and similar results were obtained. Network retraction, clump formation, and cell detachment occurred first and were more prominent in BPH than in NDM.

Development of Electrophysiological Activity in NDM and BPH Media on BMT and MCS MEAs

The percentage of active electrodes (spike frequency >0.04 Hz) per network was higher in BPH than in NDM at all measurement

TABLE 3 | Mean impedance of 30 μm TiN microelectrodes at 1 kHz before and after cell experiments performed in different cell culture media.

MEA manufacturer	TiN type	Medium	Before cell experiments		After cell experiments		Count of MEAs	Count of cell experiments**
			AVG [kΩ]	Stdev [kΩ]	AVG [kΩ]	Stdev [kΩ]		
BMT	IBAD	NDM	83	5	143	38	5	1
BMT	IBAD	BPH	87	5	35*	26*	5	1
BMT	IBAD	none	94	21	137	16	2	0
MCS	Sputtered	NDM	46	32	114	86	5	2
MCS	Sputtered	BPH	43	30	101	97	4	2

*Unreliable result as the Si_3N_4 insulator layer was almost completely corroded.
**Between impedance measurements.

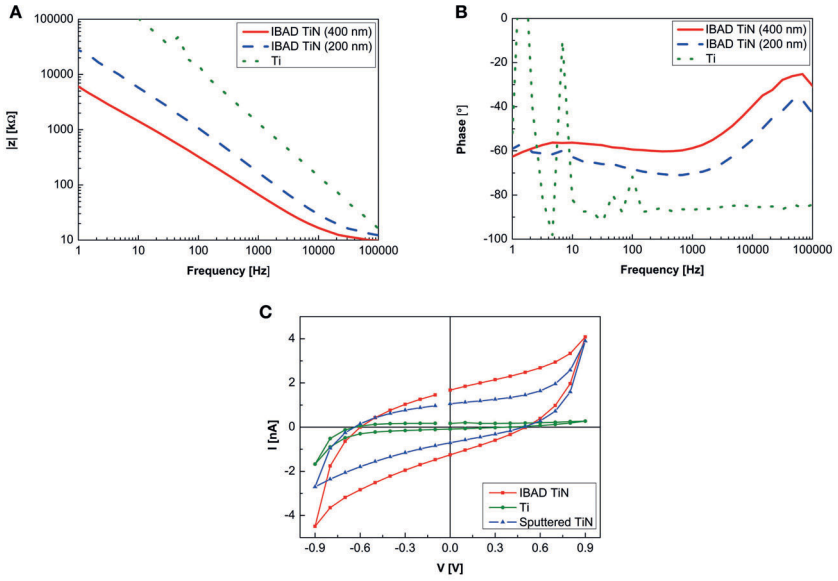

FIGURE 3 | Electrochemical analysis of 30 μm electrodes. **(A)** Magnitude and **(B)** phase of the impedance as a function of frequency of IBAD TiN and Ti electrodes, and **(C)** the third CV curves measured for calculating the charge transfer capacity of IBAD TiN, sputtered TiN, and Ti electrodes.

time points (M1 = 6 days, M2 = 11 days, M3 = 13 days, M4 = 18 days, and M5 = 19–20 days) on both BMT and MCS MEAs (**Figure 6A**). The results were statistically significant at most of the time points (BMT M1 $p = 0.005$, M2 $p = 0.035$, M4 $p < 0.001$; MCS M1 $p = 0.030$, M3 $p = 0.045$, M4 $p < 0.001$, M5 $p < 0.001$). Even though the BPH increased the amount of active electrodes, the median spike frequency in active electrodes was not clearly increased in BPH medium (**Figure 6B**). Depending on the measurement time point, more spikes were recorded in either BPH or NDM medium in both MEA types. Furthermore, the median burst count during the 10 min recording was not higher in BPH than that in NDM (**Figure 6C**). However, more electrodes recorded bursts in BPH medium. The spikes per burst medians were rather similar between the media in both MEA types (**Figure 6D**). Additional MEA analysis results are presented in **Supplementary Tables 1, 2**. Overall, BPH medium increased the amount of active electrodes but did not enhance the spike frequency or network maturation based on the burst parameters.

Insulation Layer Corrosion

Corrosion of the insulator layer in BMT MEAs not only affect the reliability of the impedance readings after the cell experiments but the vanishing of the insulation also caused a decrease in the MEA signal amplitudes. Examples of spike waveforms recorded using MEA with a badly corroded insulation layer are presented in **Figure 7a**. In comparison to spike waveforms recorded with MEA still with proper insulation left (**Figure 7b**), the signal amplitude from the badly corroded MEAs is substantially lower. In addition, the

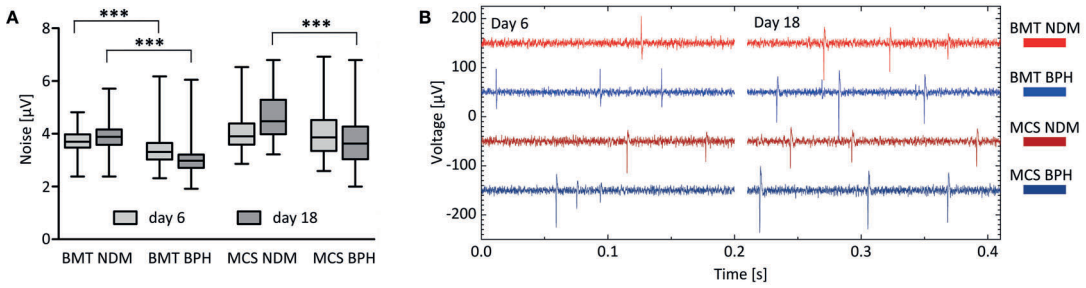

FIGURE 4 | Noise in each MEA type and medium combination. **(A)** Estimation of the standard deviation of background noise of each MEA type and medium combination at two time points. Data are expressed as the median (band inside the box) with interquartile range (IQR; box) and minimum and maximum values (whiskers) at two time points: 6 and 18 days on MEA. BMT, BioMediTech MEA; MCS, Multi Channel Systems MEA; NDM, neuronal differentiation medium; BPH, BrainPhys medium. ***$p \leq 0.001$. In addition, the noise level of BMT MEAs was significantly lower from that of MCS's sputtered TiN MEAs under the same time point and condition ($p < 0.001$ for all). **(B)** Examples of raw measurement data of each MEA type and medium combination at two time points. Curves have been shifted vertically for clarity.

amplitude of the noise was lower in the badly corroded MEAs.

DISCUSSION

The aim of this study was to demonstrate that sputtering is not the only method for fabricating TiN microelectrodes, as an alternative method exists. For the sputtered commercial TiN microelectrodes (MCS), we measured an impedance range of 30–50 kΩ, which is in line with the range provided in the manufacturer's brochure. This range is <80 kΩ as reported by Egert et al. (1998) in an early paper describing the sputtered TiN process for MEAs. Thus, it is very likely that by continuing process parameter optimization we could cut some tens of kΩ from the impedance of IBAD TiN microelectrodes. Our results showed that with IBAD TiN we reached impedance levels <100 kΩ, similar to those of current sputtered TiN microelectrodes. The signal-to-noise ratio was also very similar between these types of MEA electrodes. The CTC values reported in literature for sputtered TiN microelectrodes vary a lot. The original record by Janders et al. (1996) was as high as 42 mC/cm^2, which was later questioned by Weiland et al. (2002) who reported ∼2.4 mC/cm^2. That is in line with our result for sputtered TiN, 2.0 mC/cm^2. On the contrary, Gerwig et al. (2012) and Li et al. (2011) have reported both only 0.45 mC/cm^2. So, if Janders' record is ignored, IBAD TiN seems to perform well against sputtered TiN with its CTC of 3.3 mC/cm^2 also in this aspect. Thus, IBAD TiN microelectrodes can be expected to be competitive also in stimulation use. The produced IBAD TiN MEAs were compatible for cell measurements, especially when TiN is concerned. Overall, for in-house production, the availability of deposition equipment determines which TiN production method is used. For operators with an e-beam but no sputtering system, upgrading the e-beam coater with an ion source could be the most economical choice to obtain tools for in-house TiN deposition.

Here, the IBAD deposition parameters used in MEA fabrication were chosen based on the SAR; higher SAR was expected to result in lower impedance. Mumtaz and Class (1982) linked brownish color to more porous TiN structure, which agrees with our SAR results and color observations. Further, the coating colors of the produced samples were in line with the observations from previous studies (Mumtaz and Class, 1982; Roquiny et al., 1999). Additionally, it might be interesting to also fabricate MEAs with IBAD deposition parameters other than the ones chosen here as optimal, just to confirm whether the highest SAR is the true defining factor of the lowest impedance. The SAR results here are based on AFM sampling of only two 1 µm × 1 µm areas per sample, which may also leave room for error. However, the measured surface roughness value of 3.1 nm is in good agreement with the value of 3.0 nm by Cyster et al. (2002) for their DC magnetron-sputtered TiN. They also observed a rather strong dependency between the TiN layer thickness and roughness, which is in agreement with our observation of higher thickness meaning lower impedance. In order to keep the MEA surface rather planar and to avoid difficulties in certain process steps there is, however, not much room to play with the TiN thickness. Other parameters commonly connected to IBAD but not evaluated in this study are the substrate temperature and the ion beam incident angle which both may affect on the thin film properties. In our system adjusting those two parameters just was not possible. However, we did observe some temperature increase inside the deposition chamber after the IBAD process, but according to the ion source manufacturer, Saintech, with their ion sources the increase in the substrate temperature should be only very modest 20–30°C compared to ambient temperature, even if the ion source were operated on full power.

When comparing BMT-and MCS-fabricated MEAs, one should also note that there are some minor differences in the design. Only the electrode area of both BMT and MCS MEAs is equal in layout. Wider parts of the tracks and contact pads, on the contrary, have some "artistic" differences as we did not

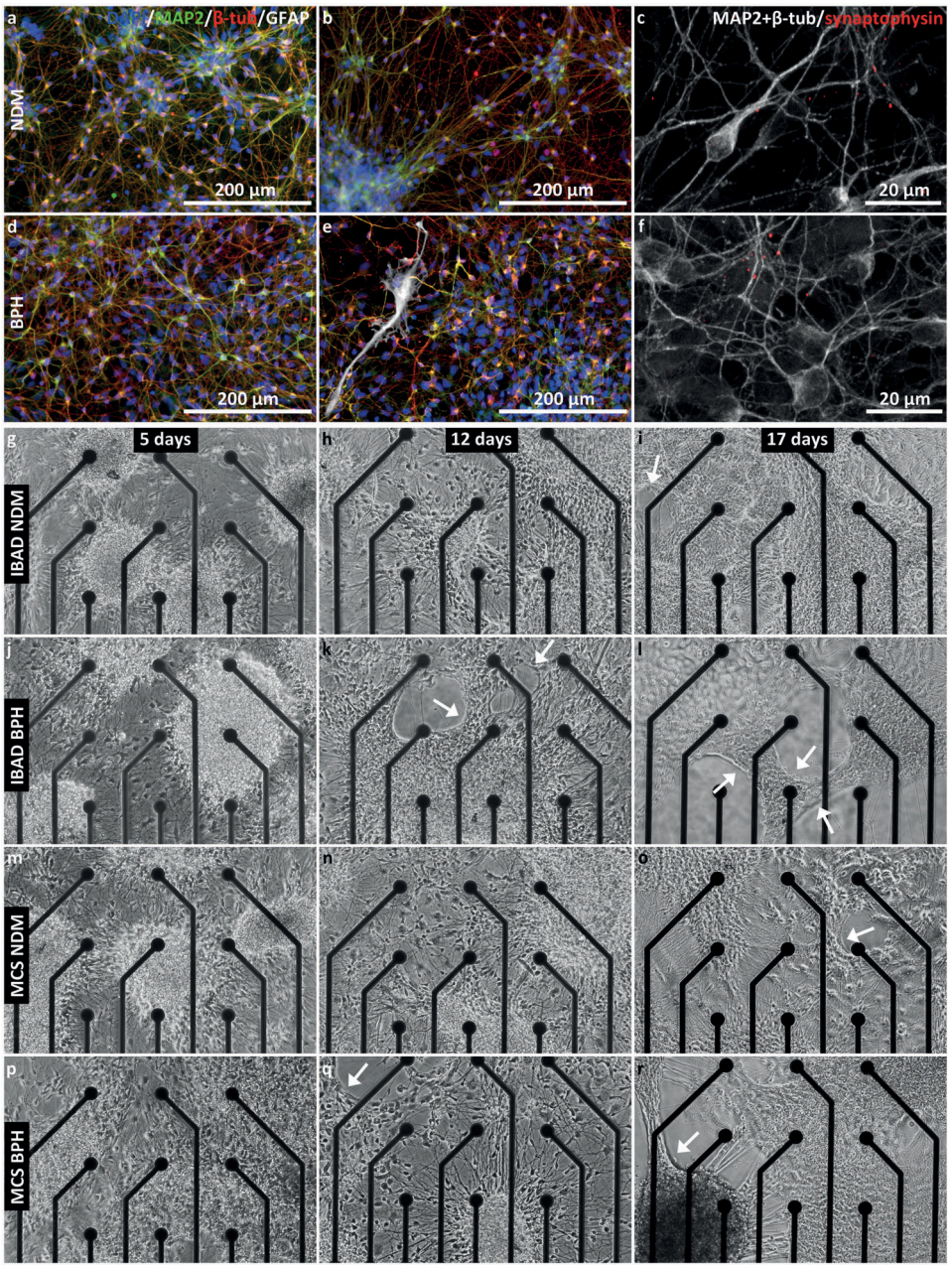

FIGURE 5 | Neuronal networks in NDM and BPH media. **(a–f)** Immunocytochemistry images from neuronal networks in NDM **(a–c)** and BPH **(d–f)** after 12 days in adherent culture. Networks in both media contained MAP2 and β-tub-positive neurons, whereas GFAP-positive astrocytes were only found in BPH medium **(e)**. Synaptophysin was expressed in networks in both media **(c,f)**. **(g–r)** Development of the network in NDM **(g–j,m–o)** and BPH media **(j–l,p–r)** on BMT MEAs **(g–l)** and MCS MEAs **(m–r)** at 5, 12, and 17 days in adherent culture. Network retraction (indicated by arrows) started earlier in BPH **(k** and **q)** than in NDM (**i** and **o**) on both MEA types.

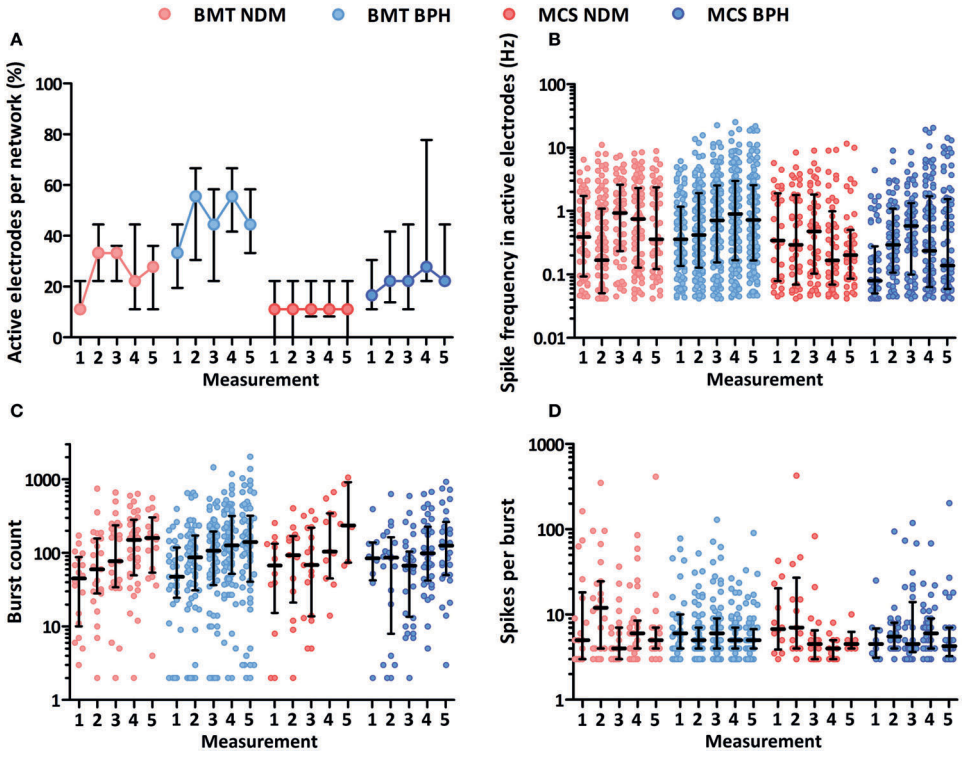

FIGURE 6 | MEA activity from NDM and BPH media on BMT and MCS MEAs. **(A)** Percentage of active electrodes per network (spike frequency >0.04 Hz). Higher percentages of electrodes were active in BPH on both MEA types. **(B)** Median spike frequency in active electrodes. **(C)** Median burst count over 10 min. **(D)** Spikes per burst median. Measurement 1 = 6 days, 2 = 11 days, 3 = 13 days, 4 = 18 days, and 5 = 19–20 days in adherent culture. Median and interquartile ranges are shown.

have MCS's mask layout CAD files available. As MCS brochures reveal only the insulator layer thickness, it is possible that Ti and TiN thicknesses are not equal in both MEA types. These differences can probably generally be ignored, but there was a notable difference in the corrosion resistance of the insulator layer even if both fabricators use 500 nm PECVD Si_3N_4. As we also observed similar corrosion in a control MEA with no IBAD TiN layer on titanium electrodes, we are confident that the IBAD TiN deposition process itself, despite potential thermal expansion-related issues, or the related rather long ultrasound bath during lift-off, is not the reason for the more corrosion-prone insulator layer in BMT MEAs. Our PECVD process only produces lower quality Si_3N_4 compared with MCS's process and requires further optimization. One should note that the IBAD TiN process introduced here is by no means connected to our PECVD Si_3N_4 process and whoever adapts IBAD TiN to their MEAs is free to use whatever insulator layer they find the most suitable for their application. If one does not want to move to polymer insulators like polyimide or SU-8, one common solution is to replace Si_3N_4 with a more stable but harder to etch sandwich structure of $SiO_2/Si_3N_4/SiO_2$ (Buitenweg et al., 1998; Yeung et al., 2007). Even if we did not observe as strong insulator layer corrosion in MCS's MEAs, these MEAs do still present some corrosion, and we have seen outside this study that, in the long run, the MCS MEA insulator layer does eventually totally wear out as well. Also Wagenaar et al. (2004) have reported long term insulator failure in MCS MEAs. In fact, there are more common studies (Schmitt et al., 2000; Herrera Morales, 2015), where not only Si_3N_4 but also many other commonly used insulator materials have been found to have a poor corrosion resistance in a biological environment. It is evident that the MEA community should stop focusing only on developing new electrode materials and put effort on studying the insulator materials as well.

Another interesting finding related to TiN was that the impedance of both sputtered and IBAD-deposited microelectrodes increased greatly during the experiments. As the impedance also increased for the control group of IBAD TiN MEAs not subject to any cell experiments, it is not necessarily only the cells or cell culture medium that either harms the electrode material or leaves some type of impedance-increasing residual on the surface of the MEA. It seems that storing the MEAs in normal room atmosphere between experiments may

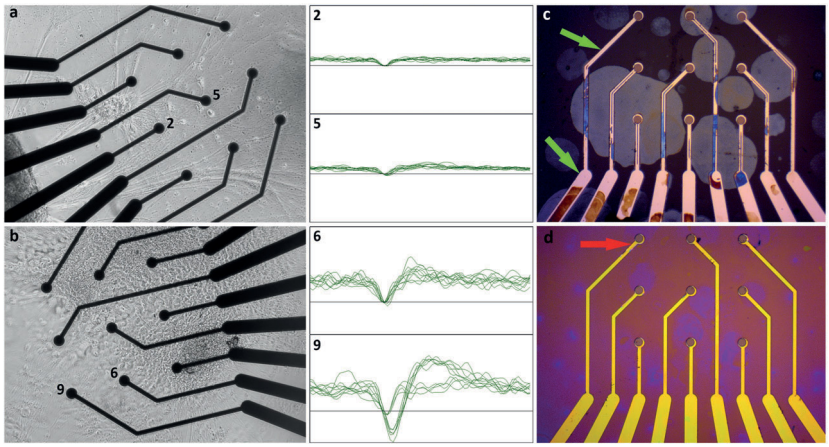

FIGURE 7 | Effect of corroded insulation on signal amplitude. **(a)** Neuronal network in BPH medium on a BMT MEA well with a badly corroded insulation layer after 21 days in adherent culture and corresponding spike waveforms from day 22 recordings from two representative electrodes (2 and 5). **(b)** Neuronal network in NDM medium at 17 days in adherent culture and recorded waveforms (6 and 9) from day 20 on a BMT MEA still with a proper insulation layer. The boxes are ±50 μV and 3 ms. **(c)** Example of insulator layer corrosion in BMT MEA after 3 weeks of cell culture in BPH medium. The green arrows indicate examples of fully corroded areas, demonstrating that most of the tracks have lost their insulation. **(d)** Example of insulator layer corrosion in BMT MEA after 3 weeks of cell culture in NDM medium. The insulator layer may have thinned all around, but it is fully corroded only from a small, barely visible area near the electrode as indicated by the red arrow.

be the primary reason for electrode degradation, likely due to the partial oxidation of Ti(N). In our preliminary tests of storing IBAD TiN MEAs in deionized water in a refrigerator, the electrodes retained constant impedance for a 1 week test period. An open question is whether the increasing impedance saturates at some point and the performance of the MEA at this point. As the condition of MEA is often controlled by checking the impedance, the combination of insulator layer corrosion and increasing electrode impedance due to oxidation makes the evaluation of the condition of MEA somewhat tricky; the impedance may stay within certain limits not because of MEA being consistent but because those two factors have compensated for each other.

In the cell culture experiments, we tested 2 media with both type of MEAs. In BPH, a significant increase in active electrode percentages was found compared to NDM. Earlier, similar results have been shown for BPH compared to standard cell culture medium (Bardy et al., 2015). Overall, our results may indicate that BPH enhanced the activity of the neurons directly or enabled denser neuronal network organization compared to NDM (see all the details in **Supplementary Table 1**). Interestingly, BPH did not increase the spike frequencies in this study in contrast to reported by Bardy et al. (2015). The burst count was neither increased in BPH compared to NDM, thus showing in both media the typical developmental increase during 3 weeks follow up as previously reported (Heikkilä et al., 2009). The median spikes per a burst (**Figure 6D**) as well as other burst parameters (**Supplementary Table 2**) showed no statistical differences between BPH and NDM. These results indicate that BPH did not enhance the maturation of the neuronal networks.

Importantly, our results revealed that BPH did not support long-term cell culturing in either of MEA types as neuronal networks started to retract and form cell clumps after 1–2 weeks and resulted in experiment termination in 3 weeks timepoint. Network retraction and cell clumping has been mentioned also in the study of Bardy et al. (2015) as a minor problem while here in our longer study it became a major problem. The long term stability of the network is most important for hPSC-derived neurons that require several weeks or even longer to develop mature neuronal activity (Heikkilä et al., 2009; Odawara et al., 2016).

In summary, we verified that IBAD is a valid method for producing TiN electrodes for MEA systems. Thus, it can be considered as an alternative TiN deposition method for sputtering. We also stated that BPH medium supported the development of neuronal activity on MEAs, although it caused problems in cell behavior and MEA insulator layer stability in long-term cultures. Thus, as insulator material, electrode material, and even cell culture medium can have detrimental effects on recording quality of MEAs especially with long-term cultures, all of these aspects should be carefully evaluated.

AUTHOR CONTRIBUTIONS

TR is responsible for the IBAD TiN process development, BMT MEA design and fabrication, AFM, impedance, and CV measurements, and technical data analysis excluding noise analysis performed together with MT and LY-O. MT is responsible for the cell experiments and cell data analysis. TS operated SEM and EDS. TR and MT wrote the manuscript. LY-O, SN, and JL participated in the project design with TR and MT

and provided additional support to analysis and writing of the manuscript.

FUNDING

This work was funded by Business Finland (formerly known as the Finnish Funding Agency for Technology and Innovation [TEKES]), the Academy of Finland (MEMO [311017, 311021 311022] and grant 286990 for LY-O), the Council of Tampere Region, and the Finnish Culture Foundation (grant for TR).

ACKNOWLEDGMENTS

Preliminary results of this study have been published previously as a conference abstract in Ryynänen et al. (2016).

SUPPLEMENTARY MATERIAL

The Supplementary Material for this article can be found online at: https://www.frontiersin.org/articles/10.3389/fnins.2018.00882/full#supplementary-material

REFERENCES

Bardy, C., van den Hurk, M., Eames, T., Marchand, C., Hernandez, R. V., Kellogg, M., et al. (2015). Neuronal medium that supports basic synaptic functions and activity of human neurons *in vitro*. *PNAS* 112, E2725–E2734. doi: 10.1073/pnas.1504393112

Bauerdick, S., Burkhardt, C., Kern, D. P., and Nisch, W. (2003). BioMEMs materials and fabrication technology : substrate-integrated microelectrodes with improved charge transfer capacity by 3-dimensional micro-fabrication. *Biomed. Microdevices* 5, 93–99. doi: 10.1023/A:1024526626016

Buitenweg, J. R., Rutten, W. L., Willems, W. P., and van Nieuwkasteele, J. W. (1998). Measurement of sealing resistance of cell-electrode interfaces in neuronal cultures using impedance spectroscopy. *Med. Biol. Eng. Comput.* 36, 630–637. doi: 10.1007/BF02524436

Cogan, S. F. (2008). Neural stimulation and recording electrodes. *Annu. Rev. Biomed. Eng.* 10, 275–309. doi: 10.1146/annurev.bioeng.10.061807.160518

Cyster, L. A., Grant, D. M., Parker, K. G., and Parker, T. L. (2002). The effect of surface chemistry and structure of titanium nitride (TiN) films on primary hippocampal cells. *Biomol. Eng.* 19, 171–175. doi: 10.1016/S1389-0344(02)00021-7

Egert, U., Schlosshauer, B., Fennrich, S., Nisch, W., Fejtl, M., Knott, T., et al. (1998). A novel organotypic long-term culture of the rat hippocampus on substrate-integrated multielectrode arrays. *Brain Res. Brain Res. Protoc.* 2, 229–242. doi: 10.1016/S1385-299X(98)00013-0

Falk, A., Heine, V., Harwood, A., PF, S., Peitz, M., Brüstle, O., et al. (2016). Modeling psychiatric disorders: from genomic findings to cellular phenotypes. *Mol. Pychiatry* 21, 1167–1179. doi: 10.1038/mp.2016.89

Gabay, T., Ben-David, M., Kalifa, I., Sorkin, R., Abrams, Z. R., Ben-Jacob, E., et al. (2007). Electro-chemical and biological properties of carbon nanotube based multi-electrode arrays. *Nanotechnology* 18:035201. doi: 10.1088/0957-4484/18/3/035201

Gahlin, R., Bromark, M., Hedenqvist, P., Hogmark, S., and Hakansson, G. (1995). Properties of TiN and CrN coatings deposited at low temperature using reactive arc-evaporation. *Surf. Coatings Technol.* 77, 174–180. doi: 10.1016/0257-8972(95)02597-9

Gawad, S., Giugliano, M., Heuschkel, M., Wessling, B., Markram, H., Schnakenberg, U., et al. (2009). Substrate arrays of iridium oxide microelectrodes for *in vitro* neuronal interfacing. *Front. Neuroeng.* 2:1. doi: 10.3389/neuro.16.001.2009

Gerwig, R., Fuchsberger, K., Schroeppel, B., Link, G. S., Heusel, G., Kraushaar, U., et al. (2012). PEDOT–CNT composite microelectrodes for recording and electrostimulation applications: fabrication, morphology, and electrical properties. *Front. Neuroeng.* 5:8. doi: 10.3389/fneng.2012.00008

Guzman, L., Bonelli, M., Miotello, A., and Kothari, D. C. (1998). Process parameters optimization for TiN and TiC formation using reactive ion beam assisted deposition. *Surf. Coatings Technol.* 100–101, 500–502. doi: 10.1016/S0257-8972(97)00679-8

Heikkilä, T. J., Ylä-Outinen, L., Tanskanen, J. M. A., Lappalainen, R. S., Skottman, H., Suuronen, R., et al. (2009). Human embryonic stem cell-derived neuronal cells form spontaneously active neuronal networks *in vitro*. *Exp. Neurol.* 218, 109–116. doi: 10.1016/j.expneurol.2009.04.011

Heim, M., Rousseau, L., Reculusa, S., Urbanova, V., Mazzocco, C., Joucla, S., et al. (2012). Combined macro-/mesoporous microelectrode arrays for low-noise extracellular recording of neural networks. *J. Neurophysiol.* 108, 1793–1803. doi: 10.1152/jn.00711.2011

Herrera Morales, J. M. (2015). *Selecting and Evaluating Biocompatible Barrier Films for Protecting Medical Micro Devices*. Dissertation. Université Grenoble Alpes.

Huang, J., Lin, C., Ma, C., and Chen, H. (2000). Low energy ion beam assisted deposition of TiN thin films on silicon. *Scr. Mater.* 42, 573–579. doi: 10.1016/S1359-6462(99)00393-0

Hubler, G. K., Vanvechten, D., Donovan, E. P., and Kant, R. A. (1988). Ion beam assisted deposition of titanium nitride. *MRS Proc.* 128, 55–60. doi: 10.1557/PROC-128-55

Janders, M., Egert, U., Stelzle, M., and Nisch, W. (1996). "Novel thin film titanium nitride micro-electrodes with excellent charge transfer capability for cell stimulation and sensing applications," in *Proceedings of 18th Annual International Conference of the IEEE Engineering in Medicine and Biology Society (1996)* Amsterdam, 245–247.

Jiang, N., Zhang, H. J., Bao, S. N., Shen, Y. G., and Zhou, Z. F. (2004). XPS study for reactively sputtered titanium nitride thin films deposited under different substrate bias. *Phys. B Condens. Matter* 352, 118–126. doi: 10.1016/j.physb.2004.07.001

Johnstone, A. F., Gross, G. W., Weiss, D. G., Schroeder, O. H., Gramowski, A., and Shafer, T. J. (2010). Microelectrode arrays: a physiologically based neurotoxicity testing platform for the 21st century. *Neurotoxicology* 31, 331–350. doi: 10.1016/j.neuro.2010.04.001

Kapucu, F. E., Tanskanen, J. M., Mikkonen, J. E., Ylä-Outinen, L., Narkilahti, S., and Hyttinen, J. A. (2012). Burst analysis tool for developing neuronal networks exhibiting highly varying action potential dynamics. *Front. Comput. Neurosci.* 6:38. doi: 10.3389/fncom.2012.00038

Kreutzer, J., Ylä-Outinen, L., Kärnä, P., Kaarela, T., Mikkonen, J., Skottman, H., et al. (2012). Structured PDMS chambers for enhanced human neuronal cell activity on MEA platforms. *J. Bionic Eng.* 9, 1–10. doi: 10.1016/S1672-6529(11)60091-7

Lappalainen, R. S., Salomäki, M., Ylä-Outinen, L., Heikkilä, T. J., Hyttinen, J. A., Pihlajamäki, H., et al. (2010). Similarly derived and cultured hESC lines show variation in their developmental potential towards neuronal cells in long-term culture. *Regen. Med.* 5, 749–762. doi: 10.2217/rme.10.58

Li, X., Pei, W., Tang, R., Gui, Q., Guo, K., Wang, Y., et al. (2011). Investigation of flexible electrodes modified by TiN, Pt black and IrO x. *Sci. China Technol. Sci.* 54, 2305–2309. doi: 10.1007/s11431-011-4436-7

López, J. M., Gordillo-Vázquez, F. J., Böhme, O., and Albella, J. M. (2001). Low grain size TiN thin films obtained by low energy ion beam assisted deposition. *Appl. Surf. Sci.* 173, 290–295. doi: 10.1016/S0169-4332(00)00912-0

Mumtaz, A., and Class, W. H. (1982). Color of titanium nitride prepared by reactive dc magnetron sputtering. *J. Vac. Sci. Technol.* 20, 345–348. doi: 10.1116/1.571461

Odawara, A., Katoh, H., Matsuda, N., and Suzuki, I. (2016). Physiological maturation and drug responses of human induced pluripotent stem cell-derived cortical neuronal networks in long-term culture. *Sci. Rep.* 6:26181. doi: 10.1038/srep26181

Peng, H., Zhou, D., Zhang, J., Guo, H., and Gong, S. (2015). Deposition of TiN by plasma activated EB-PVD: activation by thermal electron emission from molten niobium. *Surf. Coatings Technol.* 276, 645–648. doi: 10.1016/j.surfcoat.2015.05.047

Quiroga, R. Q., Nadasdy, Z., and Ben-Shaul, Y. (2004). Unsupervised spike detection and sorting with wavelets and superparamagnetic clustering. *Neural Comput.* 16, 1661–1687. doi: 10.1162/089976604774201631

Roquiny, P., Bodart, F., and Terwagne, G. (1999). Colour control of titanium nitride coatings produced by reactive magnetron sputtering at temperature less than 100??C. *Surf. Coatings Technol.* 116–119, 278–283. doi: 10.1016/S0257-8972(99)00076-6

Ryynänen, T., Toivanen, M., Narkilahti, S., and Lekkala, J. (2016). Titanium Nitride Microelectrodes Deposited by Ion Beam Assisted E-beam Evaporation. *Front. Neurosci. Conference Abstract: MEA Meeting 2016 | 10th International Meeting on Substrate-Integrated Electrode Arrays*. doi: 10.3389/conf.fnins.2016.93.00123

Samba, R., Fuchsberger, K., Matiychyn, I., Epple, S., Kiesel, L., Stett, A., et al. (2014). Application of PEDOT-CNT microelectrodes for neurotransmitter sensing. *Electroanalysis* 26, 548–555. doi: 10.1002/elan.201300547

Schmitt, G., Faßbender, F., Lüth, H., Schöning, M. J., Schultze, J.-W. and Buß, G. (2000). Passivation and corrosion of microelectrode arrays. *Mater. Corr.* 51, 20–25. doi: 10.1002/(SICI)1521-4176(200001)51:1<20::AID-MACO20>3.0.CO;2-Q

Stelzle, M., Stett, A., Brunner, B., Graf, M., and Nisch, W. (2001). Electrical properties of micro-photodiode arrays for use as artificial retina implant. *Biomed. Microdevices* 3, 133–142. doi: 10.1023/A:1011450326476

Thomas, C. A., Springer, P. A., Loeb, G. E., Berwald-Netter, Y., and Okun, L. M. (1972). A miniature microelectrode array to monitor the bioelectric activity of cultured cells. *Exp. Cell Res.* 74, 61–66. doi: 10.1016/0014-4827(72)90481-8

Wagenaar, D. A., Pine, J., and Potter, S. M. (2004). Effective parameters for stimulation of dissociated cultures using multi-electrode arrays. *J. Neurosci. Methods* 138, 27–37. doi: 10.1016/j.jneumeth.2004.03.005

Wagner, J., Mitterer, C., Penoy, M., Michotte, C., Wallgram, W., and Kathrein, M. (2008). The effect of deposition temperature on microstructure and properties of thermal CVD TiN coatings. *Int. J. Refract. Met. Hard Mater.* 26, 120–126. doi: 10.1016/j.ijrmhm.2007.01.010

Weiland, J. D., Anderson, D. J., and Humayun, M. S. (2002). *In vitro* electrical properties for iridium oxide versus titanium nitride stimulating electrodes. *IEEE Trans. Biomed. Eng.* 49, 1574–1579. doi: 10.1109/TBME.2002.805487

Xie, S., Cai, J., Wang, Q., Wang, L., and Liu, Z. (2014). Properties and morphology of TiN films deposited by atomic layer deposition. *Tsinghua Sci. Technol.* 19, 144–149. doi: 10.1109/TST.2014.6787367

Yeung, C. K., Sommerhage, F., Wrobel, G., Offenhäusser, A, Chan, M., and Ingebrandt, S. (2007). Drug profiling using planar microelectrode arrays. *Anal. Bioanal. Chem.* 387, 2673–2680. doi: 10.1007/s00216-007-1172-8

Ylä-Outinen, L., Heikkilä, J., Skottman, H., Suuronen, R., Aänismaa, R., and Narkilahti, S. (2010). Human cell-based micro electrode array platform for studying neurotoxicity. *Front. Neuroeng.* 3:111. doi: 10.3389/fneng.2010.00111

Yokota, K., Nakamura, K., Kasuya, T., Mukai, K., and Ohnishi, M. (2004). Resistivities of titanium nitride films prepared onto silicon by an ion beam assisted deposition method. *J. Phys. D. Appl. Phys.* 37, 1095–1101. doi: 10.1088/0022-3727/37/7/023

Conflict of Interest Statement: The authors declare that the research was conducted in the absence of any commercial or financial relationships that could be construed as a potential conflict of interest.

PUBLICATION IV

Microelectrode array for noninvasive cardiomyocyte measurements at the single-cell level

Ryynänen, T., Pekkanen-Mattila, M., Shah, D., Kreutzer, J., Kallio, P., Lekkala, J., Aalto-Setälä, K.

Japanese Journal of Applied Physics (2018), 57:117001, 1–7
https://doi.org/10.7567/JJAP.57.117001

OPEN ACCESS

Japanese Journal of Applied Physics **57**, 117001 (2018)

https://doi.org/10.7567/JJAP.57.117001

REGULAR PAPER

Microelectrode array for noninvasive analysis of cardiomyocytes at the single-cell level

Tomi Ryynänen[1*†], Mari Pekkanen-Mattila[2†], Disheet Shah[2], Joose Kreutzer[1], Pasi Kallio[1], Jukka Lekkala[1], and Katriina Aalto-Setälä[2,3]

[1]*BioMediTech Institute and Faculty of Biomedical Sciences and Engineering, Tampere University of Technology, 33720 Tampere, Finland*
[2]*Heartgroup, BioMediTech Institute and Faculty of Medicine and Life Sciences, University of Tampere, 33520 Tampere, Finland*
[3]*Heart Center, Tampere University Hospital, 33520 Tampere, Finland*

[*]E-mail: tomi.ryynanen@tut.fi
[†]These authors contributed equally to this work.

Received July 9, 2018; accepted August 20, 2018; published online October 19, 2018

Microelectrode arrays (MEAs) are widely used to assess the electrophysiology of human pluripotent stem cell-derived cardiomyocytes (hPS-CMs). Traditionally, MEAs have been used to record data at the cell population level, but it would be beneficial to be able to analyze also at the single-cell level using MEAs. To realize this, we present a special MEA platform for recording field potential from single beating cardiomyocytes. The size and location of transparent indium tin oxide (ITO) electrodes have been optimized to make noninvasive studies of the electrophysiological activity of cardiomyocytes at the single-cell level possible and also to enable simultaneous video imaging through transparent electrodes and thus image-based analysis of the mechanical beating behavior of the same cardiomyocytes. Because of these characteristics, this novel platform provides a powerful tool for assessing the functionality of cardiomyocytes in basic cardiac research, disease modeling, as well as drug development and toxicology. © 2018 The Japan Society of Applied Physics

1. Introduction

Microelectrode arrays (MEAs) provide a valuable tool for studying the electrophysiology of cells. In addition, they provide a platform for long-term and on-line assessment of electrophysiological parameters at the baseline as well as during pharmacological or mechanical stress. MEAs have been widely used for assessing the electrical activity of multiple cell types, such as human stem cell-derived cardiomyocytes (hPS-CMs) and neurons at the cell population level.[1–4)]

Human induced pluripotent stem (iPS) cells are derived from somatic cells with a defined set of factors.[5)] They can be differentiated, e.g., into cardiomyocytes (CMs) by multiple methods, such as using defined growth factors or small molecules, or by co-culturing with mouse endodermal-like (END-2) cells.[6,7)] With the differentiation methods, all cardiac subtypes (pacemaker, atrial, and ventricular cells) can be produced and the differentiated hPS-CMs resemble the native human counterparts in their gene and protein expression as well as functional properties. Therefore, they are suitable for modeling human cardiomyocytes and use in studies of human heart development, cardiac function, and diseases as well as in drug development and toxicology, as reviewed earlier.[8)] hPS-CMs have been used in the evaluation of cardiac safety of new drug candidates especially for their effects on the field potential duration (FPD), which is analogous to the QT interval of electrocardiography (ECG).[9)]

The electrophysiological characteristics of single hPS-CMs can be assessed using the patch clamp technique and calcium (Ca^{2+})- and voltage-sensitive dyes. The patch clamp technique is a gold standard for the assessment of cardiomyocyte action potential. However, it is labor-intensive and has a low throughput and therefore not suitable for high-throughput-type early-stage drug screening studies. Ca^{2+}- and voltage-sensitive dyes are suitable for intermediate-throughput-type studies of cardiomyocyte electrophysiology at the single-cell and cell population levels and can be used in preclinical drug testing approaches. However, all these aforementioned methods are either invasive or toxic to the cells and thus, long-term experiments are not applicable.

MEAs have been a widely used for assessing electrical activity and signal propagation as well as the conduction velocity of hPS-CMs.[10–12)] hPS-CM measurements using conventional MEAs consisting of 30 μm electrodes and 200 μm pitch have been limited to cell clusters or monolayers; therefore, signals are gained from a cell population. However, similar to single-cell transcriptomic and proteomic studies, analyses of the electrophysiological characteristics using individual cells would produce a more accurate representation of the cells than bulk measurements.

There is no fundamental reason why conventional MEAs are not applicable to single-cell studies. However, owing to the relatively small electrode size, the noise level is high and the signal amplitude of a single cardiomyocyte is low. Thus, detecting signals from single cells by conventional MEAs is very challenging. An additional difficulty is getting the single cells on the electrodes in a conventional layout. Using conventional MEAs, we have not been able to detect signals from single cells, and to the best of our knowledge there have been no reports of studies of the electrical activity of single hPS-CMs using traditional MEAs. Because of these reasons, performing single-cell studies using conventional MEAs is not feasible; thus, the single-cell-optimized MEAs were produced.

By assessing the electrophysiology or calcium transients of cardiomyocytes, the cardiac function is only measured partly while ignoring the biomechanics of the actual contraction of the cardiomyocytes. Previously, the biomechanics of the cardiomyocyte contraction have been assessed in vitro by atomic force or traction force microscopy.[13,14)] However, recent video microscopy methods have proven to provide a

relatively simple and noninvasive alternative to studying the biomechanics of cardiac contraction.[15–18] In a recent work, a video microscopy method was utilized, based on digital image correlation (DIC) and more specifically on its subtype, the minimum quadratic difference (MQD) method, which has been developed mainly for particle image velocimetry (PIV).[16] The video microscopy method quantifies the biomechanics, i.e., the movement of CMs in a noninvasive and label-free manner, enabling high-throughput-type screening, as well as long-term measurements.[15–17] Video analysis reveals information on the motion of CMs and, recently, video microscopy has also been combined with Ca^{2+} imaging.[19] By combining ionic and contraction data, a deeper understanding of the electromechanical coupling of cardiomyocyte contraction will be gained and new insights into cardiac diseases and drug effects may be revealed.

The aim of this study was to produce a MEA platform that contains electrodes that can measure the electrophysiological parameters of single hPS-CMs. The platform is designed for cell cultures where single hPS-CMs are plated on a MEA plate and only one cell is attached on the electrode. Owing the transparency of the electrodes, the platform also enables simultaneous measurement of the electrophysiological and biomechanical parameters of the contraction of single hPS-CM contraction noninvasively. The proposed platform consists of transparent electrodes, which are larger than those in conventional MEA platforms. In addition, the electrode layout is optimized for hPS-CMs. The custom-made MEA platforms are used with a conventional MEA amplifier, and the transparent electrodes enable simultaneous imaging and video analysis of the hPS-CMs. Therefore, the proposed approach provides data on both electrophysiological and biomechanical characteristics of a single cardiomyocyte, which will be utilized in studies of, e.g., iPS-based genetic cardiac disease modeling.

2. Materials and methods

2.1 MEA design, fabrication, and characterization

In measuring the field potential from a single cell with a MEA, there are two main challenges: how to 1) place a cell to be sufficiently close to the electrode and 2) optimize the signal-to-noise ratio by adjusting the size of the electrodes. If the electrode is much larger than the cell, the signal-to-noise ratio becomes small. However, too small electrodes possess a higher noise level by nature because impedance and noise are inversely dependent on the electrode area. For these reasons, the field potential signals of single cardiomyocytes are difficult to separate from noise. With the conventional MEAs having ~30-μm-diameter electrodes with ~200 μm spacing, it has been impossible to assess the electrical characteristics of hPS-CMs at the single-cell level.

The aim of this study was to design a MEA electrode layout that simultaneously increases the probability of cells to be located in optimal proximity to the electrodes and provides sufficient signal-to-noise ratio. In Layout 1, the cell culture area is covered by long and narrow electrodes resembling finger electrodes [Fig. 1(a)] to fulfill especially the first requirement for a design. For Layout 2 [Fig. 1(b)], we focus on evaluating different electrode sizes and shapes. The electrodes are circular or oval in shape, with some being split into halves or quarters. In this layout, the electrodes are located throughout the cell culture area. In Layout 3 [Figs. 1(c) and 1(d)], circular electrodes having a diameter of 80 μm are placed around the perimeter of the cell culture area. The center-to-center distance of the electrodes varies from 250 to 460 μm. Some of the electrodes have stripes or round holes to provide topography, which aims to orientate the cells or induce the cells to attach to the electrodes. Again, some of the electrodes are divided into separate halves as in Layout 2.

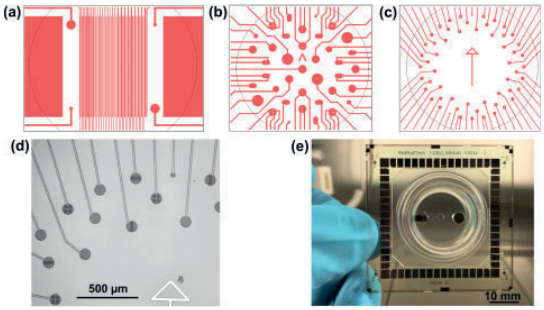

Fig. 1. (Color online) (a) Electrode Layout 1, (b) Layout 2, and (c) Layout 3. The black circles represent the central opening in the PDMS ring; diameters, 2 mm in Layouts 1 and 2, and 3.5 mm in Layout 3. (d) 5× microscopy image of Layout 3 MEA. (e) Specially designed PDMS ring on layout 3 ITO MEA. At the center there is an opening for microelectrodes and two bigger openings for ground electrodes. The right-angled ground electrode on the left was used in this study.

2.2 MEA fabrication

Figures 2(a)–2(k) show the fabrication process for Layout 3 in detail. The MEAs in Layouts 1 and 2 were fabricated using mostly the same process as that for MEAs in Layout 3. Two different versions of MEAs having Layout 3 were fabricated; one with opaque titanium (Ti) electrodes[20] and the other with transparent indium tin oxide (ITO) electrodes. The processing of MEAs with Ti electrodes started by e-beam deposition of 400 nm of Ti on $49 \times 49 \times 1\,mm^3$ soda lime glass substrates (Gerhard Menzel). Next, a positive photoresist (Futurrex PR1-2000A) was used as an etching mask in wet etching the MEA layout on the Ti layer. In the case of MEAs with ITO electrodes, a ~180 nm, 8–10 Ω/sq ITO layer was readily deposited on $49 \times 49 \times 0.7\,mm^3$ boro-aluminosilicate glass substrates (Universitywafer). In that case, the in-house process was started by lift-off patterning Ti alignment marks on the ITO-coated substrates. Next, a positive photoresist was used as an etching mask in etching the MEA layout on the ITO layer using argon in a reactive-ion etching (RIE) process. The remaining process steps were the same for the Ti and ITO versions. A 500 nm Si_3N_4 layer was deposited by plasma-enhanced chemical vapor deposition (PECVD) as the insulator layer and openings for electrodes and contact pads were dry-etched with a positive photoresist as an etching mask. Before 400 nm of titanium nitride was deposited by ion-beam-assisted e-beam deposition (IBAD),[21] to protect the contact pads, the electrode area was covered with a drop of photoresist. Finally, lift-off and resist removal were carried out using acetone in an ultrasound bath. Photolithography masks used in this work were fabricated in-house using a μPG501 maskless exposure system (MED; Heidelberg Instruments Mikrotechnik) on chrome mask blanks (Clean Surface Technology). In the case of Layout 1, part of the

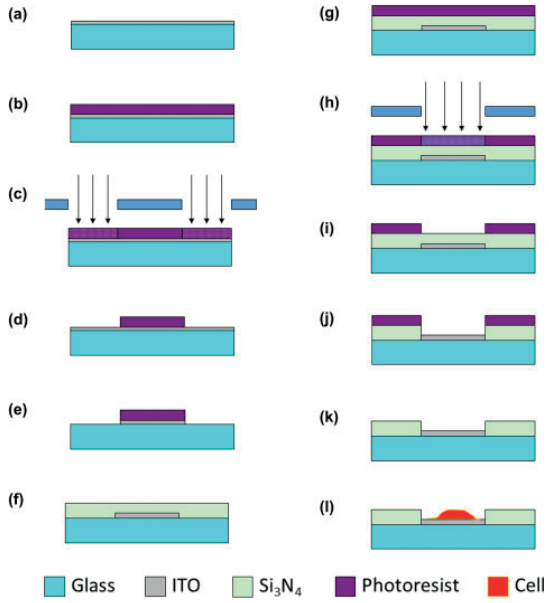

Fig. 2. (Color online) (a–k) MEA fabrication process. (a) Glass substrate coated with ITO or Ti, (b, g) spin coating with photoresist, (c, h) UV exposure of photoresist, (d, i) developed resist pattern, (e) electrode and track pattern dry etched to ITO or Ti, (f) PECVD of Si_3N_4, (j) dry etching openings for electrodes, and (k) removal of photoresist. Steps to fabricate alignment marks for ITO MEA and deposition of TiN to protect contact pads are excluded for simplicity. (l) Cardiac cell on MEA electrode. Owing to the edges formed by the Si_3N_4 insulator layer, the electrode is in a small pit, which may be favored by the cells. The dimensions in the drawing are not in scale.

exposures were, however, direct exposures using μPG501 instead of a mask aligner and the chrome masks.

2.3 MEA characterization

In order to characterize the impedance of the electrodes, a poly(dimethylsiloxane) (PDMS) ring was attached on top of the ready-made MEAs as a pool and was filled with Dulbecco's phosphate-buffered saline (PBS Dulbecco w/o Ca^{++}, Mg^{2+}, Biochrom) one day before the impedance measurements. The measurement system consisted of an Iviumstat potentiostat and multiplexers (Ivium Technologies), an MEA adapter (Multi Channel Systems MCS), and a Pt wire counter electrode (ALS-Japan). In addition, DRIREF-2 (World Precision Instruments) was used as the reference electrode for single-frequency measurements, where the impedance was measured at 1 kHz frequency. The result for both electrode types (ITO and Ti) is presented as the average of the median of 10 randomly selected nonpatterned electrodes from three MEAs. The impedance was characterized in more details for a randomly selected electrode over a frequency range from 1 to 100 000 kHz.

The simple PDMS rings used in the impedance measurements were removed and a specially designed PDMS ring was applied to the MEAs [Fig. 1(e)] providing small openings for the electrode area (2.0 mm in diameter for Layouts 1 and 2, and 3.5 mm in diameter for Layout 3) and for the ground electrodes (4 mm in diameter). The purpose of the PDMS ring is to restrict the cell culture area to enhance the cell attachment to the top of the electrodes and to prevent the cells from spreading out across the well, e.g., to the ground electrodes, where the beating of the cells would disturb the measurement by causing "reversed" signals to all of the electrodes. The silicone ring also provides a large reservoir for culture medium (1.5 ml). Silicone rings were fabricated as described previously.[22)]

Before plating hPS-CMs, the baseline noise was recorded in the cell culture medium consisting of KnockOut Dulbecco's modified Eagle's medium (KO-DMEM; Lonza), 20% fetal bovine serum (FBS; Lonza), 1% nonessential amino acids (NEAA; Cambrex), 2 mM Glutamax (Invitrogen), and 50 U/ml penicillin/streptomycin (Lonza) for 30 s with an MEA2100 MEA system (MCS). The average root mean square (RMS) noise level was calculated for each MEA and MEA type. Electrodes having an RMS noise level above 10 μV were considered faulty and were excluded from the calculations.

2.4 Cell culture and differentiation of hPS-derived cardiomyocytes

The human patient-specific iPSC line UTA.04602.WT was used in this study. The iPS cell line has been established from the fibroblasts of a healthy individual and cultured as described previously.[5,23)]

Differentiation of human pluripotent stem cells into cardiomyocytes was carried out via temporal modulation of canonical Wnt-signaling.[6)] The differentiated cells were dissociated into single cells with collagenase A (Roche Diagnostics).[7)] Single cells were suspended into the cell culture medium described above.

The MEA wells were first hydrophilized with FBS and then coated with 0.1% gelatin type A (Sigma-Aldrich). Immediately after coating, dissociated hPS-CMs were plated on each MEA by pipetting 50 μl of cell suspension consisting approximately 200–300 cells to the electrode area. The hPS-CMs were incubated in this volume of the medium for 1 h in an incubator to let the cells attach to the MEA. After incubation, the MEA was carefully filled with 1 ml of the cell culture medium described above. The medium was replaced with a fresh one for the MEAs every three days, and the MEAs were measured one day after the medium replacement.

2.5 Cell measurements and data analysis

Field potential (FP) was recorded 5–11 days after plating at 37 °C, and signals were recorded for 30 s. The sampling frequency was 20 kHz. Field potential was recorded during spontaneous baseline beating and after adding 50–100 nM E-4031 (Sigma-Aldrich) to the cell culture medium. The E-4031 solution was incubated 2 min before the measurements. The E-4031 solution was diluted and measurements performed in the cell culture medium as described above.

FP data were converted from the MCD format to Axon Binary File (ABF) using MC_DataTool software (MCS), and the ABF tile was converted to Axon Text File (ATF) using ClampFit version 10.3.0.2 (Molecular Devices). The FP signals in the ATF format were analyzed with an in-house-developed analysis module using Origin 2017 (Microcal OriginTM). Beating frequency by beats per minute (BPM), interbeat interval (IBI), and field potential duration (FPD) were extracted from the data. Bazett's formula was used to calculate the beat-rate-corrected FPD (cFPD).

The beating hPS-CMs on MEA chambers were imaged with a Zeiss Axio Observer-inverted phase contrast microscope and videos were taken with an Imperx Bobcat-camera

and JAI-Tool software. Videos were recorded for 30 s at 60 frames per second using 20× magnification. Video and MEA recordings were taken manually at the same time; therefore, the recordings were not automatically synchronized in this study.

The recorded videos were analyzed with CellVisus software (BioMediTech), which uses the digital image correlation (DIC)-based analysis method as used previously for hPS-CMs.[16,24] From the videos, the average parameters of the biomechanics of the contraction were defined: (1) duration of contraction, (2) time when hPS-CMs contracted, (3) duration of relaxation, (4) incomplete relaxation time, and (5) time when the cells relaxed.

For immunocytochemical staining, the hPS-CMs on MEA chambers were fixed with 4% paraformaldehyde (PFA; Sigma-Aldrich). The hPS-CMs were stained with a goat anti-cardiac-troponin-T (anti-Tnt; 1:2000, Abcam) antibody and incubated at +4 °C overnight. Alexa Fluor 568-conjugated polyclonal IgG (Abcam) for the goat anti-Tnt antibody was used as the secondary antibody and incubated with the cells for 1 h at room temperature. Cells were mounted with Vectashield containing 4′,6-diamidino-2-phenylindole, difydrochloride (DAPI) for staining nuclei (Vector Labs Vectashield). Fluorescence was visualized using an Olympus IX51 phase contrast microscope equipped with fluorescence optics and recorded with an Olympus DP30BW camera. The images were processed with Image-J and Adobe Photoshop 7.0 software (Adobe Systems).

3. Results and discussion

3.1 MEA layout development and technical characterization

In Layout 1, the cells plated on the MEA attached to the electrodes with high probability as the finger-type electrodes filled most of the cell culture area. Unfortunately, the area where the hPS-CM crossed the electrode was very small compared with the total electrode size and the signal from the cell was overpowered by the noise. However, one cardiomyocyte was found to attach to a circular 100 µm electrode included for the process characterization reasons. From that electrode, we were able to measure the signal and obtain a preliminary proof that a single hPS-CM is measurable by the MEA if the electrode size is increased from the conventional size of 30 µm (data not shown).

With MEAs in Layout 2, cardiomyocyte signals were detectable from some of the electrodes. However, it was observed that a notable proportion of the plated hPS-CMs tended to attach to the edges of the cell culture area, near the PDMS ring. On the basis of this finding, all the electrodes in Layout 3 were placed on the outer perimeter of the cell culture area of the MEA in order to increase the probability of the cells to attach to the electrodes. With this approach, a larger number of electrodes provided a signal. Nevertheless, no significant differences between the electrodes with stripes or holes and the plain electrodes were observed.

The impedances of ITO and Ti electrodes in Layout 3 were approximately 250 and 190 kΩ, respectively. The average baseline RMS noise in contrast was the same (5.4 ± 0.9 µV) for both materials. The phase and the magnitude of the impedance of a randomly selected round ITO electrode in a Layout 3 MEA are shown in Fig. 3 as functions of frequency.

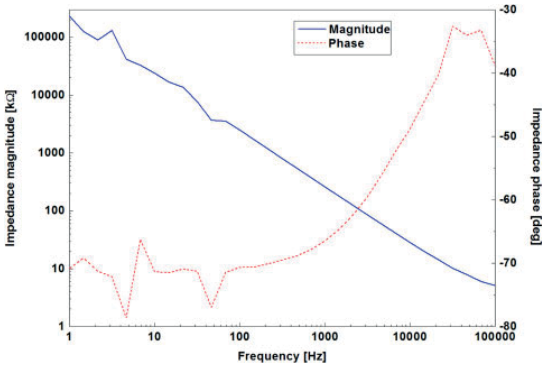

Fig. 3. (Color online) Phase and magnitude of impedance of a randomly selected round ITO electrode from a Layout 3 MEA as a function of frequency.

Compared with the standard 30 µm electrodes made of porous low-impedance materials such as titanium nitride (TiN) or platinum black, the impedances of our 80 µm ITO and Ti electrodes were 5–10 times higher despite their clearly larger sizes. Thus, one future development step in order to decrease impedance and noise level could be coating the Ti electrodes with TiN or with platinum black, as was done in a recent single-cell MEA approach in Ref. 29. These coatings, however, result in opaque electrodes. In contrast, decreasing the impedance of transparent ITO electrodes without losing their transparency is more challenging. Some improvement could be gained by increasing ITO thickness. However, because the impedance of the electrode–cell/medium interface dominates over track resistance, a more notable improvement requires new approaches, such as the development of new transparent electrode materials. Nevertheless, owing to the larger electrode size, the impedance was already 5–10 times smaller than the typical impedance of 30 µm electrodes made of ITO or Ti.[25] The baseline noise levels of both electrode types werethe same as those of commercial 30 µm TiN electrodes we previously measured for.[25] In addition to noise level and impedance, the material selection affects also the stimulation capability of the electrodes, which would enable, e.g., the pacing of hPS-CMs. That is however, left for future studies.

3.2 Cell attachment and measurements

The specific aim of this study was to grow no more than one hPS-CM on one electrode [Fig. 2(l)]. Therefore, the cell suspension was diluted and the total number of hPS-CMs plated on MEA plates was low, approximately 200–300 cells/well. The cells attached to the MEA plates during an overnight incubation and stayed attached as well as functional for at least two weeks on the MEA chambers. The hPS-CMs were beating and, therefore, functional when cultured in contact with the opaque Ti electrodes as well as transparent ITO electrodes.

The electrical activity of all the beating hPS-CMs attached to the top of the opaque and transparent electrodes in Layout 3 MEAs was detectable (4 MEA chambers used, 1–4 signals from each chamber observed). The signals were measured 5–11 days after the cell plating. The signal was very clear; therefore, the beating rate, beat-to-beat interval, and FP duration were measurable (Fig. 4, Table I). The signal character-

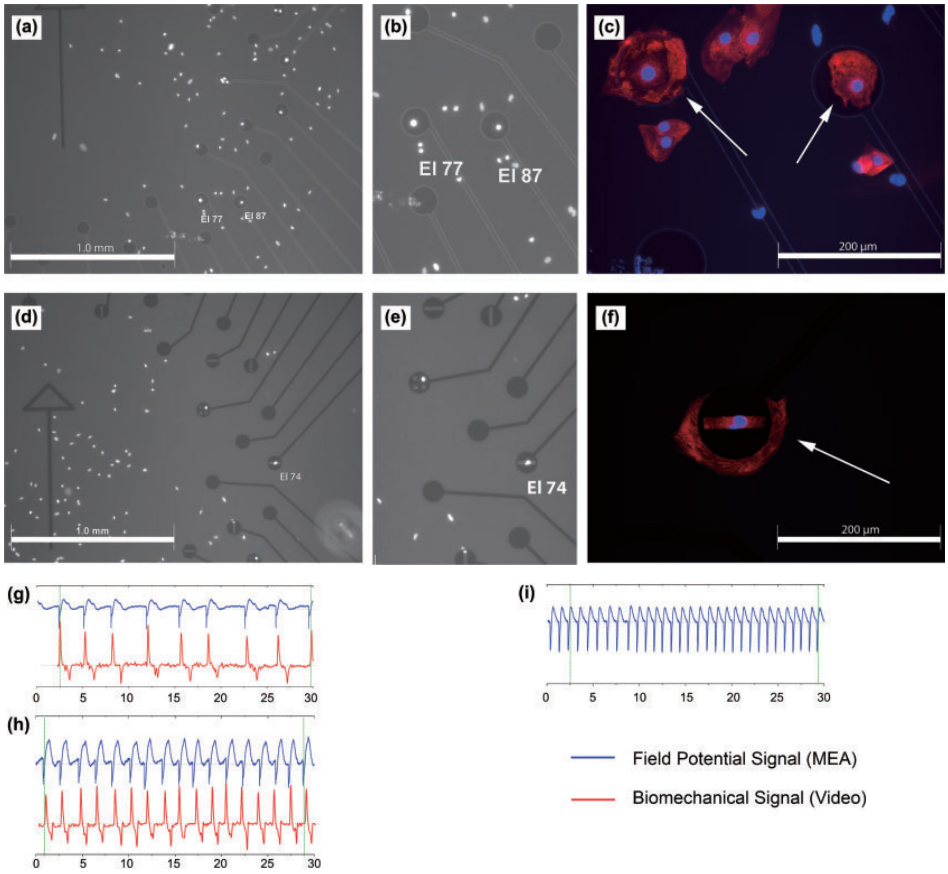

Fig. 4. (Color) (a–f) Immunocytochemical characterization of the cells plated on MEA chamber. (a) A MEA chamber with transparent electrodes and with DAPI staining indicating cell nuclei. (b) Insert in (a), indicating that both of the electrodes numbered 77 and 87 have one cell on each. (c) Immunocytochemical staining with cardiac-specific anti-troponin T antibody reveals that both of the cells on the electrodes are cardiomyocytes (indicated by arrows). (d) MEA chamber with opaque electrodes. (e) DAPI-stained nuclei are not visible on the electrodes with the inverted microscope if there are no holes on the electrode area, as on electrode 74. (f) Anti-troponin antibody staining shows that the cell on electrode 74 is a cardiomyocyte. (g–h) MEA signal (blue) aligned with the biomechanical signal of the contraction (red) analyzed by the video microscopy method from the hPS-CMs plated on the transparent electrodes. With both of the methods, a clear signal was obtained. (i) MEA signal gained from the hPS-CM on the opaque electrode.

Table I. Representative examples of the parameters describing the electrophysiology and biomechanics of the cardiac contraction of hPS-CM measured from the single hPS-CMs (Cells 1–6). The BPM and IBI gained from MEA and video data are comparable. With the single-cell MEA, the expected FPD prolonging effect of the the K^+-channel blocker E-4031 is observed. BPM, beats per minute; IBI, beat-to-beat interval; FPD, field potential duration; cFPD, corrected field potential duration.

		MEA data				Biomechanical (video) data		
		BPM	IBI (ms)	FPD B (ms)	cFPD B (ms)	BPM	IBI (ms)	Duration of mechanical activity (ms)
Cell 1	Baseline	38	1599	1055	834	38	1598	721
Cell 2	Baseline	17	3583	2623	1386	17	3461	1333
Cell 3	Baseline	93	644	480	598	94	639	164
Cell 4	Baseline	75	804	604	673	74	818	352
	E-4031	54	1112	829	786	N/A	N/A	N/A
Cell 5	Baseline	18	3426	1563	844	N/A	N/A	N/A
	E-4031	13	4508	1821	858	N/A	N/A	N/A
Cell 6	Baseline	62	965	702	714	N/A	N/A	N/A
	E-4031	48	1262	825	735	N/A	N/A	N/A

istics were comparable to those obtained from hPS-CM aggregates cultured using commercial MEA plates as reported previously.[16,23] In addition to the baseline data, the effects of the hERG-blocker E-4031 agent known to prolong the FPD interval were investigated. Prolongation of the FPD interval was detected at the single-cell level (Fig. 5 and Table I)

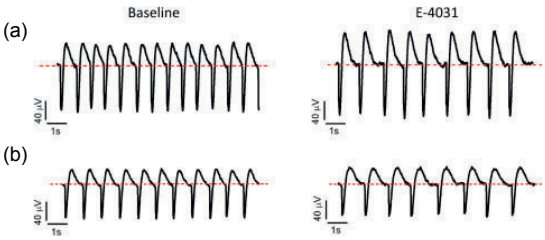

Fig. 5. (Color online) FP curves at the baseline and with E-4031 recorded from the hPS-CMs on the single-cell MEA. The FPD is prolonged owing to E-4031 as expected and this phenomenon is observed with the single-cell MEAs with transparent (a) as well as with opaque (b) electrodes.

demonstrating successfully the possibility of pharmaceutical testing on this novel single-cell MEA platform.

Owing to the transparency of the electrodes, the plated hPS-CMs could be imaged with the inverted phase contrast microscope. The videos of the hPS-CMs plated on the electrodes were analyzed by the Cell Visus software and the results of the analysis were comparable to the MEA data produced with the single-cell MEA system (Fig. 4, Table I, and video 1 in the online supplementary data at http://stacks.iop.org/JJAP/57/117001/mmedia). The obtained beating frequencies and beat-to-beat intervals were similar when recorded with the two methods.

The results showed that the MEA platform we developed can simultaneously record electrophysiological and biomechanical data and can thus be used for studies of cardiomyocyte function at the single-cell level owing to the transparency of the electrodes. Therefore, with this method, we can assess, e.g., the electromechanical coupling of hPS-CMs,[16] which provides a valuable tool for evaluating, for example, the proarrhythmic risk of novel drug candidates. However, the correlation between the electrical and mechanical functions of single hPS-CMs will be assessed in detail in future studies, since it is not within the scope of this study.

The beating was also observed from the opaque electrodes possessing gaps or holes (video 2 in the online supplementary data at http://stacks.iop.org/JJAP/57/117001/mmedia). However, video analysis was not possible and the contraction parameters could not be assessed. Therefore, to obtain both the MEA and video data, we concluded that the electrodes have to be transparent.

In this study, the entire cell culture area was coated with gelatin to support cell attachment. To increase the number of single cells attached on single electrodes, one possibility is the selective patterning of the electrodes with gelatin or other extracellular matrix proteins.[26] Recently, three-dimensional (3D) printing technologies have been applied to the generation of 3D cardiac patches composed of hPS-CMs and other supporting cell types with and without biomaterials.[27,28] Therefore, cell printing is an intriguing method that can be utilized also in the present single-cell MEA application, as the printer could print the cells exactly on the electrodes. Recently, Kaneko et al.[29] have proposed a MEA layout with small 8-μm-diameter and 1.4–3.0-μm-thick opaque platinum-black electrodes and agarose microchambers, where single CMs were seeded individually with a micropipette. With this method, the extracellular potential of a single CM was determined. However, the approach suffered from cell handling issues as well as difficulties with detecting two phases of FP peaks. We found the electrode diameter of 80 μm to be large enough to house a cell and to increase the probability of cell attachment compared with the standard 30 μm electrodes. Moreover, the diameter is sufficiently small to distinguish the cell signal from the background noise.

4. Conclusions

In this study, we introduced a MEA platform for assessing the electrophysiological characteristics (including FPD, beating frequency and beat-to-beat interval) of the hPS-CMs at the single-cell level. In addition, the transparency of the electrodes enables simultaneous video recording and analysis of the biomechanics of hPS-CM contraction and thus, enabling simultaneous electrophysiological and biomechanical characterization. With the video analysis, the durations of contraction and relaxation can be evaluated in addition to the alterations in the beating behavior such as a prolonged contraction or relaxation and oscillations in the beating.[16,24] The simultaneous electrophysiological and biomechanical characteristization provides a valuable tool for iPS-based disease modeling, as well as toxicology and drug development. In addition, the noninvasive nature of the novel platform enables the long-term assessment of the functionality of hPS-CMs at the baseline as well as the short- and long-term effects of alteration to putative drug agents. This platform opens up a new gateway to modeling cardiac diseases including genetic diseases and ischemia at the single-cell level.

Acknowledgments

This study was funded by Business Finland [formerly known as the Finnish Funding Agency for Technology and Innovation (TEKES)], the Council of Tampere Region, the Finnish Culture Foundation, and Päivikki and Sakari Sohlberg's foundation. We thank Antti Ahola for assistance with the video analysis and Haider Iftikhar for aid in ITO etching process development. We also acknowledge the Tampere Facility of Electrophysiological Measurements for their service.

1) T. J. Heikkilä, L. Ylä-Outinen, J. M. A. Tanskanen, R. S. Lappalainen, H. Skottman, R. Suuronen, J. E. Mikkonen, J. A. K. Hyttinen, and S. Narkilahti, Exp. Neurol. **218**, 109 (2009).
2) M. Pekkanen-Mattila, E. Kerkelä, J. M. A. Tanskanen, M. Pietilä, M. Pelto-Huikko, J. Hyttinen, H. Skottman, R. Suuronen, and K. Aalto-Setälä, Ann. Med. **41**, 360 (2009).
3) K. Asakura, S. Hayashi, A. Ojima, T. Taniguchi, N. Miyamoto, C. Nakamori, C. Nagasawa, T. Kitamura, T. Osada, Y. Honda, C. Kasai, H. Ando, Y. Kanda, Y. Sekino, and K. Sawada, J. Pharmacol. Toxicol. Methods **75**, 17 (2015).
4) L. Sala, D. Ward-van Oostwaard, L. G. J. Tertoolen, C. L. Mummery, and M. Bellin, J. Vis. Exp. **123**, e55587 (2017).
5) K. Takahashi, K. Tanabe, M. Ohnuki, M. Narita, T. Ichisaka, K. Tomoda, and S. Yamanaka, Cell **131**, 861 (2007).
6) X. Lian, C. Hsiao, G. Wilson, K. Zhu, L. B. Hazeltine, S. M. Azarin, K. K. Raval, J. Zhang, T. J. Kamp, and S. P. Palecek, Proc. Natl. Acad. Sci. U.S.A. **109**, E1848 (2012).
7) C. Mummery, D. Ward-van Oostwaard, P. Doevendans, R. Spijker, S. van den Brink, R. Hassink, M. van der Heyden, T. Opthof, M. Pera, A. B. de la Riviere, R. Passier, and L. Tertoolen, Circulation **107**, 2733 (2003).
8) Y. Yoshida and S. Yamanaka, Circ. Res. **120**, 1958 (2017).
9) M. Clements and N. Thomas, Toxicol. Sci. **140**, 445 (2014).

10) J. Kuusela, V. J. Kujala, A. Kiviaho, M. Ojala, H. Swan, K. Kontula, and K. Aalto-Setälä, Springerplus **5**, 234 (2016).
11) J. Kuusela, J. Kim, E. Räsänen, and K. Aalto-Setälä, Stem Cell Rev. **12**, 698 (2016).
12) H. Zhu, K. S. Scharnhorst, A. Z. Stieg, J. K. Gimzewski, I. Minami, N. Nakatsuji, H. Nakano, and A. Nakano, Sci. Rep. **7**, 43210 (2017).
13) M. Pesl, J. Pribyl, I. Acimovic, A. Vilotic, S. Jelinkova, A. Salykin, A. Lacampagne, P. Dvorak, A. C. Meli, P. Skladal, and V. Rotrekl, Biosens. Bioelectron. **85**, 751 (2016).
14) M. C. Ribeiro, L. G. Tertoolen, J. A. Guadix, M. Bellin, G. Kosmidis, C. D'Aniello, J. Monshouwer-Kloots, M. J. Goumans, Y. Wang, A. W. Feinberg, C. L. Mummery, and R. Passier, Biomaterials **51**, 138 (2015).
15) H. Välimäki, J. Verho, J. Kreutzer, D. K. Rajan, T. Ryynänen, M. Pekkanen-Mattila, A. Ahola, K. Tappura, P. Kallio, and J. Lekkala, Sens. Actuators B **249**, 738 (2017).
16) A. Ahola, A. L. Kiviaho, K. Larsson, M. Honkanen, K. Aalto-Setälä, and J. Hyttinen, Biomed. Eng. Online **13**, 39 (2014).
17) L. Sala, B. J. van Meer, L. T. Tertoolen, J. Bakkers, M. Bellin, R. P. Davis, C. N. Denning, M. A. Dieben, T. Eschenhagen, E. Giacomelli, C. Grandela, A. Hansen, E. Holman, M. R. Jongbloed, S. M. Kamel, C. D. Koopman, Q. Lachaud, I. Mannhardt, M. P. Mol, D. Mosqueira, V. V. Orlova, R. Passier, M. C. Ribeiro, U. Saleem, G. Smith, F. L. L. Burton, and C. L. Mummery, Circ. Res. **122**, e5 (2018).
18) T. Hayakawa, T. Kunihiro, S. Dowaki, H. Uno, E. Matsui, M. Uchida, S. Kobayashi, A. Yasuda, T. Shimizu, and T. Okano, Tissue Eng. Part C **18**, 21 (2012).
19) A. Ahola, R. P. Pölönen, K. Aalto-Setälä, and J. Hyttinen, Ann. Biomed. Eng. **46**, 148 (2018).
20) T. Ryynänen, V. Kujala, L. Ylä-Outinen, I. Korhonen, J. M. A. Tanskanen, P. Kauppinen, K. Aalto-Setälä, J. Hyttinen, E. Kerkelä, S. Narkilahti, and J. Lekkala, Micromachines **2**, 394 (2011).
21) T. Ryynänen, M. Toivanen, S. Narkilahti, and J. Lekkala, Front. Neurosci. Conf. Abstr. MEA Meet. 2016/10th Int. Meet. Substrate-Integrated Electrode Arrays, 2016.
22) J. Kreutzer, L. Ylä-Outinen, P. Kärnä, T. Kaarela, J. Mikkonen, H. Skottman, S. Narkilahti, and P. Kallio, J. Bionic Eng. **9**, 1 (2012).
23) A. L. Lahti, V. J. Kujala, H. Chapman, A.-P. Koivisto, M. Pekkanen-Mattila, E. Kerkelä, J. Hyttinen, K. Kontula, H. Swan, B. R. Conklin, S. Yamanaka, O. Silvennoinen, and K. Aalto-Setälä, Dis. Model. Mech. **5**, 220 (2012).
24) A. L. Kiviaho, A. Ahola, K. Larsson, K. Penttinen, H. Swan, M. Pekkanen-Mattila, H. Venäläinen, K. Paavola, J. Hyttinen, and K. Aalto-Setälä, IJC Hear. Vasc. **8**, 19 (2015).
25) T. Ryynänen, L. Ylä-Outinen, S. Narkilahti, J. M. A. Tanskanen, J. Hyttinen, J. Hämäläinen, M. Leskelä, and J. Lekkala, J. Vac. Sci. Technol. A **30**, 041501 (2012).
26) L. Wang, L. Liu, X. Li, N. Magome, K. Agladze, and Y. Chen, Microelectron. Eng. **111**, 267 (2013).
27) L. Gao, M. Kupfer, J. Jung, L. Yang, P. Zhang, Y. Sie, Q. Tran, V. Ajeti, B. Freeman, V. Fast, P. Campagnola, B. Ogle, and J. Zhang, Circ. Res. **120**, 1318 (2017).
28) C. S. Ong, T. Fukunishi, H. Zhang, C. Y. Huang, A. Nashed, A. Blazeski, D. DiSilvestre, L. Vricella, J. Conte, L. Tung, G. F. Tomaselli, and N. Hibino, Sci. Rep. **7**, 4566 (2017).
29) T. Kaneko, H. Toriumi, J. Shimada, and F. Nomura, Jpn. J. Appl. Phys. **57**, 03EB03 (2018).